Review of Aeronautical Fatigue Investigations in Germany During the Period March 2003 to May 2005

Dr. Claudio Dalle Donne
EADS Corporate Research Center Germany
SC/IRT/LG-MT

SC/IRT/LG-MT–2005-039 Technical Report
EADS Corporate Research Center Germany

Title

Review of Aeronautical Fatigue Investigations in Germany During the Period March 2003 to May 2005

Author

Dr. Claudio Dalle Donne

Phone-No.	Department	Date	Report-No.
089/607-27728	SC/IRT/LG-MT	19.04.2005	SC/IRT/LG-MT-2005-039

Abstract

The review has been prepared for presentation at the 2005 Meeting of the International Committee on Aeronautical Fatigue in Hamburg Germany, 6.-7. June 2005. German aerospace manufacturers, governmental and private research institutes, aerospace authorities as well as universities were invited to contribute summaries of aeronautical fatigue related research activities. The 50 voluntary contributions cover the whole spectrum of fatigue related research in the years 2003 to 2005, raging from full scale testing of aircraft down to fundamental studies in the field of fatigue damage.

Distribution to

SC/IRT/LG-SP- Patents
M & W Zander/FM-K2-OT-MF - Mikroverfilmung
Cover page: SC/IRT/LG – Dr. Bütje
Cover page: SC/IRT/L – Dr. Müller-Wiesner

Specialized information

pages	Figures
82	83

Documentation-No.

Classification: 1

Acceptance:

1 generally accessible

2 free distribution inside EADS

3 confidential

4 highly confidentially

Dr. Dalle Donne
Manager of the
responsible department

1 Introduction

The review has been prepared for presentation at the 2005 Meeting of the International Committee on Aeronautical Fatigue in Hamburg Germany, 6.-7. June 2005. German aerospace manufacturers, governmental and private research institutes, aerospace authorities as well as universities were invited to contribute summaries of aeronautical fatigue related research activities. These voluntary contributions are compiled here. The author acknowledges these contributions with appreciation. Enquiries should be addressed to the authors of the summaries.

Mailing Addresses of Contributing Companies and Institutes:

Airbus-D	Airbus Deutschland GmbH, Kreetslag 10, 21129 Hamburg
AvCraft	AvCraft Aerospace GmbH, PO-Box 1252, 82231 Wessling
EADS-CRC	European Aeronautic Defence and Space Company, Corporate Research Center Germany, 81663 Munich
DLR	German Aerospace Center DLR, Institute of Materials Research, 51170 Cologne
IABG	Industrieanlagen-Betriebsgesellschaft mbH, PO-Box 1212, 85503 Ottobrunn
IMA	Materialforschung und Anwendungstechnik GmbH, PO-Box 800144, 01101 Dresden
GKSS	GKSS Research Center, Institute for Materials Research, Max-Planck-Strasse, 21502 Geesthacht
LBF	Fraunhofer Institute for Structural Durability LBF, Bartningstr. 47, 64289 Darmstadt
RUAG	RUAG Aerospace Services GmbH, Airport Oberpfaffenhofen, PO-Box 1253, 82231 Wessling
UniBw-M	University of the Federal Armed Forces Munich, Department of Materials Science, 85577 Neubiberg
USI	University of Siegen, Department of Materials Science and Testing, 57068 Siegen

2 Full Scale Testing

2.1 Overview of Full Scale Fatigue Tests in Germany (May 2005)

Project	Customer	Test Structure	Time Schedule	Test Lab
A380	Airbus-D	Rear End Test: Damage tolerance certification test of CFRP parts	2005-2006	Airbus-D
A380	Airbus-D	Full scale certification test of the complete inner flap	2005-2007	Airbus-D
A380	Airbus-F	Engine pylon fwd. attachment	2004-2006	IABG
A380	Patria	Spoiler No 1 and No 4	2004-2006	IABG
A380	Airbus-D	A380 full scale fatigue test	2003-2008	IABG-IMA
A380	Airbus-D	Flap track No. 6 static and fatigue certification test	2004 - 2005	IMA
A380	Airbus-D	Flap carriage No. 3 crack propagation development test	2004 - 2005	IMA
A380	Airbus-D	Fatigue and damage tolerance tests of fuselage panels	2004	IMA
A380	Airbus-F	Flat panel test – landing gear bay/ frame 22 orbital junction	2004	IMA
A380	Eurocopter-D	Component test stop fittings of passenger doors	2003 - 2004	IMA
A380	Liebherr Aerospace	Windmilling test of an A380 rotary actuator	2004	IMA
AB139	Liebherr Aerospace	Development test NLG and MLG	2004	IMA
ERJ-145	Liebherr Aerospace	Verification test NLG	2004	IMA
M346	Liebherr Aerospace	NLG stiffness, strength and fatigue test	2004 - 2005	IMA
PC21	Pilatus	Wings	2004	IABG
PC21	Pilatus	Complete airframe	2004-2006	IABG
PC21	Pilatus	Drop tests for NLG and MLG	2004	IABG
Research	Airbus-D	Megaliner barrel	2002-2004	Airbus-D
Research	Airbus-D	Static and dynamic testing of CFRP curved fuselage panels	since 2003	IMA
Research	BMWT	Possibilities and problems with vibro-acoustic diagnostic on aircraft engines	2003	IMA
TANGO	Airbus-D	Metallic and composite barrel, curved fuselage panels	2002-2004	Airbus-D, IMA

2.2 Airbus A380 Full Scale Fatigue Test

K. Woithe (IABG)

IABG has realized a test installation for performing a full scale fatigue test of the A380 airframe structure. The test specimen consisting of the complete primary fuselage structure with both wings and a number of dummies replacing original structures (i. e. landing gears, engine pylon, horizontal tail, VTP etc.) has been delivered in September / October 2004 and was assembled by Airbus working party till end of December 2004.

Fatigue testing is planned to start in September 2005 with the aim of reaching 5.000 simulated flights by January 2006, a few months before the first A380 enters into service.

In total 47.500 flights should be completed by end of 26 month test duration in 2007, which is calculated to be equivalent to 60.000 actual flights because of a fatigue load enhancement factor of 1.1 is to be used.

The test will run for 24h a day with a high test speed of 900 flights/week. The structure will be inspected every 3800 flights for damage.

The mechanical loading of the test structure will be done by using 182 hydraulic jacks and 6 struts supporting the test specimen. The fuselage will be loaded via 1.416 loading points distributed onto all decks (passenger and cargo) as well as further loading onto the fuselage shell. The wing will be loaded by tension / compression whiffle trees positioned below the wing. The load introduction is realized by approx. 2.800 load pads bonded at the upper wing skin.

IABG has installed an advanced control and monitoring system to realize the required accuracy and high test speed during the simulation of the flight by flight program. Further more a data acquisition system has been installed to measure 7.200 strain gauges and deflection transducers.

The hydraulic system is driven from a central hydraulic power supply with 6.000 l/min oil capacity operating at a pressure of 280 bar.

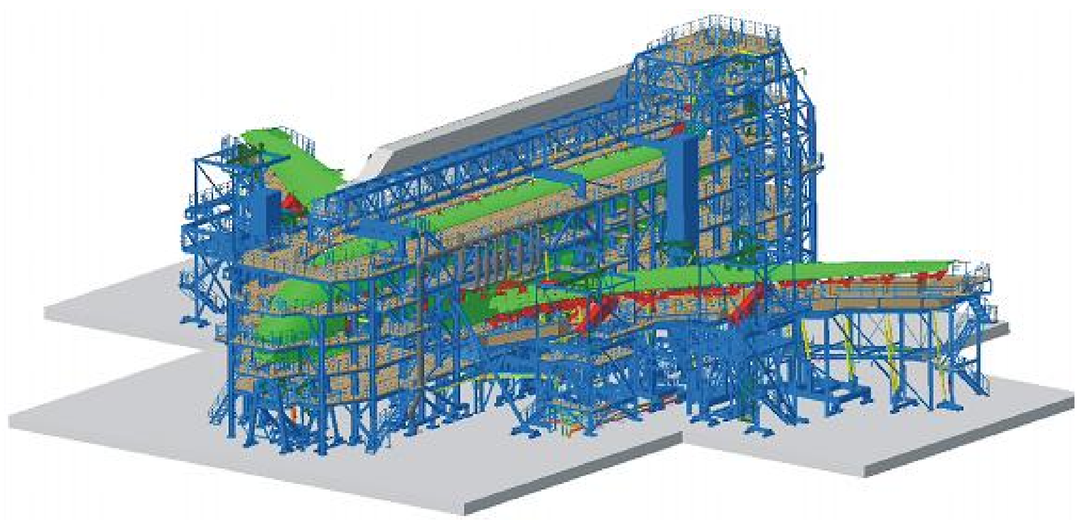

Figure 1: Schematic test setup A380 full scale fatigue test

The fuselage cabin will be pressurized by using a central pneumatic power supply to simulate the internal pressure profile during flight simulation. Figure 1 shows the schematic test setup for the A380 full scale fatigue test.

2.3 Transportation and Infrastructure for the Airbus A380 Full Scale Fatigue Test

R. Buchholz and T. Fleischer (IMA in cooperation with the main contractor IABG)

IMA GmbH Dresden is involved in the Full Scale Fatigue Test of the new Airbus A380-800. Within this project, IMA is especially responsible for important test preparations and load systems as well as for extensive work packages during the test performance and the inspection / NDT activities.

A new test hangar was built for the test near Dresden Airport. To carry the test loads a very specific strong floor of 6000 m² was developed and installed which is grounded on 200 bored piles. Furthermore, IMA was responsible for the development and installation of the hydraulic and pneumatic infrastructure. An innovative active nitrogen pressure steered accumulator system was developed for the hydraulic loading system.

The development of a sound concept for the section transports from Hamburg to the test hangar in Dresden, including the evaluation of different transport feasibility studies, was the main reason for the conduction of the A380 Full Scale Fatigue Test in Dresden. The transport was completed successfully in October 2004.

Figure 2: Pump station (left, capacity 6000 l/min, hydraulic infrastructure) and section reloading from barges to trailers near Dresden motorway bridge (right)

2.4 A380-800 Rear End Test - Full-scale damage tolerance and static test

I. Buchweitz and H. Vogelsang (Airbus-D)

This abstract provides a concise overview on the purpose and the technical characteristics of the A380-800 Rear End Test. The Rear End Test is performed in the facilities of the Airbus Test laboratory located in Hamburg Finkenwerder.

Due to the specific requirements on testing CFRP materials the test consists of five successive phases:

1. Application of pre-first-flight critical limit load cases
2. Application post-first-flight limit load cases
3. Ultimate load campaign with the load cases from phases 1. and 2.
4. Damage tolerance cyclic loading program
5. Residual strength and margin research tests

The specimen consists of the aft fuselage sections S18.3 and S19, the vertical tailplane with lower and upper rudder, the Rear Pressure Bulkhead and for load introduction purposes a horizontal tail plane dummy and a tail cone dummy. 33 hydraulic actuators are attached to the specimen structure via whiffle trees in order to simulate aerodynamic- and inertial loads. Both rudders may be deflected to the portside and loaded under deflected conditions for Limit load applications. Furthermore, for justification of rudder functionality and clearance capabilities the rudders will be moved when subjected to Limit Load in the test. During damage tolerance cycling the test specimen will be subjected to a complex flight-by-flight sequence with an average of 176 loading points per flight. Three different fatigue missions, Short-, Medium- and Long Range are simulated. Test goal is 7600 flight cycles (1/3 Design service goal = 6333 cycles). The load is increased by factor 1.287 to cover future weight variants and to reduce testing time.

The damage tolerance loading program has been developed under consideration of the experiences from former full-scale fatigue testing and taking into account the requirements of CFRP structures.

- Global component load distributions will be reproduced in the test.
- CFRP testing requires simulation of non-truncated loads spectra.
- Ground steady loads (1g) are combined with incremental fatigue loads resulting from taxiing, rotation, landing impact and braking.
- Flight steady loads (1g) are combined with vertical and lateral gusts simulated as 'round-the-clock-gusts' and with vertical and lateral manoeuvres
- Loads from airbrakes extension during descent are considered in the sequence.
- 115 flight types are processed with different flight and ground load severities implied.

Start of the static test campaign Phase I was in January 2005. The damage tolerance cyclic loading phase is scheduled for the time period from May 2005 to September 2005. After the end of all test operations presumably in November 2005 and following inspections, tear down of the test installation is planned for March 2006.

This combined static and damage tolerance test will support the certification of the carbon fibre reinforced plastic (CFRP) structure of the aft fuselage and the VTP of A380-800 Commercial Transport Aircraft in compliance with the airworthiness regulations CS/FAR 25.571.

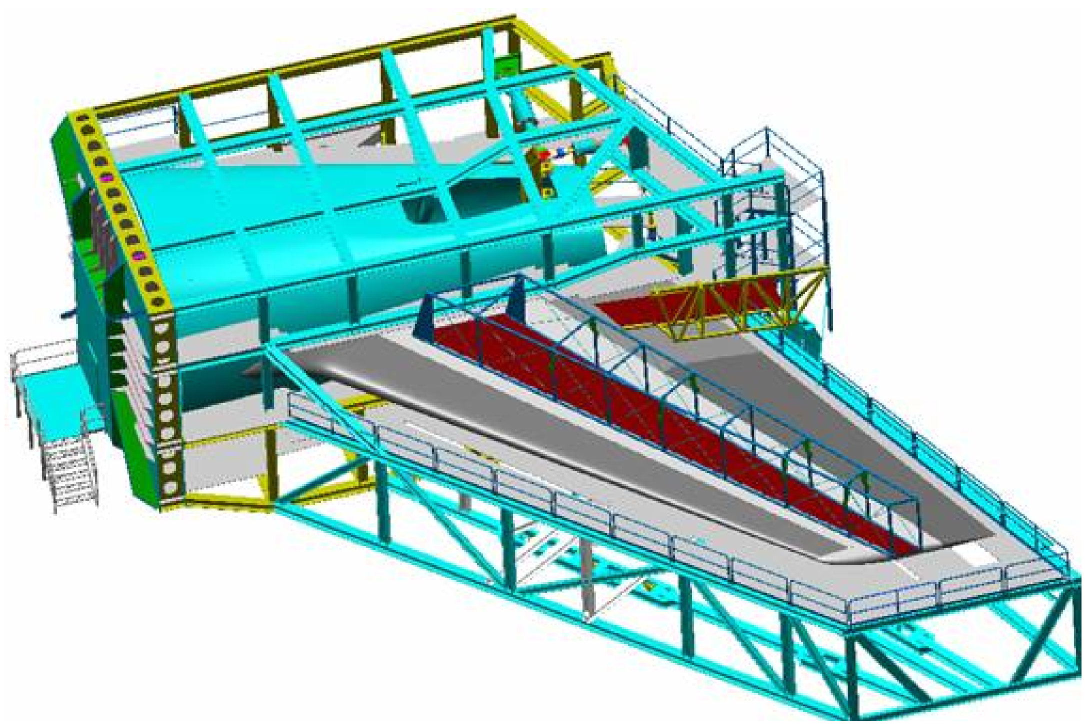

Figure 3: Rear End Test specimen installation

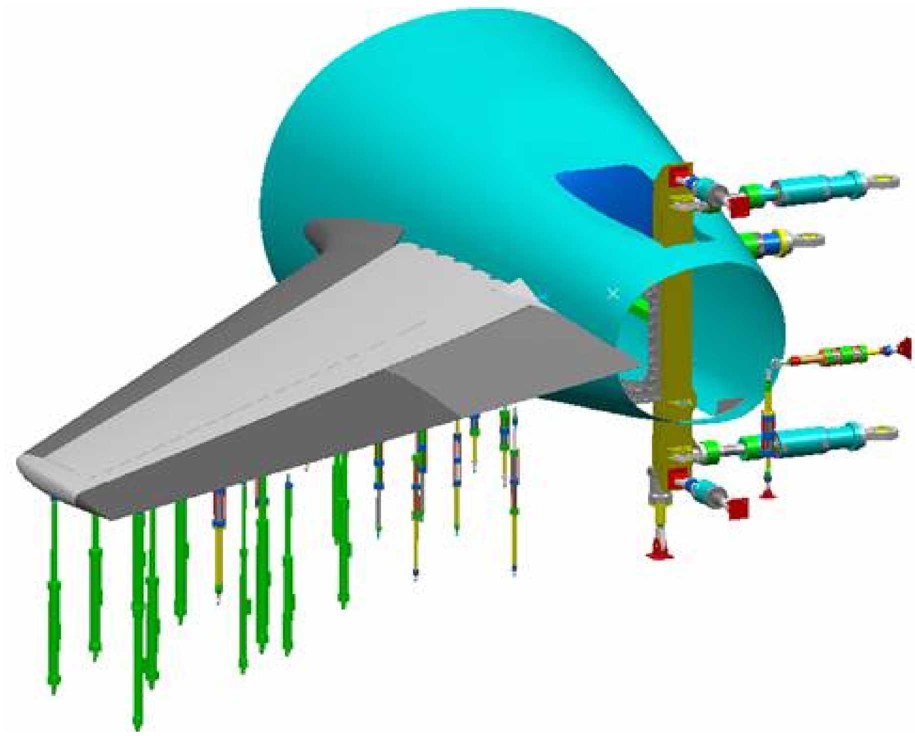

Figure 4: Rear End Test load introduction arrangement

2.5 A380 Spoiler Full-Scale Tests

U. Rüger and G. Hilfer (IABG)

Full-scale tests on two spoilers of the A380 are currently conducted at IABG, Ottobrunn, within the qualification program representative for all spoilers. The tests are made on behalf of Patria Aerostructures Oy who is responsible for design, analysis, testing, verification, manufacturing and product support of the A380 spoilers. The tests of the first spoiler started in August 2004 and the test of the other spoiler in February 2005. The completion of the entire test program is planned for the third quarter of 2006.

The spoilers chosen for testing are no. 1 and no. 4 of the left hand side. The testing of spoiler no. 1 is dedicated to the parts made of CFRP whereas the testing of spoiler no. 4 is dedicated to the metal parts. The test program contains several static test sequences up to LL and UL as well as a rupture test at the end of the complete campaign of each spoiler. Most of the static tests up to LL and UL are made at 80°C. By fatigue testing 1 DSG of 19000 flights has to be proven with a scatter factor 2,0 for spoiler no. 1 and a scatter factor 3,6 for spoiler no. 4.

When preparing the spoilers for testing strain gauges, thermocouples and attachments for displacement transducers were applied. Furthermore the introduction of artificial flaws incl. BVID and VID as well as a repeated ageing of spoiler no. 1 are part of the test program. The evolution of the artificial flaws as well as other flaw critical regions of the spoilers are monitored throughout the entire test program at several inspection stops incorporating visual and non destructive inspections.

An independent test set-up was developed for each of the spoilers. Each incorporates a restraint system with 12 struts allowing that all parts of the spoiler are supported in a statically determined way. A digital control and monitoring system allows simulation of the loading by means of up to 9 servo-hydraulic actuators in pull-push mode at each test set-up. The loads are distributed through whiffle trees or introduced at hinge fittings. A data acquisition unit records all loads, strains, displacements and temperatures during static tests.

Figure 5: A380 Spoiler full-scale test – test set-up of spoiler no. 1 ready for testing

2.6 A380 Inner Flap - Full Scale Fatigue Test

S. Schnack (Airbus-D)

This review presents the status of the A380 Inner Flap Fatigue Test. The test objective is the certification of the metal components of the inner flap and support structure.

The air load is introduced through hydraulic cylinders by means of a whiffle tree. In total 13 cylinders acting onto 50 locations are used to provide a realistic loading situation, Figure 6. At the connection to the center flap interface loads are introduced with a single cylinder. At track 1 the rear attachment is moved in order to simulate the wing deflection acting on the flap. The complete assembly is moved with the flap from retracted flap position (0°) to fully extended position (33°), Figure 7.

The loading program consists of a flight-by-flight sequence with ground cases, take off, cruise, approach, landing, breaking, taxiing and gusts. In total 50,000 flight cycles equivalent 2.5 times the design service goal will be conducted.

The test specimen is equipped with 250 strain gages, providing the information to validate the FEM analysis. Besides strain, crack growth is measured at various locations in order to validate the predictions and to proof the damage tolerant behavior of the structure. For the same reason a number of primary load paths will be disassembled to show the capabilities of the second load paths. Finally standard repairs will be installed. In order to gain maximal information on the test specimen an inspection program is defined.

Airbus and the A380 industrial partners have defined the details of the test set-up arrangement and the loading program as well as the potential test sites and will follow the test progress and collaborate on the test results.

The test specimen is delivered to Hamburg test site in March of 2005. The start of the fatigue test is planned for August of 2005. The completion of the test program is expected in 2007.

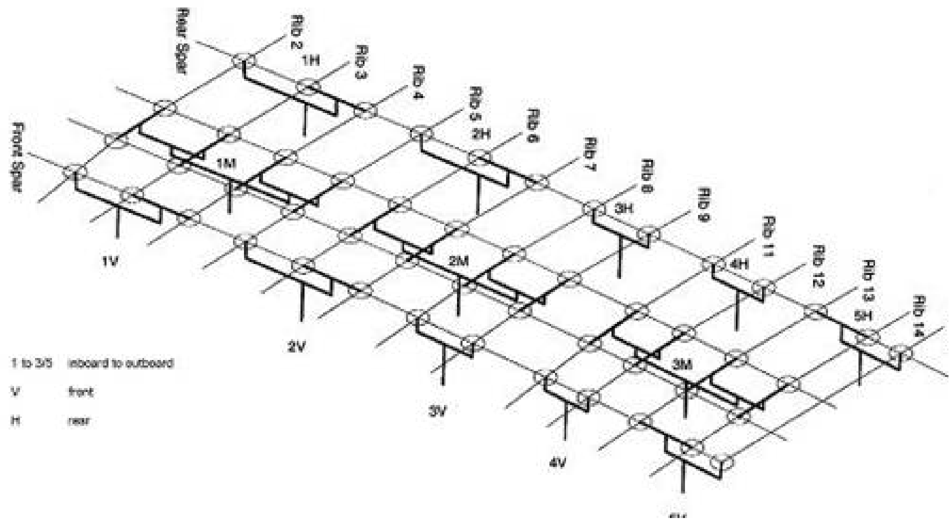

Figure 6: Air load cylinders.

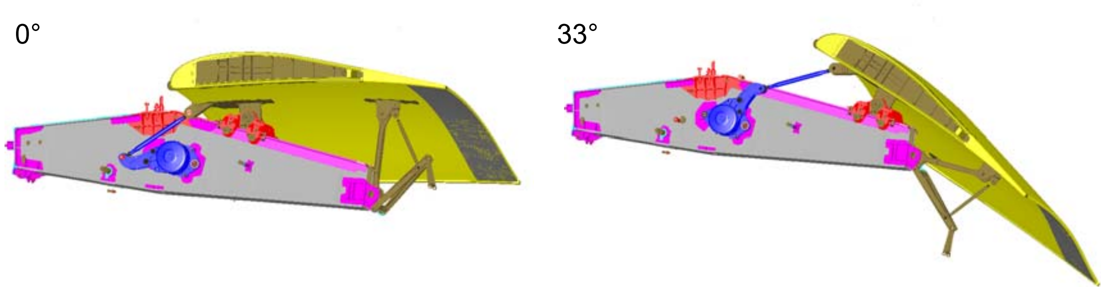

Figure 7: Inner flap movement (retracted/ extended).

2.7 A380 Flap Carriage No. 3 Crack Propagation Development Test

M. Semsch and T. Grafe (IMA)

A crack propagation test on the "A380 Flap Carriage No. 3" is carried out at IMA by order of Airbus Germany. The test contains the estimation of the crack growth under the influence of dynamic loading. Two hydraulic jacks apply the loads at one roller arm. Both jacks simulate the loads which are based on the reaction between carriage and Z-roller and side-roller respectively. The load sequence is a sine-wave with a constant amplitude and a load ratio of R = 0.1. Both loads act in-phase.

The test program contains the investigation of different crack scenarios, which were identified as critical. Therefore, artificial damages had been introduced in the carriage and were monitored during the test run.

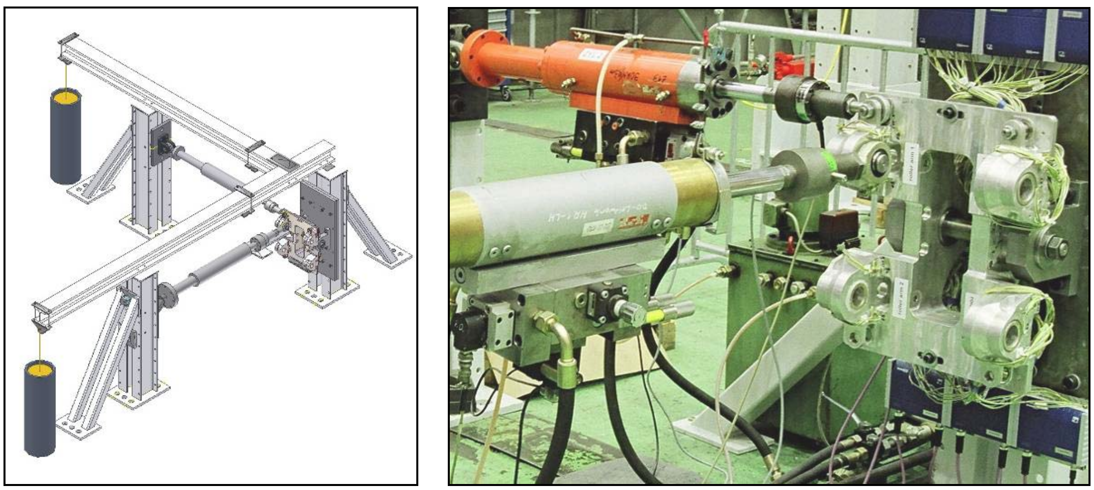

Figure 8: Flap carriage test rig (left) and flap carriage (right)

2.8 A380 Flap Track No. 6 Static and Fatigue Certification Test

M. Semsch and T. Grafe (IMA)

IMA GmbH Dresden carries out the "A380 flap track no.6 static and fatigue certification test". The test was ordered by Airbus Germany. The aim of the test is the experimental evidence of the static, fatigue and damage tolerance behaviour of the flap track. The test program includes the check of the static and fatigue performance of the manufacturing defects, damages and repair solutions.

A special test rig had been designed and made for the test. Ten hydraulic jacks apply all loads needed to simulate the real flight conditions. A load spectrum with real flight loads will be used for the fatigue test. The test concept includes the different positions of the flap and the duration of the fatigue and damage tolerance test phase is of 2.5 x DSG.

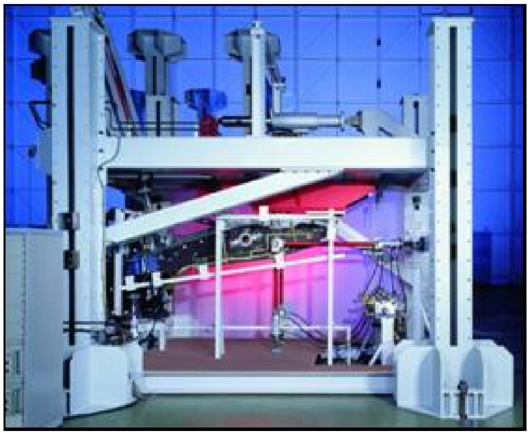

Figure 9: Test rig „A380 Flap Track No.6“

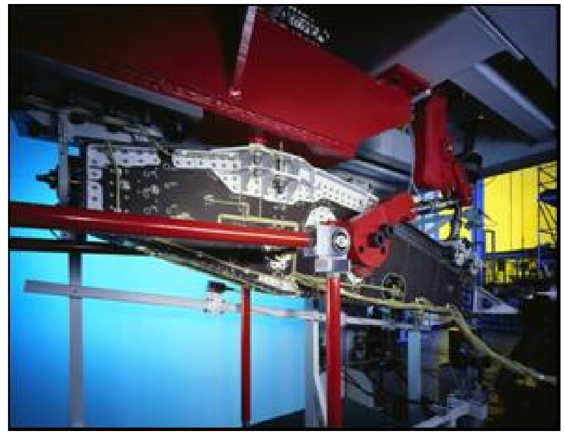

Figure 10: Detail of the loading system

2.9 A380 Component Tests on the Forward Engine Attachment Point

G. Hilfer and M. Hofstetter (IABG)

IABG is currently performing static and fatigue tests on full-scale test components of the A380 engine pylon forward attachment point (EPFA). For these tests, IABG was contracted by Airbus in March, 2004. Since then, a test set-up has been developed, built and equipped with hydraulics, control and measurement systems and testing has been started in September 2004 with one of two specimens on schedule. In April, 2005, the tests with the first specimen will be completed and the second specimen will be installed for testing until spring, 2006.

While the first EPFA specimen is dedicated to evaluate the stiffness properties and fatigue capabilities of the structure over several aircraft lives when compared to design values, the second specimen will focus on the damage propagation and damage tolerance behaviour of the component. With the first specimen several static tests have already been performed along the fatigue test program to evaluate changes in the stiffness properties. The loading program for the fatigue test consists of 12 different flight types which are grouped into a pre-defined sequence of 1000 flights. This sequence of 1000 flights is repeated thus making up the required number of aircraft lives to be simulated. The fatigue test is interrupted regularly to enable visual and non-destructive inspections of pre-defined areas. The first specimen showed an extraordinary good fatigue behaviour for which Airbus decided to anticipate the introduction of an artificial damage originally planned only for the second specimen.

The requirements for the tests with the second specimen will be refined based on the results achieved with the first specimen. Yet, it is clear that a residual strength test will be performed at the end of the test program.

The test set-up developed for the A380-EPFA tests has a basically self-contained load path design and was developed to sustain the fatigue loads of both specimens. The two actuators which load the specimen perpendicularly in Y and Z direction are attached to the EPFA by a load introduction device incorporating the original bearing used on the aircraft to suspend the engine at the forward attachment point of the engine pylon. A digital control system is used to run the test 24h/ day. During a static test a digital data acquisition system is appointed to record all load, strain and displacement sensors.

Figure 11: Test set-up for the A380 engine pylon forward attachment tests

2.10 Component Test Stop Fittings – Airbus A380-800 Passenger Doors

R. Best and T. Grafe (IMA)

IMA GmbH Dresden performed a fatigue test of stop fitting within the certification programme of the A380-800 passenger doors by order of Eurocopter Germany GmbH. Two different types of stop fittings had been tested to obtain S-N curves to verify the fatigue calculations.

During the test series big and medium-stops were tested dynamically. The load introduction in the specimen had been carried out centered to stop bolt axis. The applied load sequences describe a sine wave with constant amplitude and a ratio between lower and upper load of R=0,1 on several load levels. A residual strength test of big and medium-stop fittings was carried out after the applied dynamic testing.

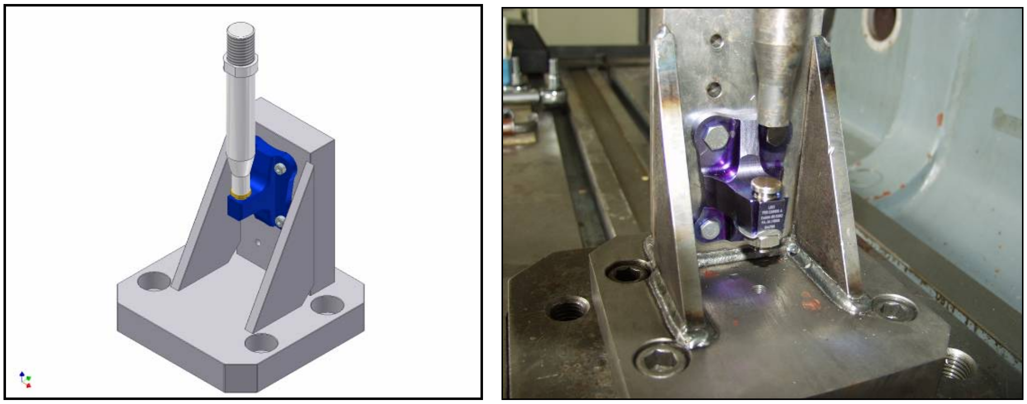

Figure 12: Stop Fittings test set-up.

2.11 Windmilling Test of an A380 Rotary Actuator

P. Frömmel, W. Fessenmayer and S. Lindner (IMA)

On behalf of Liebherr Aerospace Lindenberg GmbH, IMA Dresden performed the windmilling test of an A380 Geared Rotary Actuator Outboard.

A special test rig with an hydraulic actuator was adapted to the test requirements to simulate the final descend and approach phase (3 - 6 Hz) and the cruise phase (6-15 Hz) - with the required large amplitudes. The piston rod of the actuator was connected to the specimen by means of a stiff clamping device designed and built by IMA GmbH Dresden. Two types of clamping devices were used, one for the tests in z- and x-direction, Figure 13 left, and another one for the y-direction, Figure 13 right.

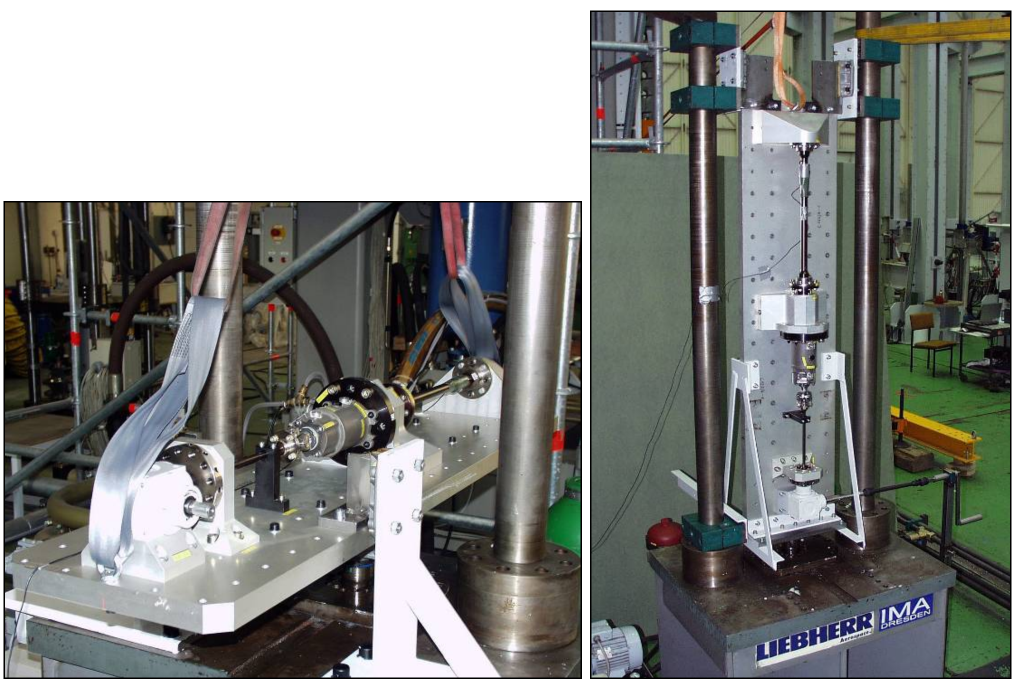

Figure 13: Test set-up for windmilling in direction z and x (left) and y (right)

2.12 A400M - Full Scale Fatigue Test

S. Berssin (Airbus-D)

This review provides the actual status of the preparation work for the A400M Major Fatigue Test (MFT). This test will be performed to support the civil and military certification of the A400M.

The A400M MFT will be a complete aircraft test, including the complete fuselage, the wings and a Vertical Tailplane for load introduction purpose. The objective of this test is to justify the metallic components of the A400M – the justification of the composite primary structure (like i.e. the wing covers) will be done by other tests.

The test specimen will be loaded by approximately 100 active hydraulic jacks, which will simulate the airloads and the inertia loads which act on the aircraft. It is intended to perform the test for a minimum of 25.000 flight simulations, which would be equivalent to 2,5* Design Service Goal.

The loading program for the A400M MFT will consist of a complex flight-by-flight sequence, which considers approx 350 load events (like gust, ground bump etc) per flight. The different possible usages of the aircraft will be reflected by 4 different missions, which describe tactical usages, training flights and logistic missions. Additionally, special events like Air-to-Air refueling maneuvers and aerial delivery conditions will be simulated.

The test specimen will be equipped with 4000 strain gauges which will provide strain and stress information for several load cases in order to validate the FEM analysis. Additionally, crack growth measurements will be performed on artificial damages to validate the predications and to demonstrate the damage tolerance capabilities of the airframe. The test specimen will also be subjected to an intensive inspection program, which should help to gain maximum knowledge out of the structure test.

Airbus and the A400M industrial partners are currently jointly defining the details of the test set-up arrangement and the loading program. In parallel, investigations about potential test sites are ongoing.

The detailed test design work will start in 2006. The test specimen will be delivered in the first half of 2008, the start of the fatigue test is envisaged for the first quarter of 2009. The test program will be completed before end 2010.

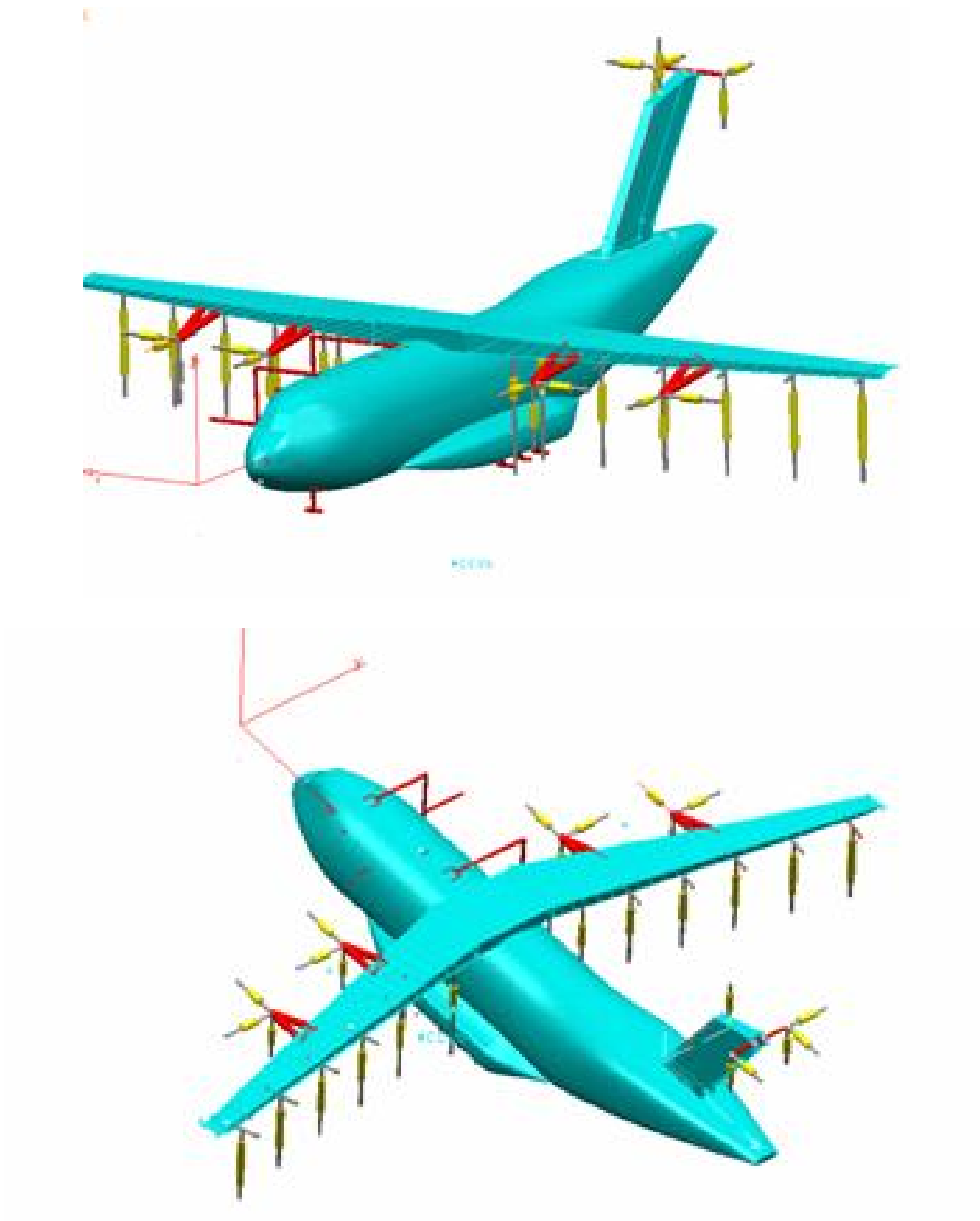

Figure 14: A400M Full Scale Test set-up overview.

3 Loads

3.1 The Effect of Steep Approach Landing Procedure on Landing Gear Loads

H. Huth and R. Brunbauer (AvCraft)

In the course of certification of the Dornier Do 328 Jet, Figure 15, for steep approach landings, e. g. at the London City Airport, fatigue ground loads had to be reviewed. The effect of new landing procedures on sinking speeds and/or main landing gear loads at spin-up und spring-back, had to be investigated.

The landing parts of the data collected during the operational load recording program DOLORES, performed with several Do 328-100 aircraft, as reported at the ICAF Symposium 1999 [1], were evaluated in more detail. The results of this comparative evaluation of 3199 landings after normal and 401 after steep approaches are plotted in Figure 16. There the Δn_z -spectra for 1000 landings are given, it could be concluded, that the landing procedure had no significant effect on landing loads. For comparison, the assumed landing load spectrum used for test and analysis is also shown. This spectrum proved to be conservative. It is derived from the ground loads during spin-up and spring-back at different sinking speeds, using the applicable sinking speed spectrum.

Figure 15: Dornier Do 328 Jet in flight

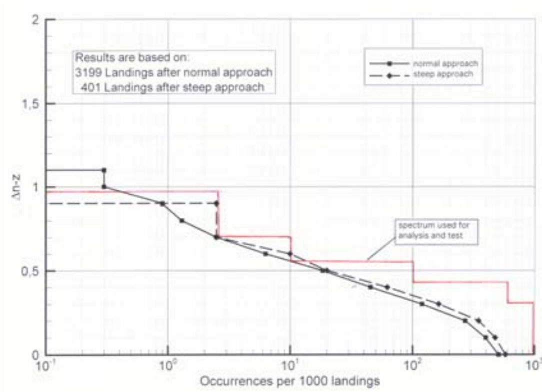

Figure 16: Comparison of measured landing load Δn_z -spectra for normal and steep approach landings

[1] Huth, H.; Mattheij, P.; Müller, M.; Peter, O.: Ableitung von Spannungsintensitätsfaktoren für Betriebsfestigkeitsnachweise von komplexen Flugzeugstrukturen. In DVM-Bericht 131 „Leichtbau und Betriebsfestigkeit“, München 2004, pp. 89-100

4 Fatigue and Fracture of Fuselage Panels and Joints

4.1 Fatigue and Damage Tolerance Test of A380 Fuselage Panels

M. Semsch and A. Kaiser (IMA)

IMA GmbH Dresden performed a fatigue and damage tolerance test of A380 fuselage panels by order of Airbus Germany. The tested panels represent upper shells of section 13 and 18 respectively. The fatigue and damage tolerance behaviour of the fuselage structure were proved within the scope of A380 certification. Therefore, the fuselage panels were loaded by

- Internal pressure
- Longitudinal tension loads
- Active frame loading

This test configuration complies with real flight condition. The applied load spectrum was correspondent to the flight-by-flight-program of the A380 for upper fuselage panels. The complete fatigue life testing program covers a span of 2.5 times of the Design Service Goal. Manufacture defects and repair solutions like

- Dents in skin
- Frame couplings
- Riveted doubler
- Scratches on skin

were included in the test program. After testing a tear-down-inspection was performed by Airbus Germany.

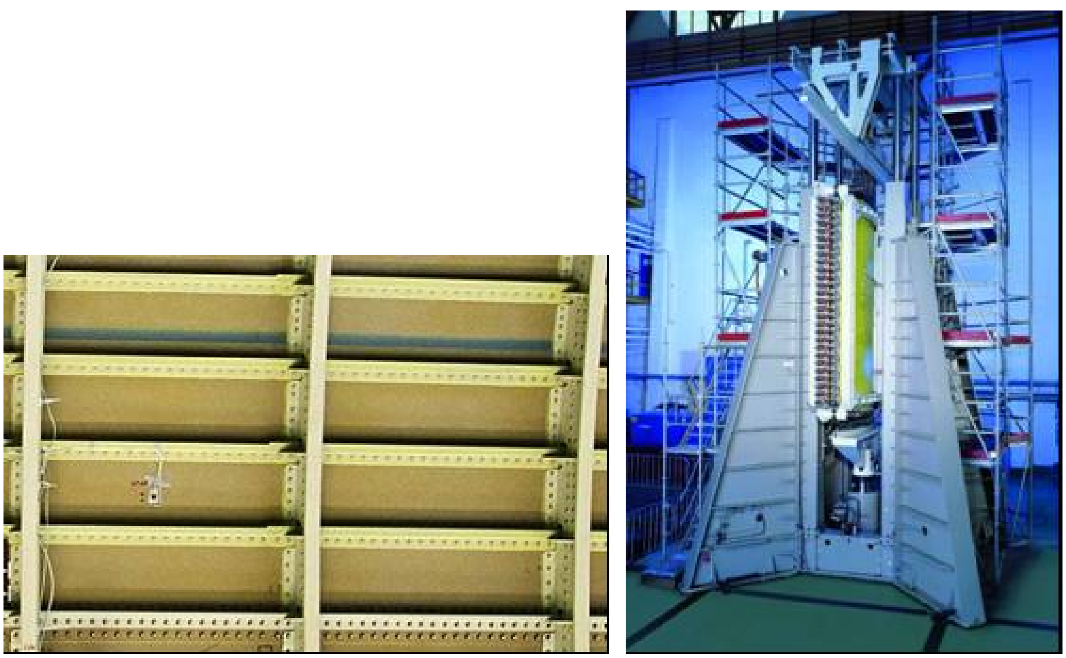

Figure 17: Test structure (left) and IMA curved fuselage panel test facility (right)

4.2 HSS GLARE® in the Airbus A380

T. Beumler and B. Borgonje (Airbus-D)

GLARE® is a Fiber Metal Laminate (FML) built up of thin aluminum sheets bonded together with glass fiber-epoxy layers. The laminate provides excellent damage tolerance characteristics and offers additional weight and safety benefits when used as skin material on aircraft. For the Airbus A380 it is applied on a large part of the upper fuselage.

HSS (High Static Strength) GLARE® has been developed as a member of the FML family with increased static properties compared with the first variant (called "Standard GLARE®"). This has been achieved by using a 7475-T761 aluminum foils instead of 2024-T3. The main improvements are found in shear properties and yield strength. Because of the high fatigue allowables for GLARE®, large parts of the A380 fuselage are statically dimensioned. For these panels, additional weight saving opportunities are provided by HSS GLARE®.

Tests have been performed, ranging from coupon tests with monolithic Al 7475-T761 specimens up to a full-scale test of a large HSS GLARE® stiffened shell. Emphasis is put on the behavior of HSS GLARE® in mechanically fastened joints. Additional tests with joint coupons of monolithic Al 7475-T761 are performed in order to establish a reference database for HSS GLARE® calculations. Shear tests have been performed by Airbus, indicating superior compression/shear behavior of HSS GLARE® compared with Standard GLARE®.

A large A380 fuselage shell has been tested at IMA in Dresden, consisting of 7 frames and 11 stringers, Figure 18. The shell includes a longitudinal joint, two longitudinal splices, a riveted aluminum doubler repair and several artificial damages. Applied was an A380 flight spectrum in longitudinal direction with internal pressure, for up to 2.5 times the A380 Design Service Goal. The test has been continued until crack initiation (defined at a = 1 mm) was reported for the lap joint and under the repair patch; the crack propagation phase has not been considered for these areas.

Figure 18: HSS GLARE® fuselage shell tested at IMA Dresden.

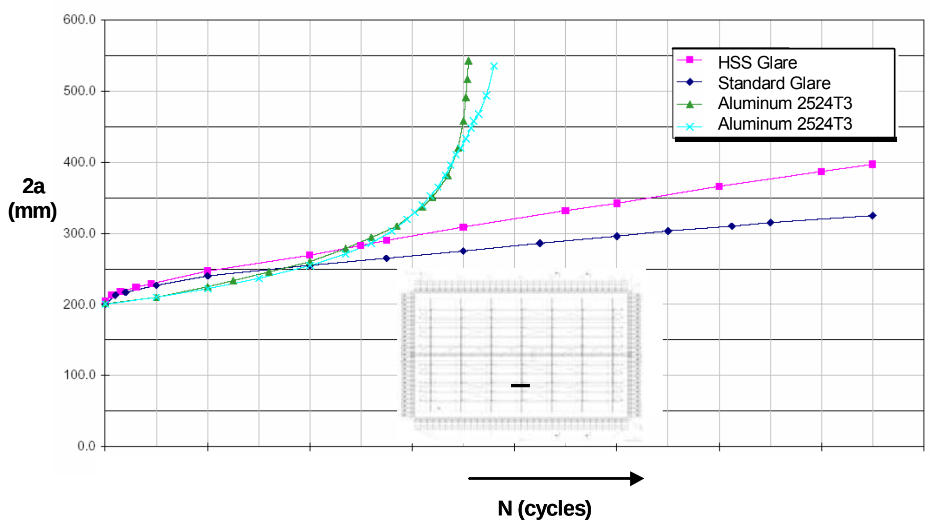

Figure 19: Comparison of crack propagation of a longitudinal crack over a broken frame in different skin materials

A parallel crack propagation test with the shell showed a minor increase of the crack propagation rate compared to Standard GLARE®, Figure 19, but still significantly lower than in monolithic Al 2524. Large damage capability was proven at 1.15 times Δp for a two-bay-crack over a broken frame.

Static testing of cutouts of the lap joint and the repair area showed comfortable residual strength, covering the 2Δp static load case. A teardown inspection did not indicate any critical damages in the backup structure, including at the locations where artificial damages were present.

The qualification program of HSS GLARE®, performed by Stork and NLR in the Netherlands, is in its final stages. Application of HSS GLARE® will commence with the freighter version of the A380.

4.3 Panel Tests – Landing Gear Bay / Frame22 Orbital Junction

M. Semsch and T. Grafe (IMA)

IMA GmbH Dresden performed a fatigue and damage tolerance test of 2 large flat panels by order of Airbus France. One of both panels represents the landing gear bay top panel of the A380. The other panel represents the structure near the orbital junction of frame 22 and stringer 24 of A380.

Both panels were tested dynamically. The applied load sequence describes a sine wave with constant amplitude and ratio between lower and upper load of R = 0.1. A certain number of load cycles were applied during the fatigue test. Artificial damages were introduced in the panels and the crack growth was monitored during cycling. After the end of the test campaign a residual strength test of each panel was carried out. The load was increased until rupture during the residual strength test.

Figure 20: Landing gear bay panel

Figure 21: Frame 22 orbital junction

4.4 Static and Dynamic Testing of CFRP Curved Fuselage Panels

R. Best and M. Sachse (IMA)

IMA GmbH Dresden developed and now operates 2 special test rigs for curved fuselage panels. Test parameters, such as loads or possible specimen strains, are specifically arranged to meet the requirements of CFRP panels. Nevertheless, panels made of metallic material may be tested, too. A third test rig being able to test panels of the whole fuselage cross section has been introduced into service, recently. Minor geometric changes of the panel, i.e. change of frame pitch, are possible at every test rig.

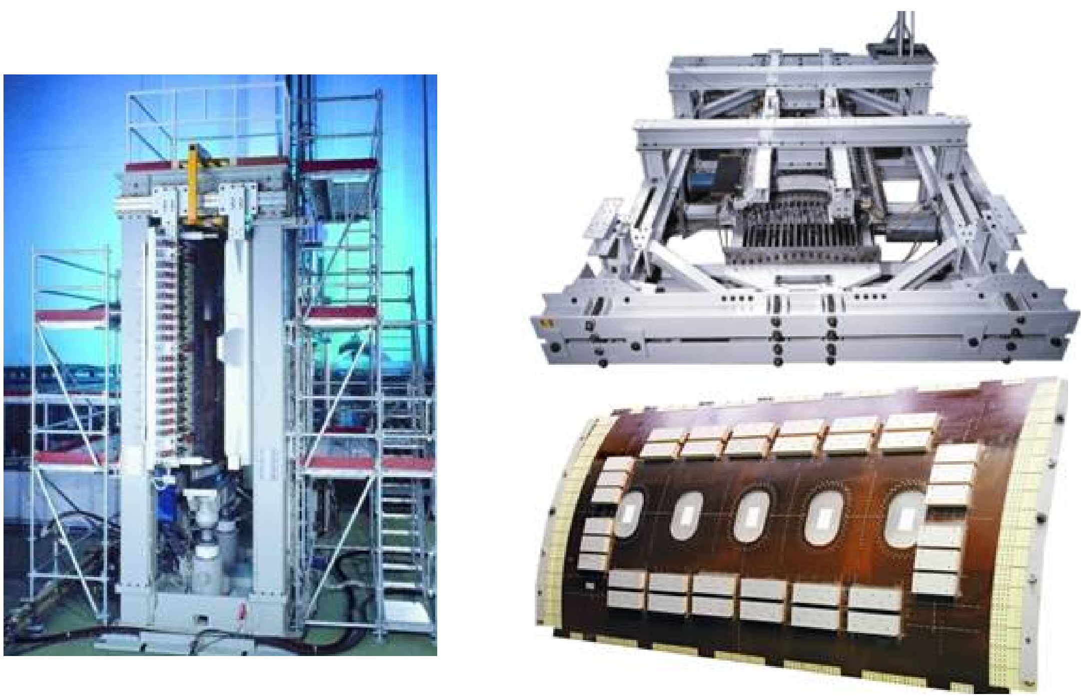

Figure 22: Curved fuselage panels test set-ups at IMA in Dresden

Specimens were loaded both with internal pressure and corresponding circumferential loads as well as

- longitudinal tension and shear
- longitudinal compression

Comparisons with FE calculations showed a good test performance.

4.5 Fatigue and damage tolerance properties of structures stiffened with bonded stringers

T. Beumler and B. Borgonje (Airbus-D)

In the past years tests on stiffened shells performed at Airbus clearly pointed out that the fatigue and damage tolerance properties of a structure can be increased by means of bonding the stringers instead of riveting them.

Bonding stringers results in an increased crack stopping efficiency of the stringer foot, in a better stress redistribution between skin and stringer and, naturally, in fewer notches in the structure. While the latter is of great advantage for fatigue (limiting the fatigue critical areas only to the few positions where a hole is drilled in the structure, i.e. coupling areas), for residual strength and fatigue crack growth, the major advantage is the better crack stopping capability of the stringer foot. In this case the stress intensity factor at the crack tip decreases dramatically as the crack reaches the stringer and continues growing under it.

The above-mentioned effect is amplified when an intrinsically bonded skin material, such as GLARE®, is used. This material consists of thin aluminium sheets bonded together in a sandwich with glass fibre-epoxy layers, so that the fibres act as bonded crack stoppers themselves. The crack bridging ability of GLARE® results in fatigue crack growth rates in an order of magnitude of few microns per cycle. This, combined with the crack stopping effect of the stringers, results in a practically not growing crack for crack lengths of about half the stringer pitch.

The residual strength of stiffened shells with bonded stringers starting from a two-bay long crack over a broken stringer increases from 10 to 15% compared to the corresponding riveted structure. Moreover, when using high fracture toughness skin materials (i.e. 2524 aluminium alloy or GLARE®), it is always the stringer that fails. This fact suggests that an efficient way of increasing the residual strength of an aircraft structure in the presence of circumferential cracks is to use high strength materials for the stringers. Tests performed with both, 2xxx and 7xxx aluminium alloy stringers and with GLARE® stringers, demonstrate that there is a relation between the ultimate tensile strength of the stringer material and the residual strength of the structure. For example, GLARE® stringers have 40% higher ultimate strength compared to high strength 7xxx stringers that results in a residual strength increase greater than 10%. GLARE® stringers have also the advantage of a 9% smaller specific weight.

Regarding skin materials, GLARE® allows a very long stable crack extension during residual strength tests. In fact, a three stringers pitch long crack in a GLARE® skin under broken stringer remains stable, Figure 23a. Even after the failure of the two neighbouring stringers, the crack does not become unstable, Figure 23b.

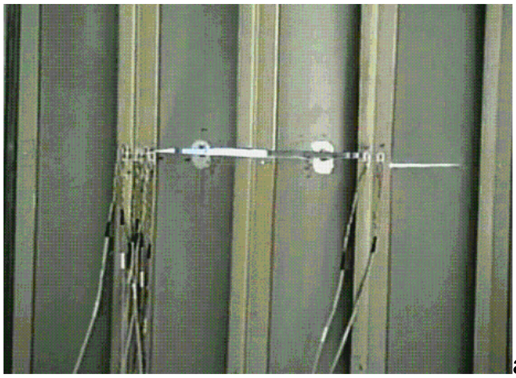

a)

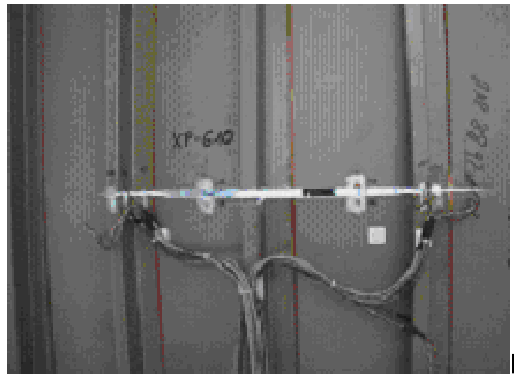
b)

Figure 23: Example of three stringers pitch long stable crack in GLARE® skins:
a) GLARE® skin with GLARE® stringers.
b) GLARE® skin with 2024 Al stringers.

Bonded stringers have also other advantages with respect to riveted stringers like modest structural weight reduction and improved shear-compression behaviour, among others. In the near future, when autoclave-free bonding processes will be available, a significant drop in both recurring and non-recurring cost will make this technology even more attractive.

4.6 Fatigue properties of metal laminates

E. Hombergsmeier (EADS-CRC) and A. Vichniakov (Airbus-D)

Metal Laminates (ML), Figure 24, as an improvement of conventional adhesive bonded panels with monolithic sheets were designed at Airbus Hamburg and investigated at EADS Corporate Research Center, Germany to asses their possible weight saving potential. Flat 7-stringer-panels were manufactured from different configurations of Metal Laminates at Airbus Nordenham and EADS. The panels were tested concerning their crack growth behaviour, Figure 25, and residual strength. Two lay-ups of the ML, the versions with relatively thick (1.2 mm) doublers below and between the stringers or application of glass fibre layers below the doublers shows significantly better damage tolerance properties as than the panels with monolithic skin. The lifetime within the “4-bay-area” of the best configuration was about 100 % higher and the reinforced configuration was about 38 % higher compared to the panels with monolithic skin and delivered a weight saving potential of 10 % and 15 % (weight of the fibres and adhesive neglected).

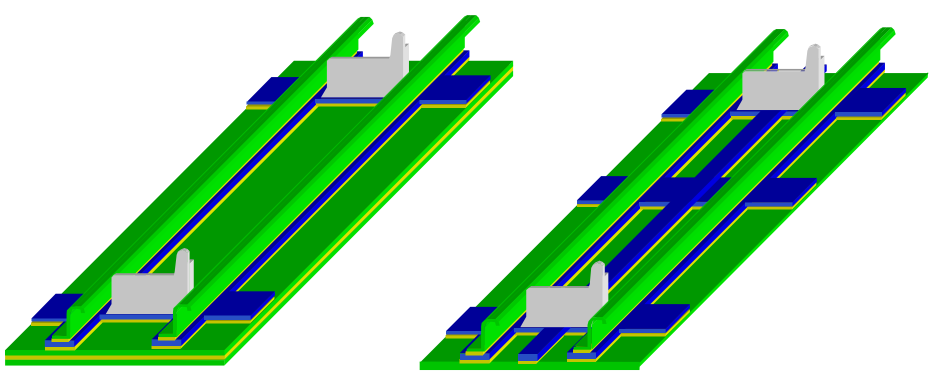

Figure 24: Examples of bonded and laminated fuselage structures.

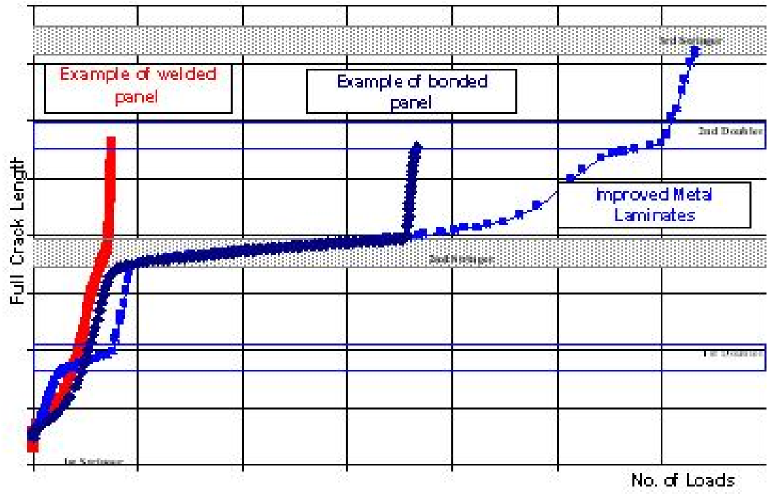

Figure 25: Crack propagation in stiffened panels of metal laminates compared to standard welded and bonded configurations.

4.7 Influence of Rivet Type and Material on Fatigue Behaviour of Fuselage Lap Joints

H. Huth (AvCraft) and O. Peter (LBF)

Comparative constant amplitude fatigue tests were performed to investigate the influence of rivet types and materials. The test specimens used represent a longitudinal fuselage lap joint, details are given in Figure 26 and in the subsequent table. The joint design of Type A is valid for the Do 328 fuselage, Type B specimens represent the 728 design. Aims of the investigation were:

- to qualify a second supplier of the 2017A solid rivets with reduced heads (Dornier Standard)
- to show the effect of using 7050-rivets (NAS 1097), which the production wanted to use instead, as they require no heat treatment
- to supply fatigue data for alternate rivet types such as Lockbolts or Briles.

The test specimens, using 2024 T351 sheet material chemically milled on one side, were manufactured in the production facilities of Fairchild-Dornier. The fatigue tests were performed at the LBF, Darmstadt. The test results, in form of S/N-curves, are given on Figure 27 and Figure 28. It must be noted, that net stresses are used.

The results in Figure 27 clearly show the detrimental effect of using 7050 rivets instead of heat treated 2017A rivets.

Furthermore, an effect of the rivet supplier for the DON 299 rivets could not be found. This is also valid for the results of specimen Type B, shown on Figure 28. Here, the expected better behaviour of the Ti-Lockbolts is seen. The S/N-curve of the Al-Lockbolts is slightly, and of the one for Briles rivets is distinctly below those of the normal Dornier rivets.

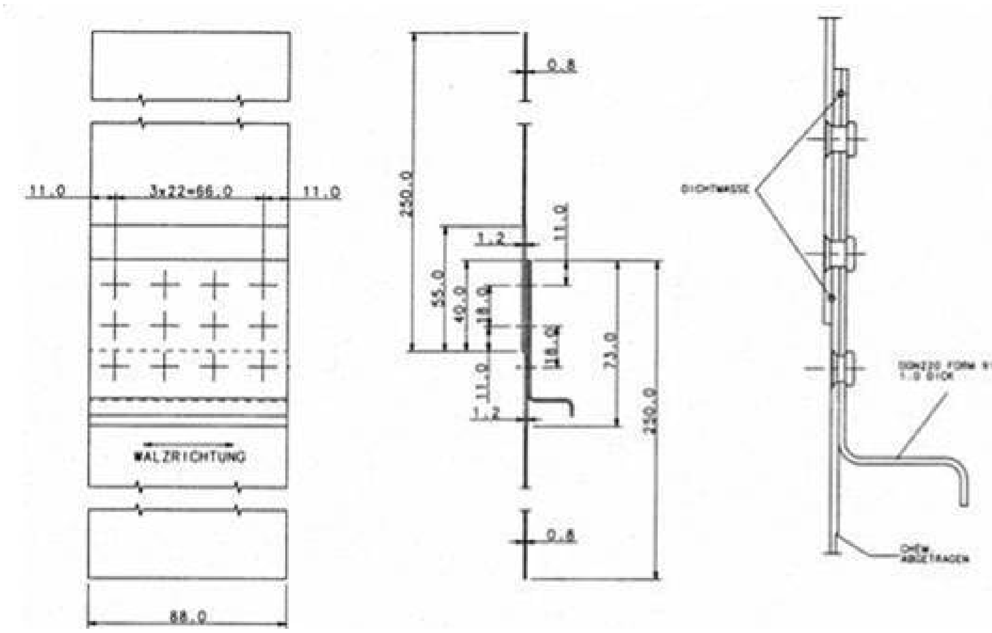

Figure 26: Single shear lap joint fatigue specimen (Geometries given are valid for Type A-1 to A-3)

Specimen	Thickness (mm)		Rivet pitch (mm)		Diam.	Fastener			
Type	s_1	s_2	t_1	t_2	(mm)	Type	Spec.	Material	Remarks
A-1	0.8	1.2	22	18	4.0	Solid rivet	DON 299	2017A T31	from SMI
A-2	0.8	1.2	22	18	4.0	Solid rivet	DON 299	2017A T31	from AHG
A-3	0.8	1.2	22	18	4.0	Solid rivet	NAS 1097 KE	7050 T73	
B-1	1.2	1.6	24	20	4.0	Solid rivet	DON 299	2017A T31	from SMI
B-2	1.2	1.6	24	20	4.0	Solid rivet	DON 299	2017A T31	from AHG
B-3	1.2	1.6	24	20	4.0	Briles	BRFZ5D	2017 T4	
B-4	1.2	1.6	24	20	4.2	Lockbolt	LGPL2S-V	Ti-6Al-4V	
B-5	1.2	1.6	24	20	4.2	Lockbolt	HLGPL2S-EB	7050	

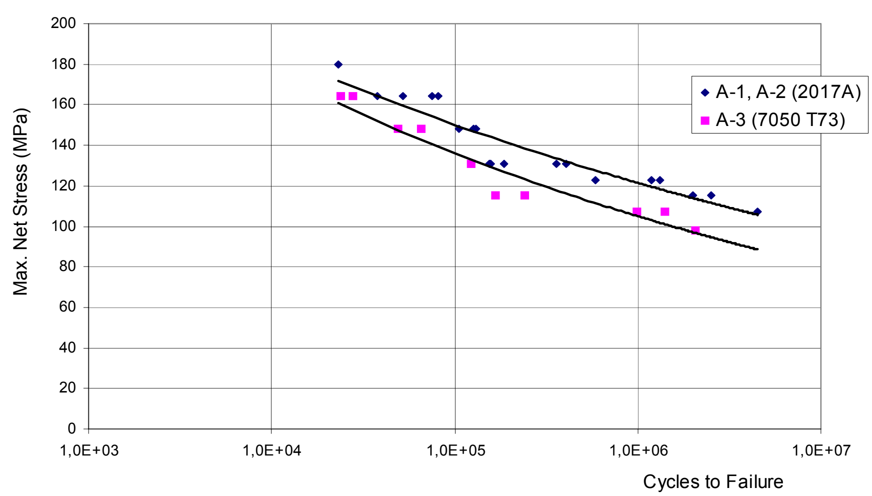

Figure 27: Results of the fatigue tests with specimens of Type A

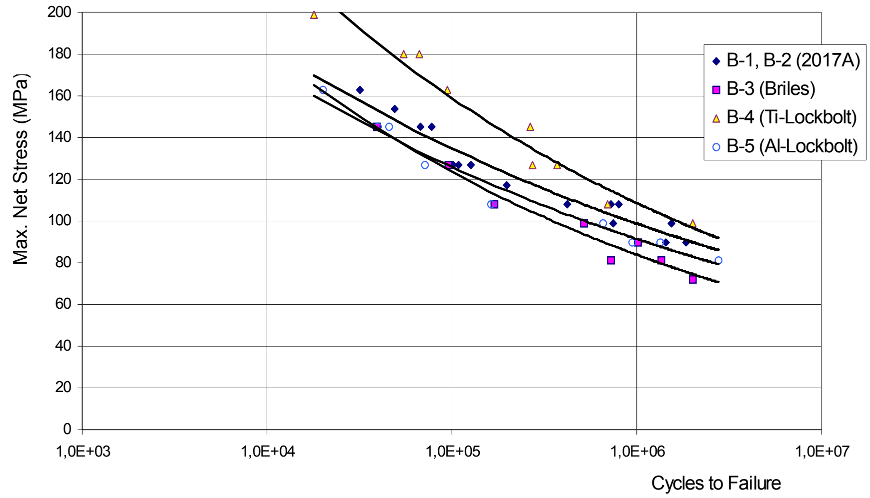

Figure 28: Results of the fatigue test with specimens of Type B

Figure 29: Example of failure mode, specimen type A-1

Concerning the failure locations, it must be pointed out, that except for two specimens of series B-5, all fatigue cracks started in the first rivet row of the external sheet where load transfer is highest, as shown on Figure 29. Thus good inspectability from outside is granted.

4.8 Derivation of Stress Intensity Factors for the Application of the Initial Flaw Concept

H. Huth (AvCraft) and O. Peter (LBF)

In order to gain experience with the application of the so-called initial flaw concept, some basic analytical and experimental investigations were performed. For the fatigue crack growth tests the following test specimens were defined:

Type I	Flat tensile specimens, 120 mm wide and 3 mm thick Edge crack specimens to derive crack growth data of the material
Type II	as Type I, with open and closed holes close to the edge, with 1.5 mm corner cracks
Type III	Double-tee-profiles loaded in 3-point bending, with 1.5 mm crack at edge or open hole

Type IV C-profiles connected by skin plates, loaded in bending, cracks at open and closed holes

Type V Component specimen, simulating a spar-rib connection, with several initial flaws (1.5 mm)

All specimens were milled out of 7475 T7351 plate material (50 mm thick). The crack growth tests and evaluations were performed at the LBF, Darmstadt (see Figure 30); the analytical work was done by former Fairchild-Dornier colleagues.

In addition to the crack growth tests, experimental and FEM-stress analyses was performed for specimens of Type III, IV and V.

By comparing experimental and analytically derived crack growth curves, stress intensity factor solutions could be verified and corrected, especially for the short crack regime. It turned out that for some applications (e.g. open holes) the existing solutions worked well, as long as the global stress distribution was considered correctly. For the more complex specimens with joints and fasteners, predictions were not very good, as load transfer by friction has a big influence on short crack growth behaviour. An example of the test results is shown on Figure 31, where the effect fastener clamping can also be seen. Although equally loaded, cracks at closed hole did not start to propagate.

Figure 30: Test set-up for test specimen type V (3-point bending)

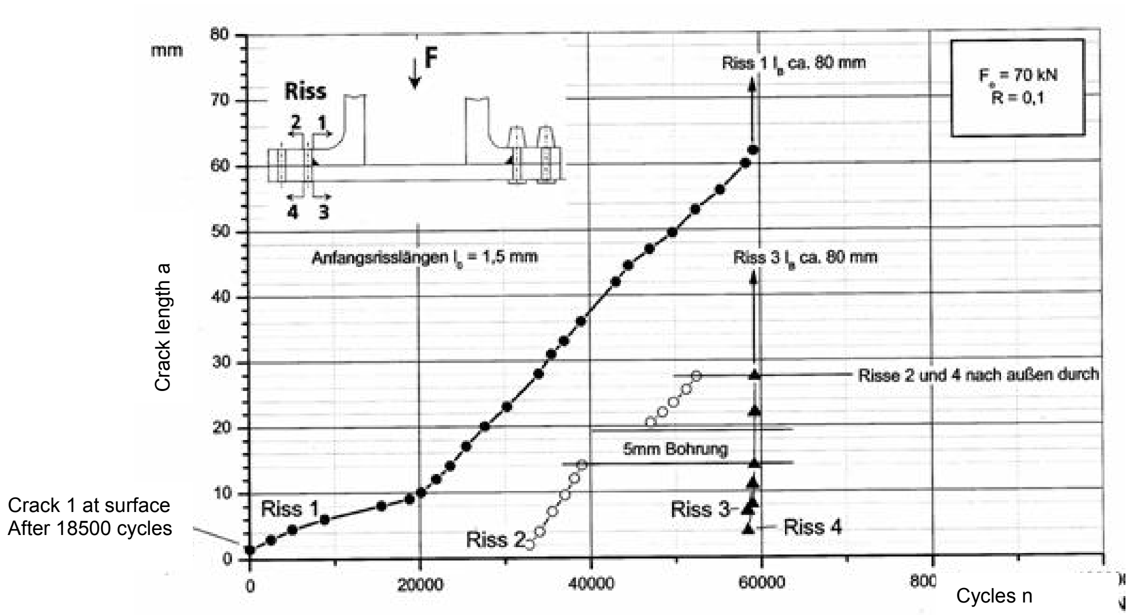

Figure 31: Results of the crack growth tests with specimen type IV

[1] Huth, H.; Mattheij, P.; Müller, M.; Peter, O.: Ableitung von Spannungsintensitätsfaktoren für Betriebsfestigkeitsnachweise von komplexen Flugzeugstrukturen. In DVM-Bericht 131 „Leichtbau und Betriebsfestigkeit“, München 2004, pp. 89-100

4.9 Fuselage Skin Repair Coupon Test

A. Pramono (Airbus-D)

In frame of the Improve and Asses Repair Capability of Aircraft Structures (IARCAS) research project, a test programme has been carried out to investigate fatigue and damage tolerance characteristics of several fuselage skin repair solutions. The objective is to show that a significant fatigue life improvement can be obtained with the proposed repair solutions. More than 180 coupons of butt-joint with increased skin plate separation type of specimen were manufactured and tested. The joint were riveted or bonded. The materials used were Al 2024 T3 for the skin and the doublers were either Al 2024 T3 or Glare®. Further details regarding the additional processes, type of fasteners, repair configurations, and bonding procedures of the riveted and bonded repair solutions investigated are listed below.

1. Baseline: 3 row countersunk rivets
2. Riveted Solutions:
   - Flap peening on the skin at the outer rivet rows
   - Hi-lok and Hi-lite with interference fit
   - Cold working in combination with interference fit
   - Increased doubler thickness
   - Additional 4th rivet row
   - Support doubler
   - Extended support doubler with additional special rivet solution
3. Bonded Solutions : cold and hot bonded

Based on the test results, the flap peened, the support doubler and the extended support doubler with 1 additional rivet row repair solutions of the riveted joint solutions were selected for further fatigue test investigation utilizing small and large flat test panels. Beside the life improvement, the selection was based on the relatively simple additional processes and repair configuration that were required for these repair solutions. Some of the coupon test results and an illustration of the baseline specimen used for the test are shown below in Figure 32. Significant fatigue life improvements were found.

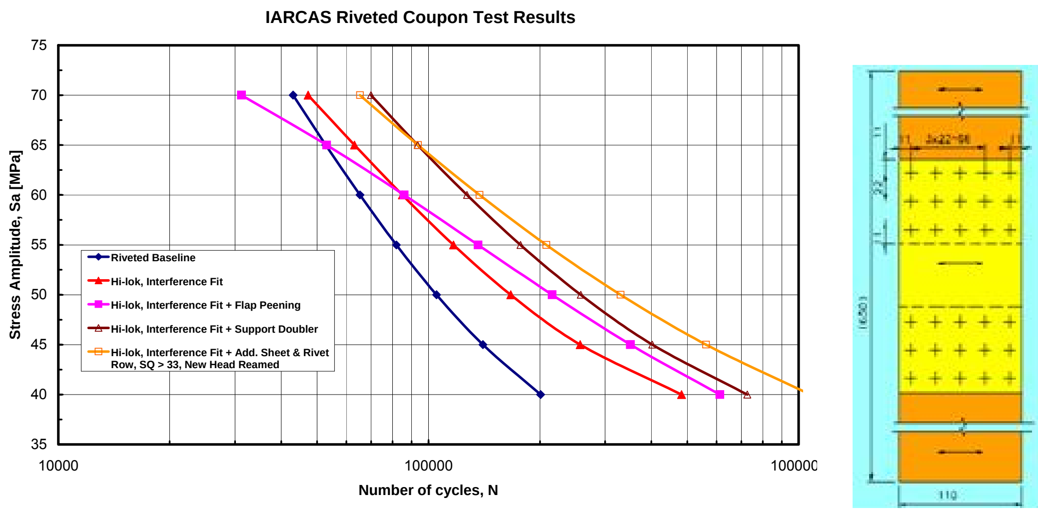

Figure 32: Coupon Test Result and Test Specimen

4.10 Equivalent Stress Concentration Factor

L. G. Gelimson (RUAG)

For predicting fatigue and fracture of fuselage panels and joints [1-3], it is very important to properly take the maximum stresses σ_{max} most dangerous into account. They are usually determined due to the nominal ones σ_{nom} via the common stress concentration factor [4]

$$C = \sigma_{max}/\sigma_{nom}$$

implicitly based on one chosen positive component of a 3-dimentional stress state. But individual stresses can be zero or negative, which naturally brings ambiguity to defining the maximum stresses (either by algebraic values or by moduli, i.e. absolute values). There are different choices of individual stresses in a non-uniaxial stress state. The roles of the chosen individual stresses in complex stress states at different places with maximal and conditionally nominal stresses can be very distinct, which can lead to great errors in determining the stress concentration factor. No individual stress alone can evaluate the danger of a complex stress state. Straightforwardly correcting the known definition leads to the necessity to consider many different cases caused by the number of the individual stresses, their signs and relations.

The *equivalent* stress concentration factor [5,6] (as σ_{enom} approaches its real value)

$$C_e = \lim \sigma_{emax}/\sigma_{enom}$$

is introduced to properly determine the maximum *equivalent*[4] stress σ_{emax} via the nominal *equivalent* stress σ_{enom}. The above limit drops by nonzero σ_{enom}. This definition holds in the general case of a complex stress state with different individual components having any signs independently from the relations between the algebraic values of these components. The roles of individual stresses at different places of a machine part are completely taken into account. The equivalent stress much more adequately evaluates the danger of a complex stress state than any individual stress does. It is not necessary to consider many different cases caused by the number of the individual stresses, their signs, and the relations between these stresses.

For the maximum stress concentrations at round holes, a design scheme is a plate infinite in the both directions and having a finite (i.e., infinitely small in comparison with the both plate dimensions besides the thickness) circular hole under two-directional uniform loading with generally unequal stresses σ_x and σ_y in the infinity [7]:

$$\sigma_{emax} = \max\{|3\sigma_x - \sigma_y|, |3\sigma_y - \sigma_x|\},$$
$$\sigma_{enom} = \max\{|\sigma_x|, |\sigma_y|, |\sigma_y - \sigma_x|\},$$
$$C_e = \lim \sigma_{max} /\sigma_{nom} = \lim \max\{|3\sigma_x - \sigma_y|, |3\sigma_y - \sigma_x|\}/ \max\{|\sigma_x|, |\sigma_y|, |\sigma_y - \sigma_x|\}$$

as $\max\{|\sigma_x|, |\sigma_y|, |\sigma_y - \sigma_x|\}$ approaches its real value (which can also vanish) by the strength criterion of the maximum shear stress [4] and

$$\sigma_{emax} = \max\{|3\sigma_x - \sigma_y|, |3\sigma_y - \sigma_x|\},$$
$$\sigma_{enom} = \{[\sigma_x^2 + \sigma_y^2 + (\sigma_y - \sigma_x)^2]/2\}^{1/2} = (\sigma_x^2 - \sigma_x\sigma_y + \sigma_y^2)^{1/2} ,$$
$$C_e = \lim \sigma_{max} /\sigma_{nom} = \lim \max\{|3\sigma_x - \sigma_y|, |3\sigma_y - \sigma_x|\}/(\sigma_x^2 - \sigma_x\sigma_y + \sigma_y^2)^{1/2}$$

as $(\sigma_x^2 - \sigma_x\sigma_y + \sigma_y^2)^{1/2}$ approaches its real value (which can also vanish) by the criterion of distortion energy[4]. In the particular case of pure shear by these criteria, respectively,

$$\sigma_{emax} = 4|\sigma_x|,\ \sigma_{enom} = 2|\sigma_x|,\ C_e = \lim \sigma_{max} /\sigma_{nom} = 2;$$
$$\sigma_{emax} = 4|\sigma_x|,\ \sigma_{enom} = 3^{1/2}|\sigma_x|,\ C_e = \lim \sigma_{max} /\sigma_{nom} = 4/3^{1/2}$$

as $|\sigma_x|$ approaches its real value which can also vanish, both instead of C = 4 due to reference [7]. The reason is that the *usual* nominal stress leaves the same by considering the second compressive stress in the infinity additionally to the first tensile one, the both having the same module (absolute value), whereas the *equivalent* nominal stress properly takes such a change into account. Analysis of C_e by all possible relations between σ_x and σ_y shows the bounds and their conditions by the above criteria, respectively:

$$C_{emin} = 2\ (\sigma_x = \sigma_y),\ C_{emax} = 3\ (\sigma_x/\sigma_y = 0 \text{ or } \infty);$$
$$C_{emin} = 2\ (\sigma_x = \sigma_y),\ C_{emax} = 14/21^{1/2} \approx 3.055\ (\sigma_x/\sigma_y = 1/5 \text{ or } 5).$$

The obtained results show many clear advantages in comparison with the known ones and properly apply to determining the maximum stresses and to predicting fatigue and fracture of responsible structural elements, e.g., fuselage panel and joints in aircraft constructions [1-3].

[1] Brunn, E. F.: Analysis and Design of Flight Vehicle Structures. Jacobs Publishing, Inc., Indianapolis (IN), 1973
[2] Military Handbook. Metallic Materials and Elements for Aerospace Vehicle Structures. MIL-HDBK-5H, 1998
[3] Handbuch Struktur-Berechnung. Prof. Dr.-Ing. L. Schwarmann. Industrie-Ausschuss-Struktur-Berechnungsunterlagen, Bremen, 1998
[4] Pisarenko, G. S. etc.: Manual de Resistencia de Materiales. Editorial MIR, Moscú, 1989
[5] Gelimson, L. G.: General Strength Theory. Abhandlungen der Wissenschaftlichen Gesellschaft zu Berlin, Publisher Prof. Dr. habil. V. Mairanowski, **3** (2003), Berlin

[6] Gelimson, L. G.: Elastic Mathematics. General Strength Theory. The "Collegium" International Academy of Sciences Publishers, Munich (Germany), 2004

[7] Timoshenko, S. P.: Theory of Elasticity, 3rd ed. McGraw-Hill, New York, 1970

4.11 Maximum Rivet Contact Pressure

L. G. Gelimson (RUAG)

It is very important for predicting fatigue and fracture of fuselage panels and joints [1], to properly take into account the maximum contact pressure between a rivet and a hole having different radii r and R, respectively, which substantially increases this pressure. It is usually determined due to the classical Hertz solution [2] for two parallel elastic cylinders externally contacting with each other (initially on a straight line parallel to their axes) under a force p linearly homogeneously distributed along the cylinders and acting in the plane of these axes. Then this line becomes a strip of width 2a. Introduce two co-ordinate systems with a common x axis and two y and Y axes from the initial contact line to the cylinders axes at any cross-section. The distribution of contact pressure q(x) is half elliptic with maximum q_{max} at x = 0:

$$q(x) = q(0)(a^2 - x^2)^{1/2}.$$

In the simplest case of the same Young modulus E and the Poisson ratio ν of the cylinders,

$$a = (\ 8/\pi\ (1-\nu^2)p/E\ rR/(R + r)\ )^{1/2},$$
$$q_{max} = 2p/(\pi a) = (\ 1/(\ 2\pi\ (1-\nu^2)\ )\ pE\ (R + r)/(rR)\ )^{1/2}.$$

This solution is usually extended also to the case of the internal contact of the surfaces with replacing R + r with R - r in the last two formulae. This is much more clear when using the curvatures instead of the radii, i.e. 1/r + 1/R and 1/r - 1/R instead of (R + r)/(rR) and (R - r)/(rR), respectively. The classical Hertz assumption [2] most important and also taken by further known works [3] is that the contact width is very small in comparison with the both radii r and R. But in the case of the internal contact of two cylindrical surfaces with the same radii (or curvatures) r = R we then obtain vanishing q(x) for any x and p, which is statically impossible. And for our rivet case with near R and r, such an assumption cannot be taken.

The simplest method of improving the classical solution for the internal contact of two cylindrical surfaces whose radii r and R (or curvatures 1/r and 1/R) can be the same seems to be adding to q_{max} a constant corresponding to the homogeneous distribution of p on width 2R:

$$q_{max} = (\ 1/(\ 2\pi\ (1-\nu^2)\ )\ pE\ (R - r)/(rR)\ )^{1/2} + p/(2R).$$

Such an approach is apparently conservative and returns the correct result by equal R and r. This would also hold for using r instead of R in the last addend but this is too conservative especially when r/R is essentially smaller than 1. Fix r, for any R not less than r consider q_{max} as a function of R, and define the maximum contact pressure multiplicator

$$M = q_{max}(R) / q_{max}(r).$$

Its physical sense is showing the increase of the maximum contact pressure when R being increased in comparison with r. In the limiting case of equal R and r, M is 1; otherwise (by R greater than r) we have M greater than 1. The formula for $q_{max}(R)$ shows nonlinearly depending $q_{max}(R)$ on p (or p/E). In order to provide a formula more suitable for our purpose, let us use the diameters d and D rather than radii r and R, as well as introduce load factor k:

$k = p/(2rE)$,
$q_{max}(R) = ((k /(2\pi (1-\nu^2)) (1 - d/D))^{1/2} + k\, d/D) E$.

When using common strength criteria [4] and general strength theory [5,6], we obtain that the maximum equivalent stresses [4] hold not on the middle line of the contact surface, but in a certain depth under it (e.g., they are about 0.3 $q_{max}(R)$ in a depth of about 0.8a by data[3]). That is why it is necessary to consider unusual limits corresponding to the ultimate strength multiplied by 10/3 for the above load factor. The obtained tables for it seem to be slightly conservative. Before dividing the bearing strength [7,8] (or multiplicating the holding stresses) by the values of the maximum contact pressure multiplicator, it is reasonable to divide these values by ones corresponding to the minimum realizable difference between R and r.

All the obtained results show many clear advantages in comparison with the known ones and successfully apply to properly determining the maximum contact stresses between a rivet and a hole edge and to predicting the fatigue strengths of responsible structural elements, e.g., fuselage panels and joints in aircraft constructions [1,7,8].

[1] Brunn, E. F.: Analysis and Design of Flight Vehicle Structures. Jacobs Publishing, Inc., Indianapolis (IN), 1973
[2] Hertz, H.: Über die Berührung fester elastischer Körper. J. reine und angewandte Matematik, **92** (1882), 156-171
[3] Pisarenko, G. S. y otros: Manual de Resistencia de Materiales. Editorial MIR, Moscú, 1989
[4] Gelimson, L. G.: General Strength Theory. Abhandlungen der Wissenschaftlichen Gesellschaft zu Berlin, Publisher Prof. Dr. habil. V. Mairanowski, **3** (2003), Berlin
[5] Gelimson, L. G.: Elastic Mathematics. General Strength Theory. The ”Collegium” International Academy of Sciences Publishers, Munich (Germany), 2004
[6] Johnson, K. L.: Contact Mechanics. Cambridge University Press, N. Y. etc., 1985
[7] Military Handbook. Metallic Materials and Elements for Aerospace Vehicle Structures. MIL-HDBK-5H, 1998
[8] Handbuch Struktur-Berechnung. Prof. Dr.-Ing. L. Schwarmann. Industrie-Ausschuss-Struktur-Berechnungsunterlagen, Bremen, 1998

5 Fatigue and Fracture of Integral Panels and Welded Joints

5.1 Welding of Fuselage Structures

M. Pacchione and S. Werner (Airbus-D)

Stringer welding

Laser beam welding of skin stringer joints has replaced the riveting in some areas of the lower fuselage, Figure 33. The main arguments for the welding process are reduction of manufacturing cost and weight saving.

The welded area is designed in such a way that there is absolutely no risk of multiple side damage within an extended service life goal. Furthermore fatigue tests on coupon and full scale articles have demonstrated that welding deviations up to a certain level can be tolerated without loss of fatigue strength.

Damage tolerance is the main issue of the integral structure. For the stringer welding in the lower shell a longitudinal crack in the weldline is the dimensioning criterion. Therefore Airbus has done a variety of residual strength and crack propagation test. The aim is to find effects which have an influence on the damage tolerance behaviour. The main parameter of the study are skin thickness, stringer thickness, heat treatment and environmental effects. This has led to a profound knowledge of the damage tolerance properties of the weldline.

Future work has to concentrate on the further improvement of the residual strength of integral structures. An optimized design of the overthickness under the weldline could result in a crack turning out of the weak zone. Another challenge will be the use of new materials, e.g. an AlLi-Alloy, for the welding process.

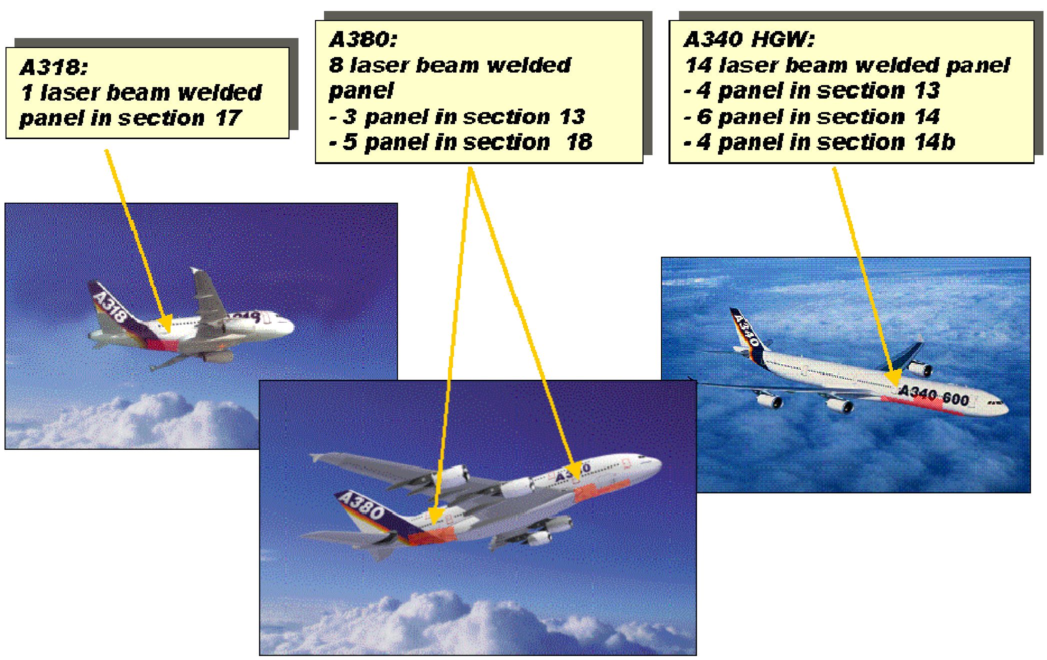

Figure 33: Laser Beam Welded Panels in the different Airbus Programs

Friction stir welding of the longitudinal joints in the pressurized fuselage

The riveted longitudinal lap joint in the pressurized fuselage of a transport aircraft is of large practical importance. It is dimensioned mainly by fatigue and damage tolerance; it is expensive to manufacture; it is prone to corrosion if not adequately protected and can be an issue for aging aircraft due to the possibility of widespread fatigue damage originating from rivet holes. Moreover it introduces a weight penalty caused by the material overlap, the application of doublers, rivets, sealant, and titanium crack stoppers.

AIRBUS has developed the Friction stir welding technology to replace the longitudinal splice with a welded butt joint (see Figure 34). This manufacturing modification, which goes in direction of monolithic structure design, creates challenges related to the design for damage tolerance. Materials with outstanding toughness properties and optimized design solutions have been investigated to achieve a high damage tolerance of the welded joint.

The maturity of the technology has been validated with investigations carried out in several research programs. The fatigue and damage tolerance aspects have been confirmed with full-scale tests in frame of the European research project TANGO (pressurized curved shells and barrel test with longitudinal and circumferential welds).

Compared to the riveted splice the weight saving is in the range of 0.8 kg per meter of joint. Since the longitudinal joints in the fuselage of a transport aircraft extend for several hundred meters the weight saving which is possible to achieve in case of extensive use of the FSW technology is significant. Friction stir welding also reduces the manufacturing costs of the joint of up to 25%. Other advantages compared to the riveted splice are the improved inspectability and no susceptibility to multi site damage.

Next steps are the qualification and certification: the first application of a FSW shell is anticipated for the front fuselage of the A340 HGW lower shell. A demonstrator of the A340 design has already been successfully produced. Extensive application of FSW is planned for the new A350.

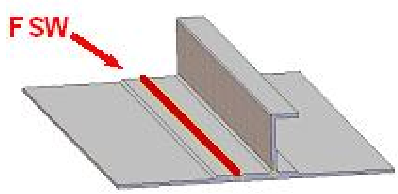

Figure 34: Longitudinal FSW in the pressurized fuselage

5.2 Fatigue Tests for Repair and Re-work Solutions of Stringer Run-outs

H. Huth (AvCraft)

In the full-scale fatigue test of the Dornier Do 328 some fatigue cracks started to develop at stringer run-outs in the lower outer wing panels at a rather late phase of the test. Although crack propagation was very slow, an investigation on possible repair and re-work procedures was initiated.

Six test specimens as shown on Figure 35 have been manufactured out of 7475 T7351 plate material. Flight-by-flight fatigue and crack growth tests will be performed at the IMA-Dresden.

After derivation of crack initiation life and crack growth behaviour, a repair by stop-drilling, cold-working and hole-closing will be tested. Furthermore, the effect of different re-work solutions on crack initiation life will be investigated.

Figure 35: Stinger run-out test specimen

5.3 Fatigue and Fatigue Crack Propagation Behaviour of Laser Beam Welded Aerospace Aluminium Alloy Butt Joints for Skin-Skin Applications in Airframes

W. V. Vaidya, M. Koçak (GKSS) and J. Hackius (Airbus-D, Bremen)

The laser beam welding (LBW) technology has now become available on the industrial scale and has opened new perspectives for weight reduction and cost savings in airframes. In contrast to a conventional heat source which develops a broad seam and an extended heat affected zone (HAZ) in a weldable Al-alloy, the laser beam source has a high energy power density which makes it feasible that both the weld seam and HAZ can be restricted to a very narrow width of a few millimetres. The availability of laser sources on one hand and the development of new fusion-weldable 6XXX Al-alloys on the other hand have led to a new design concept: *integral structures*, whereby the riveted joints (i.e., differential structure) are replaced by the welded joints. Such shells with T-joints (stringer-skin joints) have already been used in some AIRBUS civil aeroplanes and have contributed substantially to weight reduction and cost savings. Welded butt joints (skin-skin joints) is the next step towards the all-welded (rivet-free) airframe. In this context, along with the alloy AA6013, AA6056 is considered to be a prosperous airframe candidate.

Fusion welding does have some inherent problems but can be solved, e.g., hot cracking in welds can be avoided with suitable filler wire. Formation of defects such as pores or undercuts, and dilution of solute in the fusion zone may affect microstructure, strength and performance, in particular the damage tolerance. Since information on properties of LBW butt joints of aerospace Al-alloys is not yet available, the initial study was undertaken within a national project (LuFoII) and then continued in an EC project (IDA).
In LuFoII project it was demonstrated that with certain precautions it is possible to obtain high quality defect-free butt welds of AA6013 and AA6056, particularly for sheet thickness of less than about 4.5 mm. These alloys are susceptible while fusion welding for pick-up of moisture and gases, and when the latter get entrapped, pores may result. In turn, pores may act as internal notches. Notch effect leading to degradation of fatigue strength may also be induced by excess weld metal and undercuts. How good fatigue properties can be achieved on welds is shown as an example in Figure 36. When through LBW process optimisation pores are reduced, the weld width is decreased and undercuts are avoided, the fatigue strength can be improved. It must be pointed out here that the surface of the LBW fatigue specimens in Figure 36 was retained *as-welded* (i.e., without smoothening by milling as is usually done for

friction stir welds) and should have been prone for the notch effect. Nevertheless, the fatigue strength in the high cycle regime was found to be relatively high, which verifies the sound quality of welds.

Filler is essential for avoiding hot cracking and for achieving an acceptable strength in welds. On the other hand, the filler dilutes the solute concentration and also increases material heterogeneity. Additionally, precipitation behaviour, and hence strength, can be adversely affected. Open questions such as which mechanical properties are affected to what extent, and whether certain properties can be restored through a post weld heat treatment (PWHT) was investigated for LBW butt joints of AA6056-(HDT) within the project IDA (Investigation on Damage Tolerance Behaviour of Aluminium Alloys). It was found that for LBW in T4, PWHT (T6 and T78) improves hardness and strength within the fusion zone. As regards fatigue crack propagation (FCP), however, PWHT was not found to be beneficial in the present case. The FCP results are summarized in Figure 37 and show that resistance to FCP is at its maximum in the T4 condition (naturally aged) for the base metal and to some extent also for the fusion zone, particularly at high ΔK levels. When peak-aged (T6) or over-aged (T78), the FCP response was found to be in fact inferior. Usually, parameters which improve strength, fracture resistance and fatigue, may not necessarily improve the FCP behaviour. Nevertheless, it is essential to find out a balance of properties for acceptable damage tolerance. It is this area, in which further research is being conducted at GKSS Research Center.

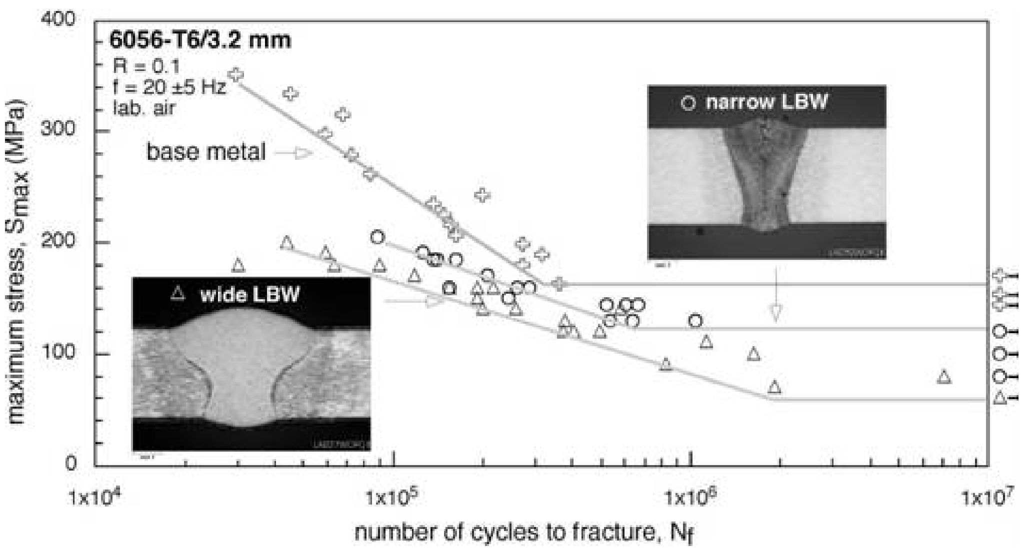

Figure 36: Fatigue behaviour of laser beam welded butt joints 6056-T6/3.2 mm alloy. The welded specimens were tested in the “as-welded” surface condition.

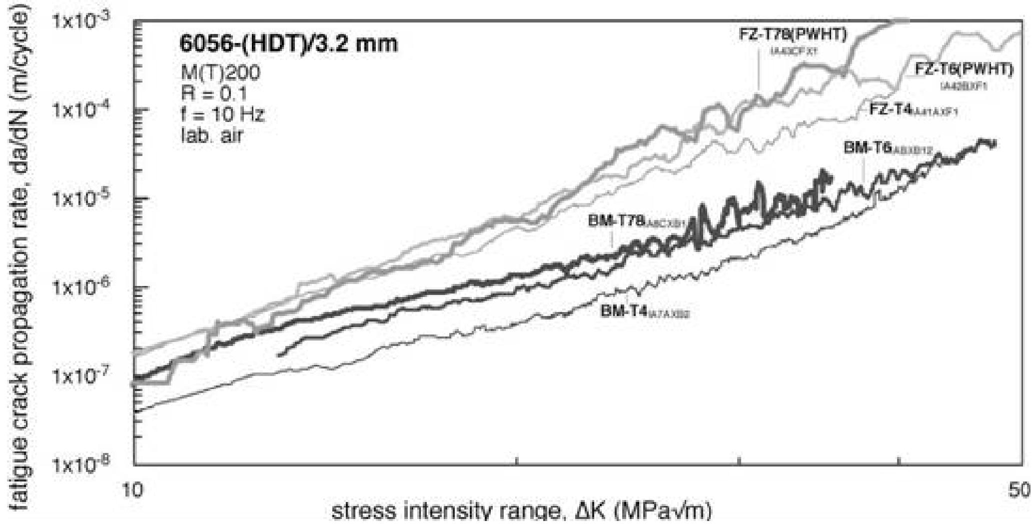

Figure 37: Fatigue crack propagation behaviour of laser beam welded butt joints 6056-(HDT)/3.2 mm alloy. The alloy was welded in T4 and then post weld heat treated to peak-ageing (T6) and over-ageing (T78).

5.4 Fracture Assessment of Laser Beam Welded Stiffened Panels for Airframe Applications

E. Seib and M. Koçak (GKSS), H. Assler and M. Pacchione (Airbus-D)

The change from the differential (riveted) to integral (welded) design of stiffened fuselage panels has introduced new aspects need to be considered in the damage tolerance analysis of panels containing crack. Hence, a joint project between AIRBUS and GKSS has been conducted to develop an advanced fracture assessment route to predict the residual strength of the integrally stiffened welded AA6013 panels. Testing of welded stiffened panels (Figure 38) with one and two bay cracks under static loading have shown that the crack approaching a welded stringer (in 90° angle) exhibits crack branching propagating both into the skin and stringer. The proposed analysis method has incorporated the crack branching (into skin and stringer) effect and is based on the FITNET Fitness-for-Service-FFS (*formerly called SINTAP*) flaw assessment procedure [1, 2]. The FITNET FFS predictions are validated using experimental results of 2-stringer panels with a one-bay (crack between two stringers) and 3-stringer panels with a two-bay crack (large central crack with a broken central stringer) configurations.

The FITNET FFS procedure yielded conservative residual strength predictions for tension loaded panels with one and two-bay cracks, Figure 39. The proposed residual strength analysis method based on the elastic-plastic fracture mechanics approach is able to predict the stringer failure either due to plastic collapse (as the riveted stringer) or due to the instability of the stringer crack. The overall failure of the cracked stiffened panel is governed by the skin or stringer failure, whichever occurs first. Hence, this study has provided an analytical flaw assessment tool for the residual strength analysis of integrally stiffened welded panels validated using structure-like large panels. Currently, similar approach is being applied for welded panels with central through thickness crack parallel to the welded stringer. In this case, analysis considers the strength undermatching (weld metal has lower strength than base material) effect on the crack driving force due to the confined plasticity (partial) at the weld.

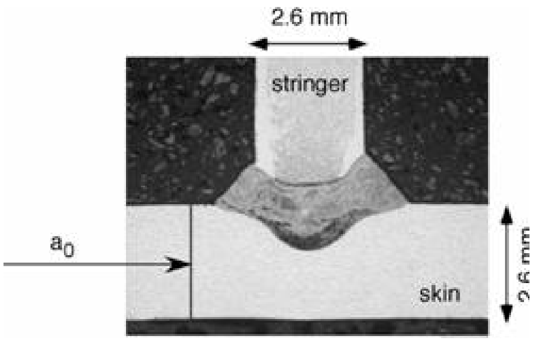

Figure 38: Macrosection of the LBW T-joint (stringer-to-skin joint) and the location of the initial crack, a_0, in stiffened welded panels.

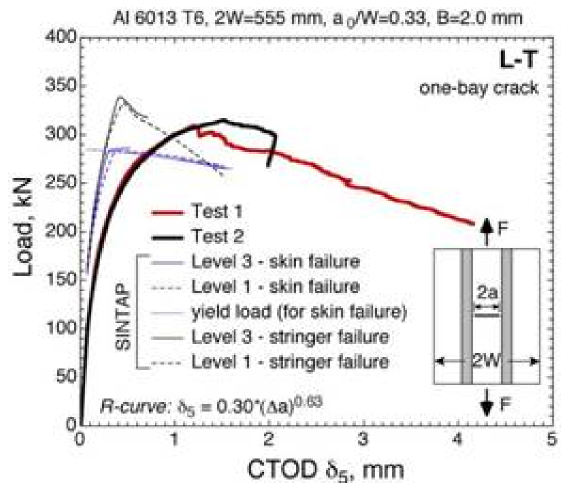

Figure 39: Comparison between the predicted and experimental load-displacement curves of the 2-stringer panel. Two FITNET analysis levels (Level 1 and Level 3) are used.

[1] SINTAP: Structural Integrity Assessment Procedures for European Industry', Brite-Euram Project No. BE95-1426, Contract No. BRPR-CT95-0024, Final Report, September 1999

[2] FITNET: European Fitness-for-Service Network, Proposal No. GTC1-2001-43049, Contract No. GIRT-CT-2001-05071, www.eurofitnet.org.

5.5 Investigation on the influence of stringer foot reinforcements on the fatigue crack growth behaviour (FCGR) in laser beam welded skin-stringer test panels

F. Palm (EADS CRC)

Integral welded structures have become reality in AIRBUS aircraft (A318 and A380). Currently this application is limited to lower shell panels in the pressurized fuselage because loading is dominated by compression and/or shear.

Extension of laser beam welding into more tension (damage tolerant) loaded area is intended for future aircraft structures but the well known crack propagation deficiencies of integrally stiffened panels hinder this approach. Principal parametric studies were initiated and performed in order to create an improved crack growth behaviour characterized by a "differential" crack growth behaviour, i. e. significant crack growth retardation if the crack tip reaches the perpendicular stringer. The 3 step approach consists of:

- Manufacturing of locally reinforced stringer (in collaboration with ALU-Menziken, Switzerland)
- Manufacturing of so called 4-stringer test pieces by laser beam welding
- Testing on FCGR (cyclic. loading, R = 0.1, σ = 100 MPa)
- Interpretation and assessment of results

In order to minimize risks and costs the profiles were manufactured from AlMgSiCu type material (AA 6013 T6) reinforced by a high strength nickel base wire (INCO 718). The skin sheet was made from AA 6013 T6 as well. The strength of the reinforcement wire was 1400 MPa.

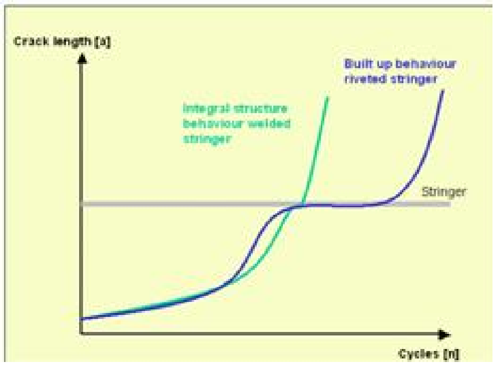

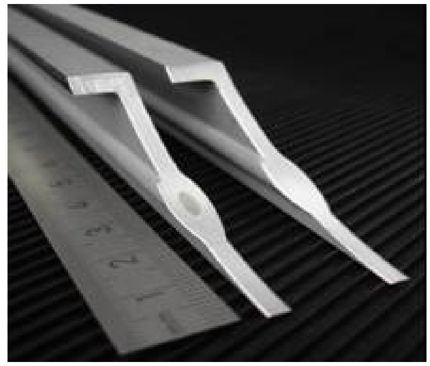

Figure 40: Increased crack propagation rates in integral structures (schematic, left) and wire reinforced stringer (left).

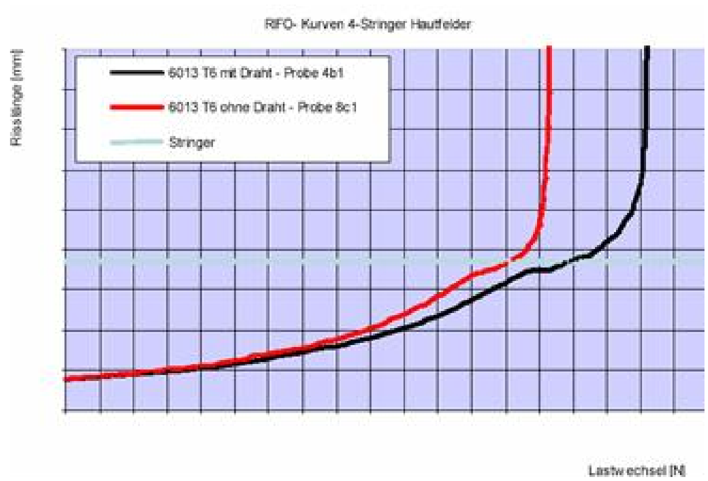

Figure 41: 4-stringer panel and crack propagation curves (x: cycles, y: crack length, black line: reinforced stringer, red line: standard stringer).

After laser beam welding (Nd-YAG laser, from both sides simultaneously) the panels were cut in the center between stringer No 2 and No 3 and FCGR testing was performed (R = 0.1). Comparison of crack growth data of not reinforced and reinforced stringer revealed interesting features.

- Crack retardation is achieved
- The manufacturing procedure of such kind of locally reinforced profiles is reliable and opens further design approaches for locally ”tailored” profiles
- Higher strength reinforcements (up to 3500 MPa, i. e. Co base wires) are feasible
- Higher strength reinforcement would probably lead to more distinct crack retardation
- Principal advantages of laser beam welding remaining. Extrusion of reinforced profiles could be scaled up. Therefore it is not penalizing this new concept by higher costs.

5.6 Parametric studies dedicated to improve residual strength in integral welded skin-stringer fuselage panels (circumferential crack scenario) via a simplified test bar

F. Palm (EADS CRC)

Modern aircraft structures have to fulfil certain requirements in order to assure safe service over a very long time (> 20 years). Hence residual strength capabilities are of specific concern and depending on the location in the aircraft structure different loading scenarios have to be checked properly.

Circumferential cracks in the pressurized fuselage characterized by broken longitudinal stiffeners (stringer) are one of the challenges the integral (welded) structure design is faced with. Experiences from different previous studies (like NASA IAS study) and own investigations revealed reduced limit load capabilities of these monolithic solutions compared to bonded or riveted ones. Therefore extension of integral design into upper shell application in a commercial transport aircraft fuselage seems to be critical.

A parametric study was initiated in order to assess the impact of different parameters on the residual strength capability of stringer reinforced skin panels (crack is perpendicular to the stringer and crack tip just at stringer foot).

Observations during testing revealed the importance of certain parameters:

- Materials (to be welded incl. type of filler material) and their behaviour (strength, toughness and notch sensitivity)
- Design of the stringer connection and particular stringer foot design
- Relevance (positively or negatively) of post weld heat treatments
- Process (welding) parameters

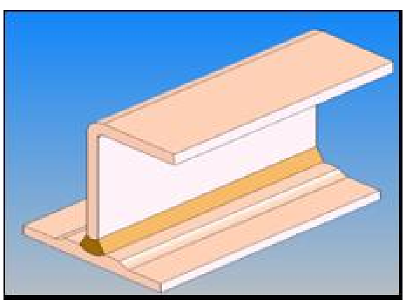

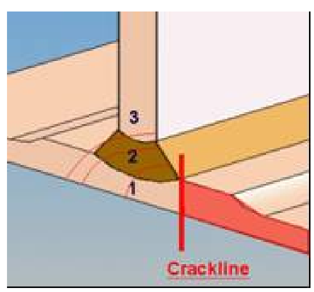

Figure 42: Investigated welding configuration and crack position.

Crack tip stress intensity and plasticity is strongly influenced by the above mentioned parameters and consequently defining the point where sudden instability limits the load sustained by the chosen configuration

As extensive testing on larger skin-stringer panels elements is long lasting and expensive and modelling is currently not able to predict failure accurately enough in those material combinations, a so called residual strength test bar was deisgned.

Assuming that the measured overall residual strength of the panel configuration can be simply described as combination of the residual strength of the skin (➔ R-curve) and the residual strength of the stringer-skin connection, a fast estimation method was established, which allows to increase the developing speed and the amount of data of different materials and welded material combinations.

The static chevron notched test bar consisted of a small portion of skin and the entire stringer material hold together by the laser beam weld seam. The residual strength results obtained with this bar, demonstrated very good conformity (qualitatively and into some extend also quantitatively) with results generated on real skin-stringer panels.

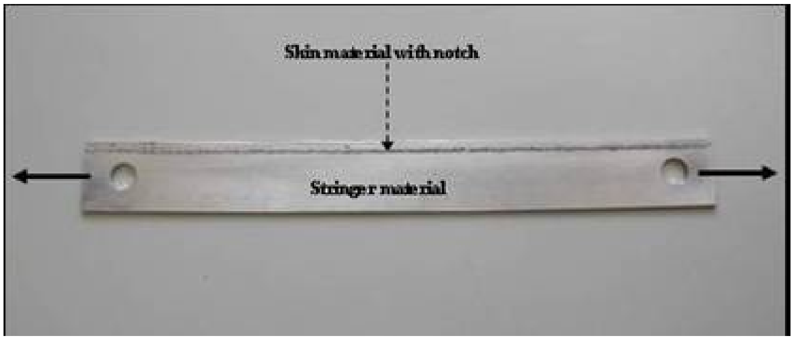

Figure 43: Simplified test bar for residual strength investigations of skin-stiffener welded configurations.

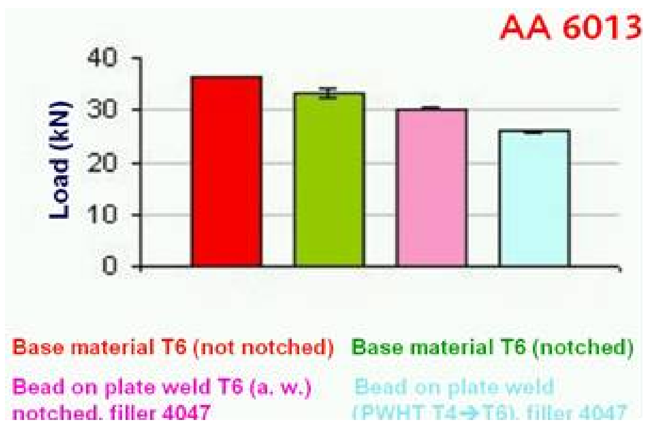

Figure 44: Residual strength values obtained with the simplified test bar.

The results welded AA 6013 samples in Figure 44 showed a permanent decrease in residual strength starting from unaffected (but sharply notched) base material over a laser beam welded one to a laser beam welded one plus PWHT. The same behaviour is observed during testing of stringers reinforced panels with identical material conditions.

On the basis of a simple an estimation of load distribution (done by an linear elastic simulation on the commercial simulation tool STRESS CHECK) it is possible to predict the residual strength of a 4 stringer panel, Figure 41. In the specific case of an AlMgZnMnZr alloy (AA 5059) the ultimate load of the cracked reinforced panel was 366 kN. The measured test bar value (28 kN) was weighted by the calculated load distribution in the 4 stringer of the panels (inner stringer 100% and outer stringer 66%) and added to the residual strength value of the non reinforced skin (276 kN). The results of this estimation gave very good agreement with the experimental value (366 km ⇔ 369 kN).

5.7 Residual Strength Analysis of Laser Beam and Friction Stir Welded Aerospace Al-alloys

E. Seib and M. Koçak (GKSS), H. Assler and M. Pacchione (Airbus-D)

Developments in weldable aluminium alloys combined with advanced joining technologies (laser beam and friction stir welding) have provided new design route (integral structure) for metallic fuselage. Numerous damage tolerance investigations have been conducted at the GKSS Research Center on the “skin-stringer” and “skin-skin” joints. This study has jointly been undertaken with AIRBUS to analyse the residual strength behaviour of such joints using European Fitness-For-Service Network (FITNET FFS, *formerly called SINTAP*) flaw assessment procedure [1, 2] in combination of extensive experimental programme for generation of input and validation data. The weld strength mismatch analysis option of the FITNET FFS Procedure has been applied to middle cracked laser beam and friction stir welded (skin-skin joints) 750 mm wide aluminium panels (2.6 mm thick AA6013T6) to predict their maximum tensile load carrying capacities. The fracture resistance curves for the base and weld materials were experimentally generated from small scale standard C(T)50 specimens and used to assess weld flaws in the structure-like thin-walled welded panels. The FITNET FFS procedure yielded conservative predictions of the failure loads for both welds [3, 4]. Hence, this study has significantly contributed to the; better understanding of the plasticity development and fracture behaviour of such joints, Figure 45.

development of an advanced residual strength assessment route, Figure 46, for thin-walled welded fuselage components by taking into account of the strength undermatching (i.e. weld zone has lower strength than the base metal) of the both LBW and FSW weld zones.

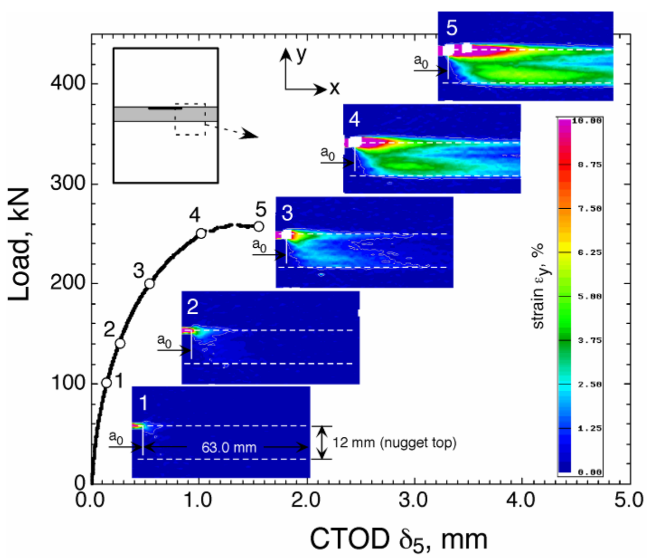

Figure 45: Stages of the plasticity development of the M(T) panel with FSW weld (notch at the edge of the weld showing the confined plasticty within the weld zone due to strength undermatching of the FSW.

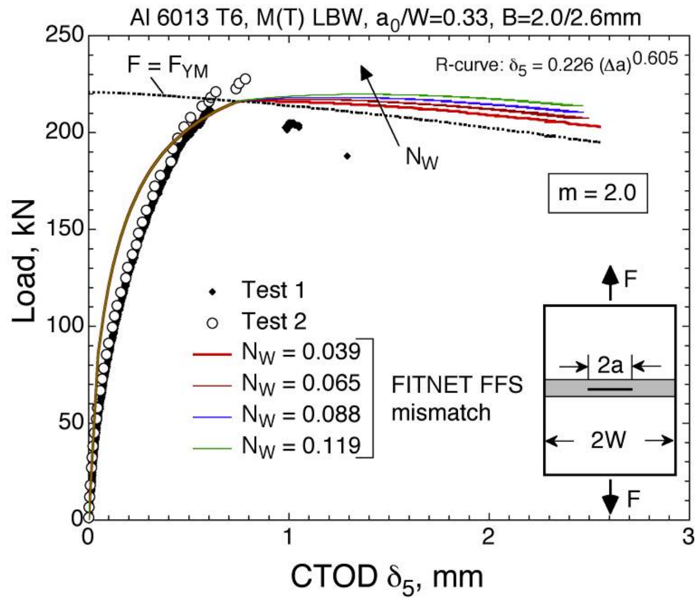

Figure 46: The comparison between experiments and FITNET predictions with sensitivity analysis for strain hardening exponent (N_W) of the laser beam weld material.

[1] FITNET, European Fitness-for-Service Network, Proposal No. GTC1-2001-43049, Contract No. GIRT-CT-2001-05071, www.eurofitnet.org

[2] Koçak M : Fitness for Service Analysis of Structures using the FITNET Procedure – An Overview. Proc. of the 24th Int. Conf. on Offshore Mechanics and Arctic Eng. (OMAE/ASME), Halkidiki, Greece, 12-17 .06. 05.

[3] Seib E, Koçak, M and Assler, H: Structural integrity assessment of welded aerospace aluminium alloy using SINTAP route. MP Materialprüfung Jahrg. 46 (2004)11-12, pp. 556-564.

[4] Seib E, Koçak, M and Assler, H: Fracture assessment of welded aerospace aluminium alloy using SINTAP route. Welding in the World, Vol. 48, no° 11/12, 2004 . 46 (2004)11-12, pp. 2-8.

5.8 Prediction of Fatigue Crack Propagation in Friction Stir Welds under Flight Loading Conditions

T. Ghidini (DLR), C. Polese and A. Lanciotti (University of Pisa, Italy), C. Dalle Donne (EADS CRC)

Since Friction Stir Welding has been identified as “key technology” for primary aerospace structures [1], the recent FAR regulations for damage tolerance and fatigue evaluations of aircraft structures require fatigue crack growth testing and modelling, [2]. Even if flight simulation testing is a generally accepted fatigue testing procedures in aeronautics (it is adopted in full-scale tests as well as for component and comparative testing), there is a complete lack of information regarding the fatigue crack propagation in friction stir welds under variable amplitude loading and flight loading conditions, both from an experimental as well as from a prediction point of view. In the present investigation an exploratory test program was carried out to improve the general understanding of sequence effects: the work offers a basis both for a better experimental documentation and for an evaluation of existing crack propagation prediction models. The experimental investigations have been performed on 4 mm thick centre cracked AA2024-T3 base metal and FSW specimens: regarding the

FSW samples, the crack was placed 5 mm out of the weld centre, in the most critical part of the joint. It was propagating in the Thermomechanically Affected Zone (TMAZ), on the retreating side of the weld, where the minimum value of the hardness is located. All the coupons have been tested under simple variable amplitude load sequences such as single overloads, overloads and under loads, overloads and compressive under loads, and a standardized flight-simulation loading history, FALSTAFF, [3]. The fatigue crack propagation was also predicted using the widespread aerospace fracture mechanics software packages AFGROW [4] and NASGRO 3.0 [5].

A simple engineering approach based on a relatively solid background and checked against fatigue test data for various test conditions was developed. It may provide a practical and reliable basis for the analysis of fatigue tests of integral structures under service loading conditions. Among others, the most evident effects acting on a structure subjected to variable loading histories are the retardation and acceleration of the fatigue crack growth, the so called interaction effects. In welded structures, the fatigue crack propagation is also affected by the presence of residual stresses. Interaction effects and internal stresses were firstly separately simulated and than combined in order to evaluate the ability to predict the fatigue crack propagation on FSW welded structures under service loading conditions, as described, for easier loading spectra, in [6]. To keep the model simple and reliable the following basic assumptions were used:

- base material dadN/ΔK curves were used for all the predictions (also for the welds)
- existent retardation models with suggested parameters were used to predict the fatigue crack propagation under variable amplitude loading
- an easy approach was used to measure the residual stresses. K_{res} was measured with the cut compliance method [7, 8] and simply added to the K_{app}. Crack growth rate was than calculated with base material dadN/ΔK curves

An overall comparison between experimental and predicted values of base and friction stir welded material is presented in Figure 47 and Figure 48. The estimated lives are in good agreement with the actual lives showing the viability of the assumptions made in the analysis.

[1] Collins, R.A., Campassens, D., Kimmins, S. T., Rodrigo, P., Advanced Materials and Manufacturing Techniques on Future Airbus Aircraft. ICAF 2003- Fatigue on Aeronautical Structures as an Engineering Challenge, Guillaume, M. (Ed.), EMAS, 2003.
[2] JAA-FAA, Damage Tolerance and Fatigue Evaluation of Structure. JAR 25.571, 1998.
[3] FALSTAFF, Descripiton of a Fighter Loading Standard for Fatigue Evaluation. Combined Report (LBF, NLR, IABG and F&W), 1976.
[4] Harter, J.A., AFGROW, User's Guide and Technical Manual. AFRL-VA-WP-TR-2002-XXXX, September 2002.
[5] NASA-ESA, ESACRACK 4 User's Manual. TOS-MCS/2000/41/In, 2000(1).
[6] Ghidini, T., Dalle Donne, C., Prediction of Fatigue Crack Propagation in Friction Stir Welds. 4th International Conference on Friction Stir Welding, Park City, Utah, 2002.
[7] Cheng, W., Finnie, I., Measurement of Residual Hoop Stresses in Cylinders Using the Compliance Method. Journal of Engineering Materials Tech., 1986. 108: p. 87-92.
[8] Schindler, H.-J., Cheng, W., Finnie, I., Experimental Determination of Stress Intensity Factors Due to Residual Stresses. Experimental Mechanics, 1997. 37(3): p. 272-277.

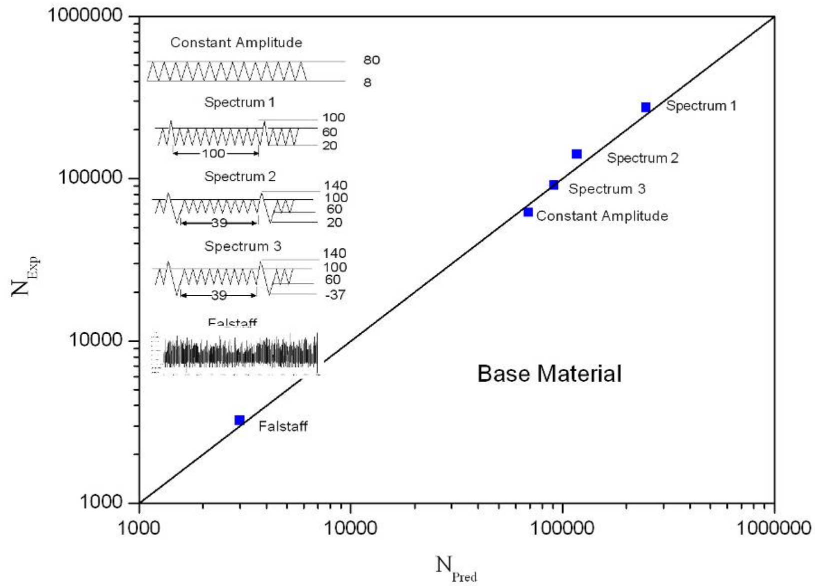

Figure 47: Predicted fatigue life of the base material compared to the observed lives.

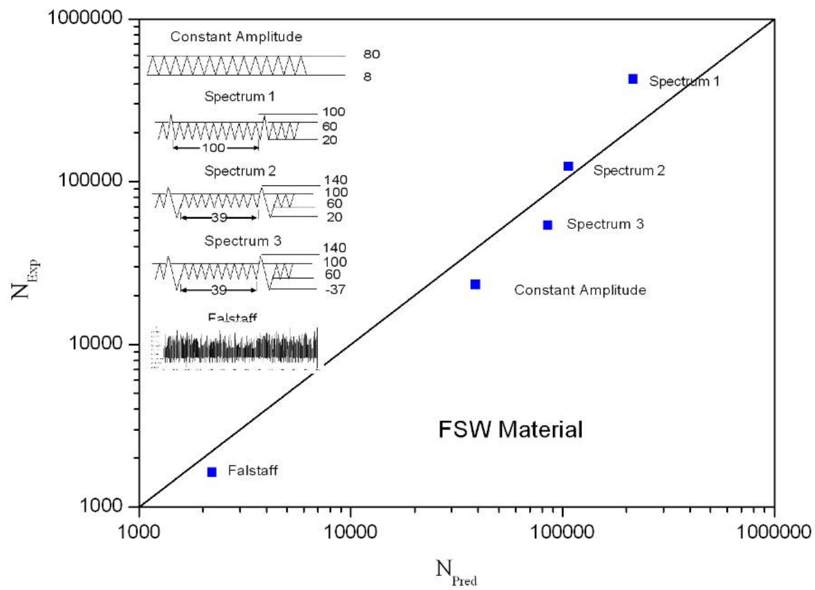

Figure 48: Predicted fatigue life of the FSW material compared to the observed lives.

5.9 Fatigue Life of Friction Stir Welded Joints in Presence of Corrosion Damage: Experiments and Calculations

T. Ghidini and U. Alfaro (DLR), C. Dalle Donne (EADS-CRC)

Aircrafts operate around the world in corrosive environment. If friction stir welding is considered for primary aircraft structures, prediction methodologies have to be adopted for this specific joint type also in presence of corrosion. However, in the case of friction stir welds there is little experimental work done [1-5] and a complete lack of prediction activities regarding pre-corroded FSW welded structures, even though for some alloys the corrosion susceptibility of the joint area is higher than that of the base material [6, 7]. One of the open questions concerning the application of friction stir welding in primary aircraft structures is the long term service behaviour of precipitation hardening aluminium alloy joints. In this view, specifically impact of corrosion on the fatigue life of 2XXX and 7XXX series alloys friction stir welds has to be investigated.

As a first step to assess this problem, the fatigue behaviour of pre-corroded 2024-T3 joints was investigated. Un-notched specimens of 4 mm thick 2024-T3 base material and FSW joints were pre-corroded by alternate immersion in 3.5% NaCl solution, following the ASTM G44 standard, for 100, 250 and 1000 hours. Subsequently pristine and pre-corroded coupons were tested under constant amplitude loading and lab environment at a load ratio F_{min}/F_{max} of R=0.1 (loading direction perpendicular to the weld).

The diagram reported in Figure 49 shows the effect of corrosion attack on the fatigue life of 2024-T3 friction stir welded joints and base material. Corrosion has obviously a detrimental effect reducing the fatigue strength for both types of specimens. The FSW joint shows a similar drop in fatigue strength as the base material; this drop is virtually independent of the corrosion time, since the test results of 100 h, 250 h and 1000 h pre-corrosion specimens follow in the same scatter band.

The fatigue lives of base and FSW pre-corroded materials were also predicted by using widespread aerospace software packages, AFGROW [8] and NASGRO 3.0 [9], and a simple fracture mechanics approach [10]. The calculations are in very good agreement with the experimental results. The following basic assumptions were taken:

- by neglecting the different weld microstructures on the basis of [9, 10] and the very low transverse residual stresses, the welded material is treated as base material
- pitting and inter-granular corrosion are treated as a single corrosion damage source and the model surface crack comprehends this damage
- the several corrosion damaged areas of the specimen surface are simulated by a single semi elliptical surface crack having the dimensions of the deepest and the widest corrosion damage area found on the specimen, Figure 50.

For brevity purposes just the simulation results regarding the 250 h pre-corroded FSW specimens are reported, Figure 51, but all the experimental fatigue curves could be successfully predicted.

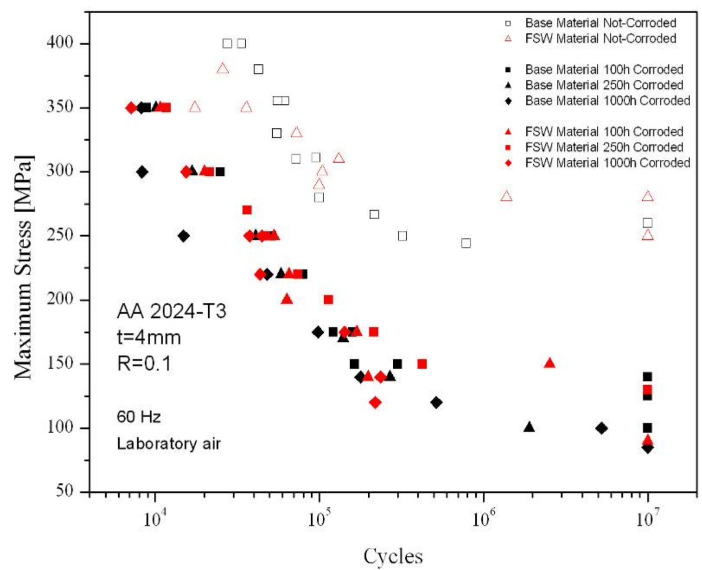

Figure 49: Comparison between not corroded and 100 h, 250 h, 1000 h corroded base and FSW material.

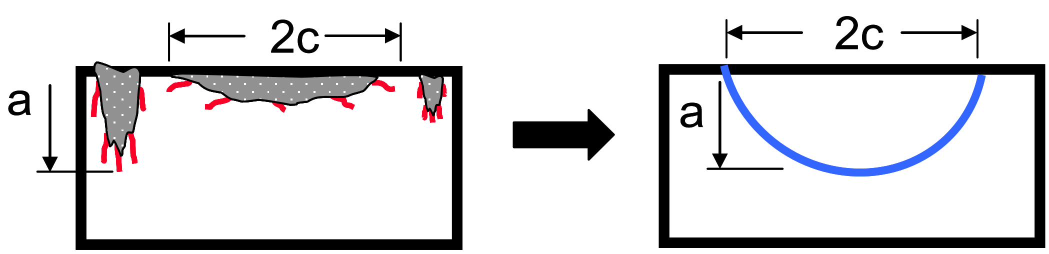

Figure 50: The model surface crack has the dimension of the deepest (a) and widest (2c) corrosion damages.

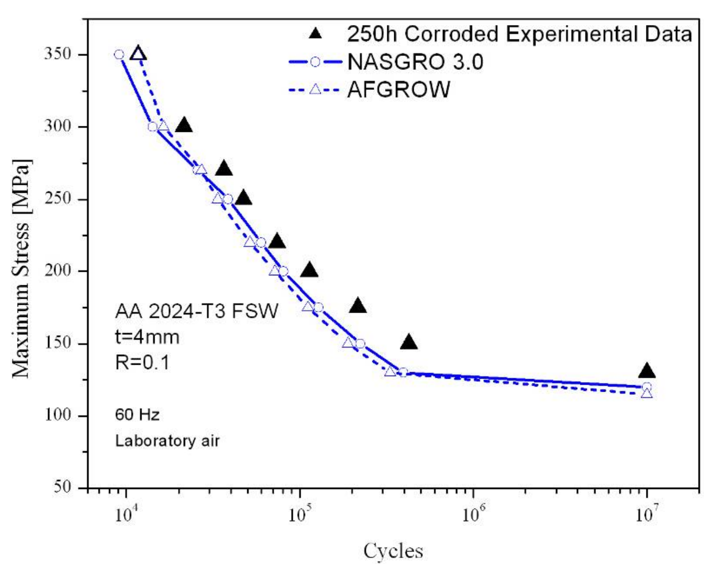

Figure 51: Comparison between 250h corroded FSW material and computer simulation.

[1] Pao, P.S., et al., Corrosion-Fatigue Crack Growth in Friction Stir Welded Al 7050. Scripta Materialia, 2001. 45(5): p. 605-612.
[2] Sankaran, K.K., Smith, H. L., Jata, K. V., Pitting Corrosion Behaviour of Friction Stir Welded 7050-T74 Aluminum Alloy. 6th International Trends in Welding Research, Pine Mountain, GA, 2002.
[3] Dunlavy, M., Jata, K., High-Cycle Corrosion Fatigue of Friction Stir Welded 7050-T7451. TMS Friction Stir Welding and Processing, 2003. II: p. 91-98.
[4] Pao, P.S., Lee, E., Feng, C. R., Jones, H. N., Moon, D. W., Corrosion Fatigue in FSW Welded Al 2519. TMS Friction Stir Welding and Processing, 2003. II: p. 113-122.
[5] Alfaro Mercado, U., Ghidini, T., Dalle Donne, C., Braun, R., Fatigue and Corrosion Properties of Friction Stir Welded Dissimilar Aluminium Alloys. 5th International Conference on Friction Stir Welding, Metz, France, 2004.
[6] Paglia, C.S., Ungaro, L. M., Pitts, B. C., Carroll, M. C., Reynolds, A. P., Buchheit, R. G., The Corrosion and Environmentally Assisted Cracking Behavior of High Strength Aluminum Alloys Friction Stir Welds: 7075-T7651 vs. 7050-T7451. TMS Friction Stir Welding and Processing, 2003. II: p. 65-75.
[7] Connolly, B.J., Davenport, A. J., Jariyaboon, M., Padovani, C., Ambat, R., Williams, S. W., Price, D. A., Wescott, A., Goodfellow, C. J., Lee, C.-M., Localised Corrosion of Friction Stir Welds in Aluminium Alloys. 5th International Conference on Friction Stir Welding, Metz, France, 2004.
[8] Harter, J.A., AFGROW, User's Guide and Technical Manual. AFRL-VA-WP-TR-2002-XXXX, September 2002.
[9] NASA-ESA, ESACRACK 4 User's Manual. TOS-MCS/2000/41/In, 2000(1).
[10] Ghidini, T., Alfaro, U., Dalle Donne, C., Fatigue Life of Friction Stir Welded Joints in Presence of Corrosion Damage: Experiments and Calculations. Deutscher Verband für Materialprüfung e. V. Bericht 131, 2004: p. 283-292.

5.10 Fatigue behaviour of conventional and non-conventional Friction Stir Welded specimens in AA6056

A.-L. Lafly(DLR and EADS-CRC France), D. Alléhaux and F Marie (EADS-CRC France), G. Biallas (DLR)

Within a common research project of EADS-CRC France in Suresnes and the Institute of Materials Research of the German Aerospace Center (DLR) in Cologne, conventional and non-conventional (Bobbin Tool) Friction Stir Welding (FSW) processes are analyzed. The effects of pre and post FSW heat treatments on mechanical properties are evaluated through hardness profiles, tensile strength, S-N fatigue tests, fatigue crack propagation and corrosion properties. The specimens made from 4mm thick sheets of AA6056 receive different heat treatments designated as follows:

- T4 directly welded
- T4 welded and subsequent T6 artificial aging (called T6 post-welded)
- T6 artificial aging and afterwards welded (called T6 as-welded)
- T4 welded and subsequent T78 artificial aging (called T78 post-welded)
- T78 artificial aging and afterwards welded (called T78 as-welded)

S-N fatigue tests:

Tests have been performed only on AA6056-T78 tempers pre and post-aging for both Kt=1 (polished and unpolished conditions) and Kt=2,3.

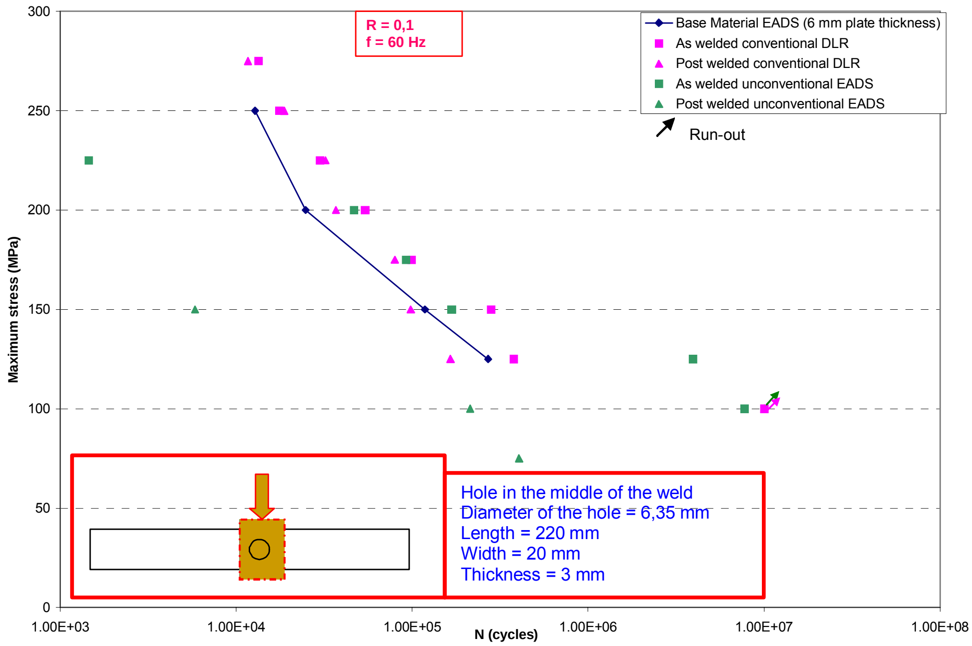

Figure 52: S-N fatigue tests for Kt=2.3, specimens with hole in the weld nugget. AA6056 Base Material and welded joints in two different aging conditions: T78 as welded and T78 post welded. Specimens' dimensions are shown in the insert.

Data related to the base material performance come from previous investigations carried out on 6 mm thick alloy: this could explain the trend highlighted by lower performance for the unwelded material. Nevertheless, the weld nugget, especially after post welding heat treatment, can also present a hardening in the weld nugget, which allows a mechanical recovery up to or above the base material level.

Tendencies seem to be identical for both technologies, conventional and bobbin tool processes: the as welded condition gives better results.

The fatal cracks are developed at different positions starting from the hole as shown in Figure 53.

Crack propagation

Crack growth experiments are also carried out at room temperature in laboratory air with a computer controlled servo hydraulic testing machine with CCT specimens in AA6056-T78 at different mean stress levels (R-ratio) following ASTM E 647. Cracks are initiated and propagated in the minimum of hardness for each specimen. This location is situated on the retreating side for both welding procedures but the distance to the weld center is 4,5mm for the conventional DLR joints and 8mm for the Bobbin Tool EADS-CRC F joints, respectively (see insert in Figure 54). Base Material data are provided by EADS-CRC F and referred to C(T) specimens.

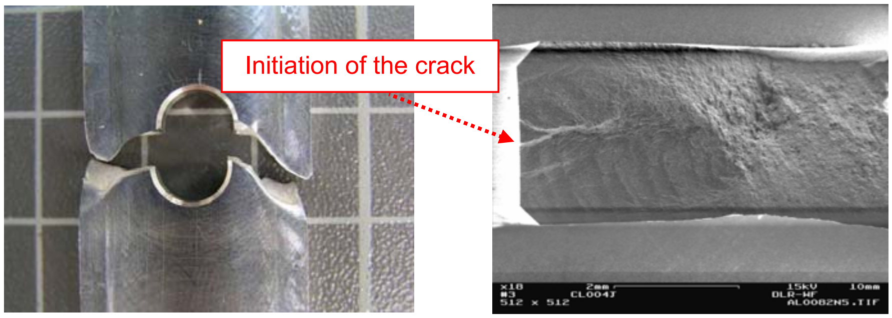

Figure 53: Fatigue Cracks (Kt=2.3) – example of post welded conventional DLR specimen

The tests reveal comparable behaviour for both technologies, at least in the post welded condition.

Differences between welded joints and base material are probably caused by internal residual stresses. Further investigations related to this effect are currently ongoing: residual stresses level and distribution will be estimated thanks to the “cut compliance method” for the calculation of ΔK_{eff} in case of the welded joints.

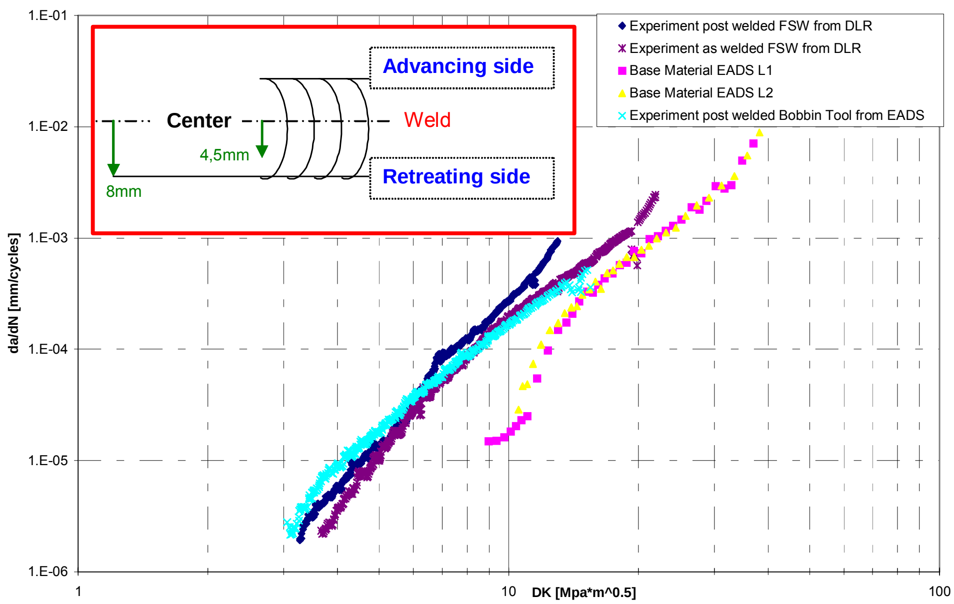

Figure 54: Crack propagation curves for AA6056-T78 and with stress ratio R=0,1.

5.11 Fatigue Behaviour of Fibre Metal Laminates with Friction Stir Welded Aluminium Sheets

R. Starikov (Airbus-D)

Fibre metal laminated material, GLARE®, is widely applied as a skin material for the upper and side shells in the forward and rear fuselage body of A380. In order to manufacture large GLARE® panels, the so called bonded splice concept was developed. In practice, splice design solutions are not standardized. Therefore, a specific design approach for each splice configuration is often required. In order to reduce the number of bonded splices and, therefore, to decrease design work and labour cost, the application of friction stir welding (FSW) in manufacturing GLARE® skin panels has been proposed. A screening program on the applicability of friction stir welding technique in manufacturing of GLARE® materials has been performed in collaboration between the German Aerospace Centre (DLR) and Airbus.

In order to investigate the effect of FSW on the fatigue behaviour of GLARE®, different number of crack initiation, crack propagation, and shear specimens were prepared with FSW Al-sheets and tested in fatigue (R = 0.1, room temperature). In addition, several skin panels with a dummy stringer were subjected to fatigue loading until different numbers of cycles and then quasi-statically loaded till failure in order to obtain residual strength data. The test results were compared with the fatigue properties of the base GLARE® material.

In general, the fatigue behaviour was similar between GLARE® with FSW Al-sheets and the base GLARE®. A comparison of the crack initiation results for FSW (closed dots) and base GLARE® (open dots) is shown below.

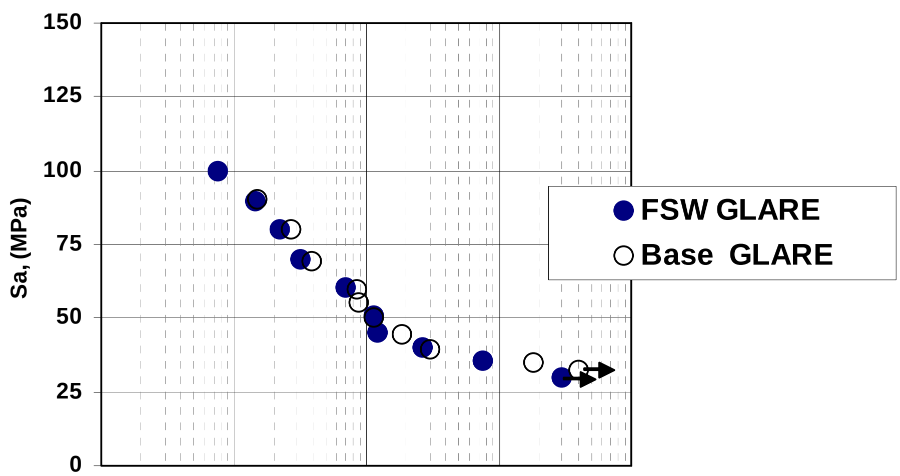

Figure 55: Crack initiation in FSW GLARE® and base GLARE®.

However, the behaviour of crack propagation specimens and skin panels with a dummy stringer was characterized by early multiple crack initiation in the FSW line. As fatigue loading proceeded the cracks grew and linked up together, cracking the FSW line. Since the FSW process had to be adjusted for each pair of Al sheets, different welding parameters could have influence on the quality of FSW, and therefore, on the behaviour of the specimens tested in fatigue. Hence, the FSW process should be optimised for thin Al-sheets.

The obtained results of the experimental screening program will be used as an input for a further systematic investigation to be performed in the near future.

5.12 Residual Stress Analysis of Laser and Friction Stir Welded Aerospace Aluminium Alloys

P. Staron, M. Koçak and W.V. Vaidya (GKSS)

The residual stress induced by the welding thermal cycles can have a significant effect on the fracture and fatigue properties of welds. Guidance on residual stress distributions for various joints is provided by some codes for consideration in flaw assessment. However, these residual stress distributions, usually presented in the form of a series of equations that were derived from either simple heat flow and residual stress generation models or experimental data, are mainly for conventional electric arc welds, but information on residual stress in any laser beam welds (LBW) or friction stir welds (FSW) is not mentioned. A recent review on residual stress distributions in welded joints by Stacey et al. [Incorporation of residual stresses into the SINTAP defect assessment procedure, *Engineering Fracture Mechanics*, 67 (2000) December 2000, pp. 573-611] summarised the data available in the public domain, again mainly for conventional welds but without information on LBW and FSW welds. Although FSW is a solid-state joining process and LBW produces exceptionally small fusion zone, significant levels of residual stresses can be present within and adjacent to the weld area. Clearly, there is a need to generate wide range of residual stress data on both LBW and FSW Al-alloys and investigate influence of residual stresses on the damage tolerance behaviour of these welds in butt- and T-joint configurations. Therefore, during the last years, GKSS has made a special effort in this direction within the framework of various national (e.g LuFo II programme) and European (WAFS, IDA, WELAIR) aerospace projects.

The use of non-destructive advanced residual stress measurement techniques such as neutron and synchrotron scattering provides a complete information on the nature of the residual stresses. A number of investigations undertaken with the neutron diffractometer ARES at the Geesthacht Neutron Facility (GeNF) at GKSS has provided information on the distribution of the residual stresses for:

- similar and dissimilar FSW joints in various heats and thicknesses of Al-alloys 2024, 6013, 6056
- the effects of CO_2 cooling and mechanical tensioning during the FSW process
- LBW butt-joints of 6013-T6, 6056 (T4, T6 and T78 tempers) in 3.0, 4.5 and 6.0 mm sheet thicknesses

Within the joint work with the BAE Systems-UK, it has been found that the mechanical tensioning parallel to the welding direction during the FSW process can generate compressive longitudinal stresses (contrary to the presence of the tensile stress peak) in the weld zone, Figure 56, and also leads to the reduction of the distortion of the FSW butt-joint welded Al-sheets. This has contributed to the process modification and optimasation.

The residual stress distribution of the 6 mm thick LBW 6056 is given in Figure 57, showing the magnitude of the tensile stress peak approaching to the yield strength (dotted line) of the sheet in as-welded condition. This information is being used for the process optimisation.

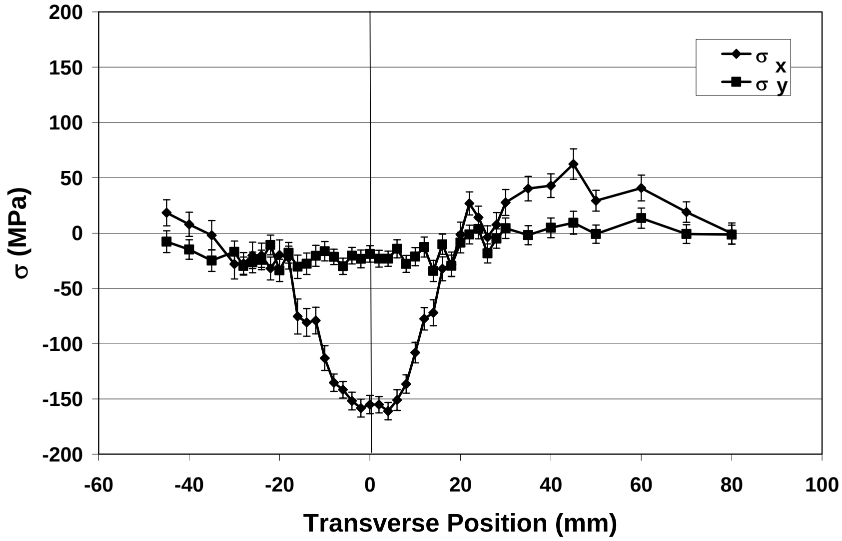

Figure 56: Presence of compressive residual stress in the FSW zone due to mechanical tensioning.

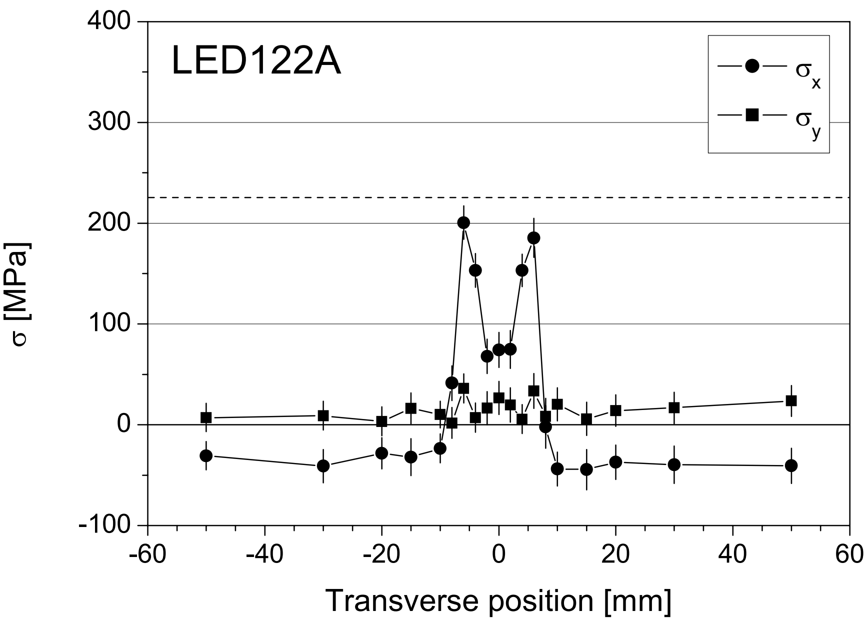

Figure 57: Residual stress distributions measured on 6.0 mm thick LBW 6056 sheets.

6 Fatigue and Fracture of Metallic Fuselage Materials

6.1 General Reserve Theory

L. G. Gelimson (RUAG)

For predicting fatigue and fracture of materials incl. metallic fuselage ones [1-3], it is necessary to realistically determine the reserves of the stress states vs. the critical ones. Usual safety factor [4] n_l as limiting stress σ_l divided by equivalent stress σ_e by a strength criterion [4] defines a limiting surface only and is not sufficient. By the second of the both equivalent approaches

$$F(\sigma_1, \sigma_2, \sigma_3) = \sigma_l,\ F^\gamma(\sigma_1, \sigma_2, \sigma_3)/\sigma_l^{\gamma-1} = \sigma_l;$$
$$\sigma_e = F(\sigma_1, \sigma_2, \sigma_3),\ \sigma_{e\gamma} = F^\gamma(\sigma_1, \sigma_2, \sigma_3)/\sigma_l^{\gamma-1};$$
$$n_{l\gamma} = \sigma_l/\sigma_{e\gamma} = \sigma_l^\gamma/F^\gamma(\sigma_1, \sigma_2, \sigma_3) = n_l^\gamma$$

takes on any positive values when choosing suitable values of γ and even by its common unit value can take on too optimistic and therefore very dangerous values. In example 1

$$(\sigma_1 = 250 \text{ MPa},\ \sigma_2 = 240 \text{ MPa},\ \sigma_3 = 210 \text{ MPa},\ \sigma_l = 235 \text{ MPa}),$$
$$n_l = 5.9,\ n_l\sigma_1 - \sigma_3/n_l = 1439 \text{ MPa} >> \sigma_l.$$

In example 2, a bar with strengths 100 MPa in tension (σ_t) and 800 MPa in compression (σ_c) is simultaneously contracted and stretched by two force pairs independently causing stresses

$$\sigma = \sigma^- + \sigma^+ = -500 \text{ MPa} + 400 \text{ MPa} = -100 \text{ MPa},$$
$$n_l = \sigma_c/|\sigma| = 8,\ n_l\sigma^- + \sigma^+/n_l = -3950 \text{ MPa} << -\sigma_c,\ \sigma^-/n_l + n_l\sigma^+ = 3137.5 \text{ MPa} >> \sigma_l.$$

The main idea [5, 6] to realistically determine the reserve of a system under consideration is separately taking the reserves of its original parameters into account, each of these reserves being expressed via a common additional number. It is obtained from the condition that, by the worst realizable combination of the values of these parameters arbitrarily modified within the bounds determined by the corresponding reserves, the state of at least one element of the system becomes limiting, no element of it being in an overlimiting state. In a general problem, for any function of an arbitrary set of variables, where (α) means that index $\alpha \in \mathrm{A}$ is optional,

$$z = f[_{\alpha\in\mathrm{A}}\ z_\alpha],\ Z = f[_{\alpha\in\mathrm{A}}\ Z_\alpha],\ z_{(\alpha)} \in Z_{(\alpha)}.$$

The genuine values of the independent variables, z_α, and of the dependent one, z, usually deviate from their values calculated. Those should belong to their admissible sets (domains), $[Z_{(\alpha)}]$, if the problem has certain limitations like strength criteria in strength problems. Otherwise, it is necessary to determine such a combination of the restrictions, Z_α, of the admissible sets, $[Z_\alpha]$, that $[Z]$ contains $f[_{\alpha\in\mathrm{A}}Z_\alpha]$. For the numeric measures of those restrictions, or the reserves of the independent variables, it is sufficient that, for any $\alpha \in \mathrm{A}$, $[Z_{(\alpha)}]$ is included into a certain Hilbert space, $L_{(\alpha)}$. It has the norm, $||z_{(\alpha)}||_{(\alpha)}$, of each element, $z_{(\alpha)}$, and the scalar product, $(z_{(\alpha)}, z'_{(\alpha)})_{(\alpha)}$, of each pair of elements, $z_{(\alpha)}$ and $z'_{(\alpha)}$. An additive approach extends the relative error and naturally determines the neighborhood, $Z_{(\alpha)}(\delta_{(\alpha)}, z_{0(\alpha)})$, of set $Z_{(\alpha)}$ with respect to element $z_{0(\alpha)} \in L_{(\alpha)}$ with error $\delta_{(\alpha)} \geq 0$ as the set of all $z'_{(\alpha)} \in L_{(\alpha)}$ with

$$||z'_{(\alpha)} - z_{(\alpha)}||_{(\alpha)} \leq \delta_{(\alpha)}||z_{(\alpha)} - z_{0(\alpha)}||_{(\alpha)}.$$

The additive reserve of set $Z_{(\alpha)}$ by set $[Z_{(\alpha)}]$ with respect to element $z_{0(\alpha)}$ is defined as

$$n_{a(\alpha)} = 1 + \sup\{\delta_{(\alpha)} \geq 0: Z_{(\alpha)}(\delta_{(\alpha)}, z_{0(\alpha)}) \subseteq [Z_{(\alpha)}]\}.$$

The multiplicative approach develops, generalizes, and extends the safety factor:

$$n_{m(\alpha)} = \sup\{n_{(\alpha)} \geq 1: Z_{(\alpha)}(n_{(\alpha)}\exp(i\varphi_{(\alpha)}), z_{0(\alpha)}) \subseteq [Z_{(\alpha)}]\}(0 \leq \varphi_{(\alpha)} \leq \pi).$$

By any of the both approaches, reserves n_α can be expressed via different nondecreasing functions of an additive reserve, n_{fa}, or a multiplicative one, n_{fm}, respectively, the both being common for reserves n_α and determined by the condition that there is an element $z \in Z$ in a limiting state by the worst realizable combination of all z_α:

$$n_{fa} = \sup\{n \geq 1: f[_{\alpha\in A}Z_\alpha(n_\alpha(n), z_{0\alpha})] \subseteq [Z]\},$$
$$n_{fm} = \sup\{n \geq 1: f[_{\alpha\in A}Z_\alpha(n_\alpha(n)\exp(i\varphi_\alpha(\ n_\alpha(n))), z_{0\alpha}) \subseteq [Z]\}.$$

For simply (proportionally) loading, the multiplicative reserve is obtained from the condition

$$F(n_{fm}\sigma_1, n_{fm}\sigma_2, n_{fm}\sigma_3) = \sigma_l.$$

By the equal reserves of all z_α, in example 1 we have for n_{fa} and n_{fm} 1.423 and 1.5, in example 2 for n_{fmt} in tension and n_{fmc} in compression 1.25 and 2, i.e., much less than n_l, which is very important for predicting fatigue and fracture of materials incl. metallic fuselage ones.

[1] Brunn, E. F.: Analysis and Design of Flight Vehicle Structures. Jacobs Publishing, Inc., Indianapolis (IN), 1973

[2] Military Handbook. Metallic Materials and Elements for Aerospace Vehicle Structures. MIL-HDBK-5H, 1998

[3] Handbuch Struktur-Berechnung. Prof. Dr.-Ing. L. Schwarmann. Industrie-Ausschuss-Struktur-Berechnungsunterlagen, Bremen, 1998

[4] Pisarenko, G. S. etc.: Manual de Resistencia de Materiales. Editorial MIR, Moscú, 1989

[5] Gelimson, L. G.: General Strength Theory. Abhandlungen der Wissenschaftlichen Gesellschaft zu Berlin, Publisher Prof. Dr. habil. V. Mairanowski, **3** (2003), Berlin

[6] Gelimson, L. G.: Elastic Mathematics. General Strength Theory. The "Collegium" International Academy of Sciences Publishers, Munich (Germany), 2004

6.2 Monotonic and Fatigue Fracture in Crack Propagation Tests

M. Broll, J. Bär, H.-J. Gudladt (UniBw-M)

To predict fatigue lifetime, in most cases, a linear damage accumulation after Miner [1] has been used. In case of specimens that contain micro- or macro-cracks increasing damage is given by the propagation of these cracks. Unfortunately, a simple linear damage accumulation cannot predict the fatigue lifetime for a load spectrum. Consequently, crack deceleration or crack arrest after a single overload in a sequence of constant amplitude loading have to be taken into account. At first a large amount of crack acceleration has been detected after a single overload. The further crack propagation is influenced by this phenomenon. The aim of this work was to focus on the comparison of crack growth during the overload cycle and the expected fatigue fracture based on crack propagation curves.

Fatigue tests have been undertaken with SEN – specimens of the aluminium alloy 6013 T 62. To estimate the actual crack length, a DC potential drop method has been used. The corresponding actual crack length measurement allows crack propagation tests under the control of the stress intensity factor K. The latter has been named K constant loading. These tests lead to a constant crack growth velocity. Therefore they are more sensitive even to small influences to crack propagation than tests with constant amplitude loading where both, the stress intensity factor and the crack growth rate, increase with increasing crack length. A single overload leads to a crack growth acceleration during one half-load cycle and is continued by a large amount of da/dN – deceleration. Consequently, a benefit on total life time has been found [e.g. 2].

The crack growth curves in Figure 58 show a crack growth rate of about 10^{-8} m per cycle for a loading of ΔK = 12 MPa√m for a stress ratio of R = -1. A single overload at R = -1 with an amplitude of 3 times to the basic load leads to a ΔK = 36 MPa√m for one load cycle and, consequently, to an expected fatigue fracture of 0.8 µm per cycle. In Figure 59 the crack length relative to the mean stress of basic loading versus time relative to the overload can be seen. The difference between the maximum of basic loading and the maximum of the overload clearly shows a crack growth of Δa_B = 33.9 ± 0.5 µm during the overload cycle. This is about 42 times greater than the expected fatigue fracture. In addition, tests show that the structure of the fracture surface changes during the overload [3]. After a sufficient amount of cycles, crack propagation as it has expected for cyclic loading at the given load level was found. This amount depends on the stress ratio of basic loading and overload, furthermore on the level of basic loading. Therefore the crack propagation during the overload cycle can be seen as a monotonic fracture. During the first half cycle of overload the crack propagation can be described by a classical concept of fracture mechanics.

Further tests will be done to examine and understand the difference of fatigue and monotonic fracture in more detail and to describe the fracture behaviour in the light of an energy concept.

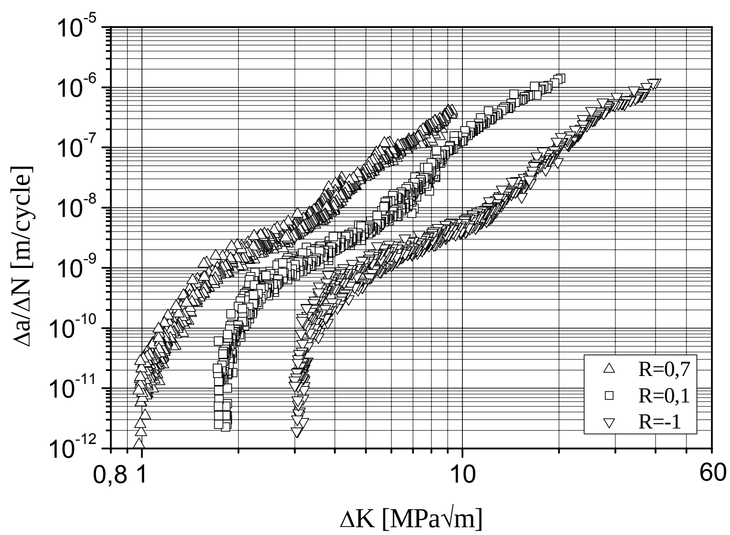

Figure 58: Crack propagation curves of AA 6013 T62 in ambient air [3]

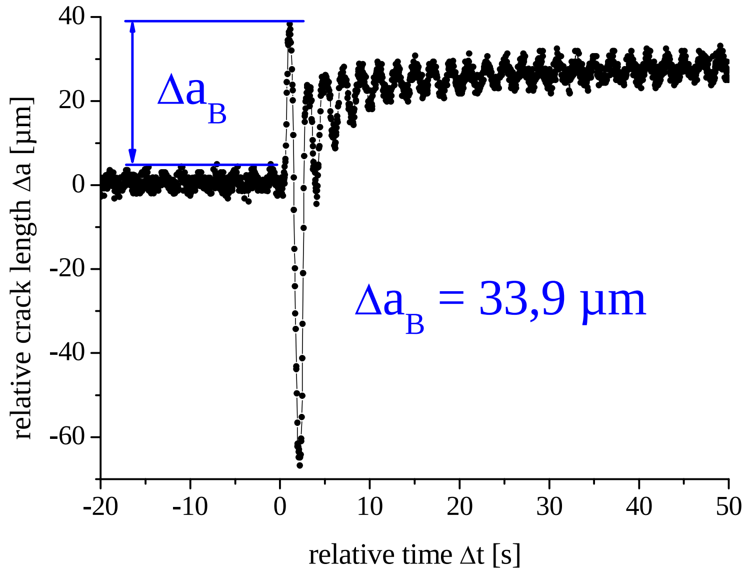

Figure 59: Relative crack length Δa versus relative time Δt after a symmetric overload of 200% in a sequence of a basic loading of ΔK = 12 MPa□m. The crack length is calculated from potential drop method.

[1] Miner M., Cumulative damage in fatigue, Journal of Appl. Mechanics (1945), pp. 159-169

[2] Suresh S., Fatigue of Materials, Second Edition, Cambridge University Press (1998)

[3] Rödling S., Einfluss von Überlasten auf das Rissausbreitungsverhalten von Aluminiumlegierungen aus dem Bereich der Luft- und Raumfahrt, Ph. D. thesis, University of the Armed Forces Munich (2003)

6.3 Positron Lifetime Measurements as a Tool for Damage Analytics: Defect Structures in Cyclically Deformed and in Monotonically Fractured Hardenable Al-Alloys

W. Egger, G. Kögel, P. Sperr and H.-J. Gudladt (UniBw-M)

For models of fatigue-lifetime prediction it is essential to determine a proper damage parameter. The determination of this parameter requires an accurate knowledge of defect structures on a microscopic scale.

Slow positrons are very sensitive probes to analyse small open volume defects, e.g. vacancies, vacancy clusters, and dislocations. The positron annihilation rate is related to the electron density at the annihilation site and, consequently, different lifetimes, characteristic for the type of defect and the material are observed in positron lifetime spectroscopy.

A modern positron beam technology allows to investigate defect structures in the sub-μm range in positron lifetime measurements: In a pulsed positron beam experiment, monoenergetic positrons are implanted into the sample. The mean positron implantation depth depends on the beam energy and on the density of the sample. By varying the beam energy, it is possible to analyse the defect structure in a layer which extends from the surface to approximately a micrometer in depth. The time between the arrival of the pulse and the annihilation photon is measured and yields an exponential decay spectrum. At present, from this spectrum up to three lifetimes and their corresponding intensities can be determined. Consequently, three different types of defects can be simultaneously studied.

Two positron beam systems were developed at our university: a pulsed low energy positron source (PLEPS), and a scanning positron microscope (SPM). The PLEPS allows for depth profiling of defect layers with a pulsed monoenergetic beam of several mm diameter that operates within a positron energy range of 0.5-20 keV. Additional, very high lateral resolution (>2μm) can be achieved with the SPM. Consequently, the PLEPS can be used for investigations of crack surfaces and the SPM for investigations of defect structures at arbitrary distances from the crack, as illustrated in Figure 60 [1].

This technique has been tested on samples of pure copper and a peak-aged Al-Mg-Si alloy (Al 6013). In the corresponding case study the defect distributions close to crack surfaces created by monotonic and cyclic deformation have been investigated with PLEPS and SPM:

In the fatigued samples, besides a high dislocation density, a high concentration of large vacancy clusters close to the fatigue crack has been observed, whereas a high dislocation density, but no vacancy clusters have been found in the monotonically fractured sample [2,3].

The presence of small vacancy clusters seems to be characteristic of the cyclic deformation process. If this observation holds as a general rule, positron lifetime spectroscopy allows distinguishing quantitatively monotonic from fatigue fracture without any further fractographic studies. Finally, the quantity of damage, identified by these vacancy clusters offers the possibility to gain a better understanding of the damage development und allows improving damage accumulation models.

Figure 61 shows the mean positron lifetime as a function of the mean implantation depth as obtained by PLEPS for differently treated Al 6013 specimens: At higher energies the sample in the as received state shows a mean lifetime of 220 ps. Here, all positrons were trapped in Mg/Si-clusters. The monotonically fractured sample shows a higher mean lifetime of 240 ps. Again, all positrons were trapped in the same kind of defect, in this case dislocations. The fatigued sample, however, shows an even higher mean lifetime. A decomposition of the mean lifetime into two different lifetimes was possible, corresponding to a high concentration of dislocations and the presence of vacancy clusters. The increase in the mean lifetime at lower energies is due to back-diffusion of positrons to the surface, and a consequently increasing admixture of a longer lifetime typical for the annihilation in the surface zone. From the intensity variation with the mean implantation depth of this surface lifetime it is possible to determine the defect concentration, if the type of defect and its trapping coefficient is known [4].

Figure 62 shows a positron mean lifetime map of the crack-tip region as registered with the SPM. Close to the crack tip almost all positrons are trapped in dislocations, whereas in the more distant regions most positrons are trapped in precipitates. From this data it was possible to estimate the mean dislocation density in the near crack-tip region.

In the near future the two beam systems will be moved at the new reactor FRM-II. The highly increased count rate and, consequently, much better statistics obtainable in much shorter measuring times will make these instruments invaluable tools for damage analytics [5].

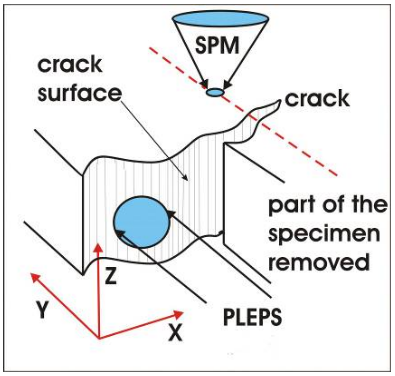

Figure 60: Employment of PLEPS and SPM in the investigation of a cracked specimen.

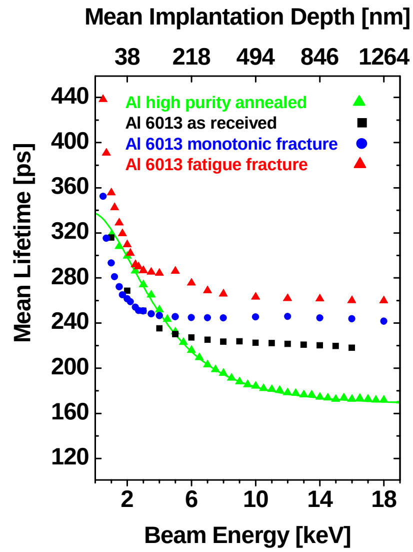

Figure 61: Mean positron lifetime as a function of mean implantation depth.

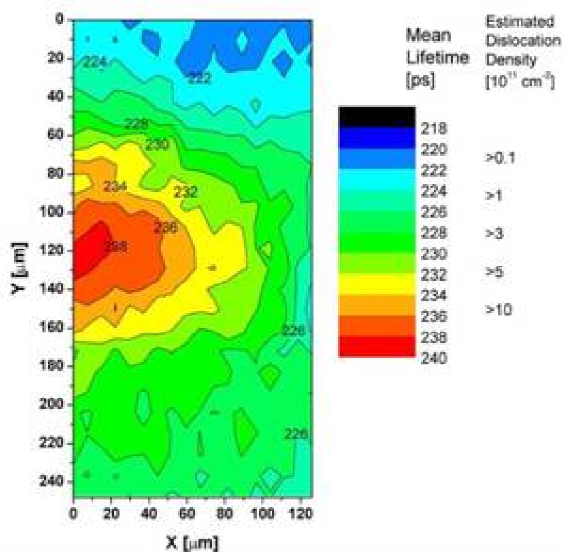

Figure 62: Positron lifetime map close to a crack tip in Al6013

[1] W. Egger, G. Kögel, P. Sperr, W. Triftshäuser, J Bär, S. Rödling, H.-J. Gudladt, Z. Metallkd. 94 (2003) 687
[2] G. Kögel, W. Egger, S. Rödling, H.-J. Gudladt, Mat. Sci. Forum 445-446 (2004) 126
[3] W. Egger, G. Kögel, P. Sperr, W. Triftshäuser, J Bär, S. Rödling, H.-J. Gudladt, Mat. Sci. Eng. A 387-389 (2004) 317
[4] A. Dupasquier, G. Kögel, A. Somoza, Acta Mat. 52 (2004) 4707
[5] G. Kögel, G. Dollinger, submitted to Appl. Surf. Science A

6.4 New Testing Procedure to Determine da/dN- ΔK Curves at Different, Constant R-Values Using one Single Specimen

A.Tesch (DLR), R.Pippan (Austrian Acad. Of Science) and H.Döker (DLR)

A new concept for fatigue crack propagation tests has been developed. With this concept it is possible to gain fatigue crack growth curves (da/dN-ΔK) for every R-ratio between R=0,9 and R= -1 with a single specimen. Figure 63 shows the important steps in this concept. The basis of the concept is a line up of step wise increasing constant K_{max}-tests. These tests were originally developed to get threshold values for the stress intensity range ΔK at high stress ratios R and without load history effects. Therefore the K_{max}-values in this type of tests are quite high (e.g. 20, 30 $MPam^{1/2}$ for Al-alloys) and the starting R ratios are bigger than 0,5. In the new testing procedure the starting values for R were always negative (R < 0) and the K_{max}-values were increased in steps from 3 $MPam^{1/2}$ up to 40 $MPam^{1/2,}$ as sketched in Figure 63a. The results are da/dN-ΔK curves (Figure 63b) with varying R-values, which cover the whole fatigue region from R= -1 to R=0,9. By laying straight lines at constant ΔK-values and transferring the intersection points with the da/dN-ΔK curves to a diagram da/dN vs. R, a set of curves is gained as shown in Figure 63c. From this diagram da/dN-ΔK curves with constant stress ratio R for every R-value can be generated. At the desired constant stress ratio R a straight line is drawn (See Figure 63c) and the intersection points with the da/dN-R curves are plotted in a graph da/dN vs. ΔK (Figure 63d). The da/dN-ΔK curves generated from the K_{max} constant tests fit very well to the da/dN-ΔK curves generated with different specimens, according to the procedures described in the ASTM Standard E 647. Additionally the new concept also provides thresholds values for fatigue crack growth. The tests were performed under computer control on servo hydraulic testing machines. The crack length was measured with the DC potential drop method. The program was developed by INSTRON according to DLR requirements. The program allows, amongst other things, the automatic performance of a series of constant K_{max}-tests. In combination with an automated crack length measurement tool like the DC potential drop method, these tests can be run with little expenditure in personnel and testing time.

In Figure 64 the da/dN -ΔK curves generated with the new testing procedure are compared to da/dN tests performed according to ASTM E647. The correlation is perfect from the threshold region up to crack growth rates of 10^{-3} mm/cycle. It should be noticed, that the da/dN -ΔK data from the K_{max}-constant tests are obtained with decreasing ΔK in contrast to the da/dN -ΔK data obtained from the da/dN tests, where the ΔK is increasing.

The monotonic plastic zone in front of the crack tip is constant during each test, because the maximum stress intensity is constant. This ensures that there are no load history effects due to plasticity induced crack closure. As a fact one can use much higher ΔK decreasing rates as for threshold test according to ASTM E647. Nevertheless all essential requirements of the standard are satisfied. The authors thank Airbus Deutschland for the provision of the testing material.

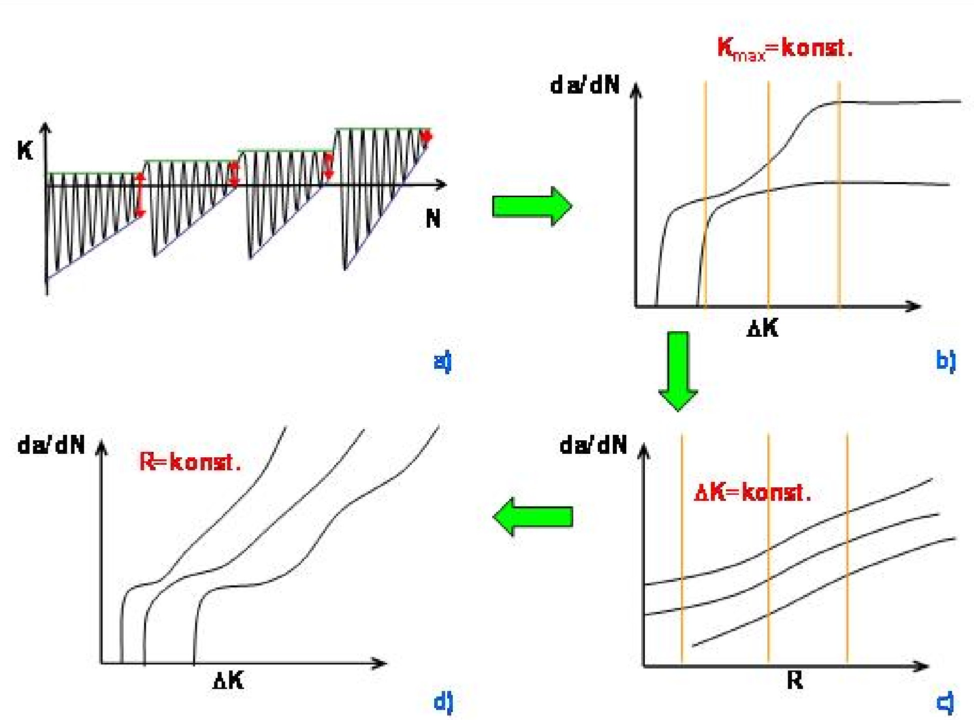

Figure 63: The basic steps of the new testing procedure.

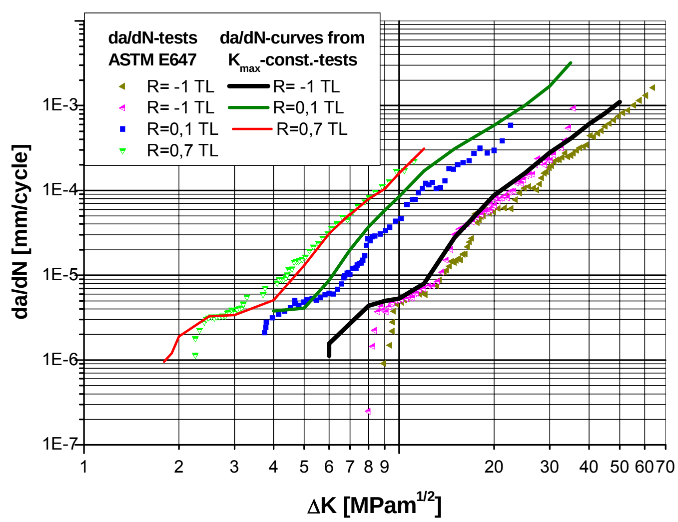

Figure 64: Comparison of the da/dN-ΔK curves generated with the new testing procedure with da/dN tests performed according to ASTM E647.

6.5 Short Crack Growth Al 2524-T351 and Al 6013-T6

A.Tesch, H. Döker and K.-H. Trautmann (DLR), R.Pippan (Austrian Acad. Of Science), C. Escobedo (Airbus-D)

In a joint research project of AIRBUS in Hamburg and the Institute of Materials Science of the German Aerospace Centre (DLR) in Cologne basics of the Initial Flaw Concept were investigated. This three-year project, which started in January 2002, included the following tasks:

1. Literature study on the crack growth behaviour of short and small cracks
2. Characterisation of the materials (tensile tests, da/dN- ΔK curves at different R-ratios, thresholds for crack growth, both for long cracks)
3. Investigation of the behaviour of short and small cracks emanating from a rivet hole (influences of different R-ratios, residual stresses, loading spectra)
4. Investigation of the behaviour of short and small cracks emanating from a rivet joint
5. Modelling the short and small crack behaviour and generating an analytical computer code to predict the fatigue life of components.

The goal of the project was to develop analytical tools to calculate the crack growth of short and small cracks in structures.

The experimental investigations were performed with the Aluminium alloys Al 2524-T351 and Al 6013-T6. Crack growth tests were performed according to ASTM E647 with M(T) (middle cracked tension) specimens under computer control on closed loop servo-hydraulic testing machines at room temperature in laboratory air. The load wave form was sinusoidal at a test frequency of 30-50 Hz.

First, long crack test data were obtained to characterise both materials. A comparison of the da/dN-ΔK curves for different R-ratios is shown in Figure 65.

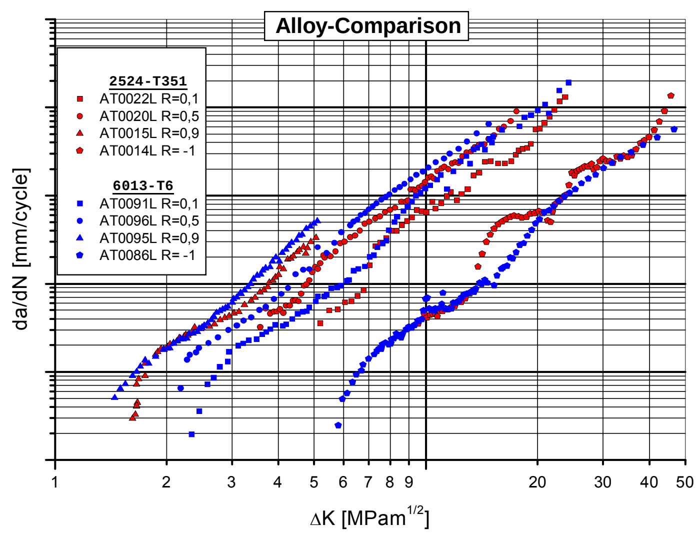

Figure 65: Comparison of the fatigue crack growth behaviour of long cracks in Al 2524-T351 and Al 6013-T6

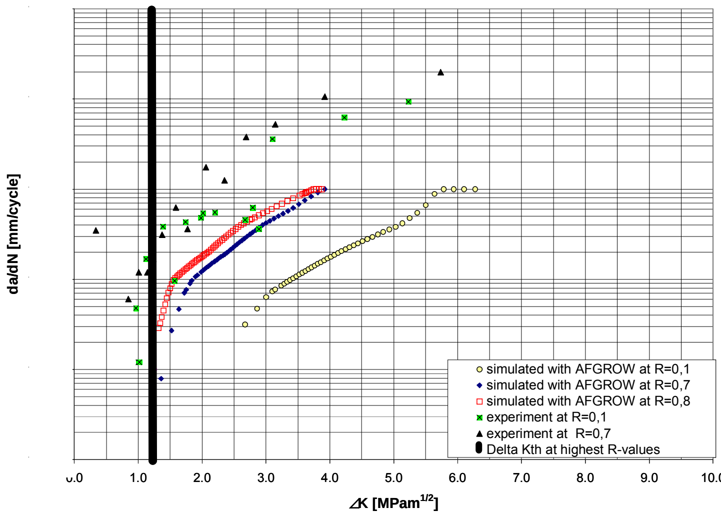

Figure 66: First short crack growth results for different stress ratios R, compared with simulated corner cracks based on long cracks growth data for 6013-T6.The black line defines the scatter band for the highest ΔKth-values.

Second, short corner cracks were introduced into the specimens at one side of the rivet hole by compression loads (R=20). The length of the cracks varied between 30µm and 200µm.

In Figure 66, first results of the tests with short corner cracks are compared with the long crack test data mentioned in the previous paragraph for the 6013 T6 alloy . The AFGROW simulation of the da/dN- ΔK curves is based on long crack growth data. The stress intensity factor solution used in the simulation was for a corner crack at a hole. The stress intensity factors for the experimental data were calculated with the same formula as in AFGROW, but for the crack growth rates the optically measured crack lengths were used. Five important differences can be seen in this comparison in Figure 66:

1. Short cracks grow at ΔK values below the threshold for long cracks at the same stress ratio R.
2. At the same ΔK-values short cracks propagate with crack growth rates approximately 10 times faster than simulated with the long crack data.
3. The difference in the crack propagation rate between the experimental data and the simulated data becomes bigger at smaller R-ratios.
4. The short crack growth is not influenced by the stress ratio R.
5. The threshold value for short crack growth (~1MPam$^{1/2}$) is just a little bit smaller than the threshold for long cracks (~1,2 MPam$^{1/2}$) at the highest stress ratios (0,965<R<0,985) reachable in experiments.

6.6 Crack Turning on Aeronautical Structures

Ll. Llopart and E. Hombergsmeier (EADS-CRC)

Integral structures offer weight reduction, cost savings and more corrosion-resistance compared with differential structures. However, integral structures have lower damage tolerance; skin crack slows more when crossing a mechanically fastened stiffener than an integral stiffener.

On 1991 crack turning was identified as an arrest criterion (Kosai). Besides, during tests on thin skinned relatively narrow-body fuselages, crack turning was observed to occur reliably enough (Pettit), which allows and arguments the use of crack turning on thin skinned fuselages as a promising behaviour to improve damage tolerance.

The aim of this investigation is to provide a tool and a reliable criterion to asses and predict crack turning under pure Mode I loading on three dimensional structures. The deliverables should permit to evaluate design modifications on structural behaviour, specially its influence on crack turning, which will be helpful to increase damage tolerance of integral structures.

First a screening on the existent tools was carried out regarding fracture mechanics capabilities on three dimensional models, design abilities, implementation capacity as well as "easy to use" conditions. The more performing software were analysed and compared. The best option congruent with the pre-defined conditions was purchased and implemented according to the need of the existent crack turning criteria. Its reliability was satisfactorily proved by means of literature and test data.

In order to evaluate the existing crack turning criteria specially under pure Mode I loading, crack propagation tests and simulations, both under stable tearing and dynamic loading, were carried out on 2024-T3 Double Cantilever Beam-DCB and cruciform-CFS specimens.

Modelling analysis showed that boundary conditions, notch effect and other details have a great influence on the crack path predictions ,Figure 67. Moreover, the existing criteria can be divided on four general groups, regarding its path prediction.

Effects due to orthotropy and three dimensional modelling seems to be relevant on crack path and they are in process to be analysed, moreover a combination of criteria seems to be needed to have a reliable assessment on crack turning phenomenon under pure Mode I loading.

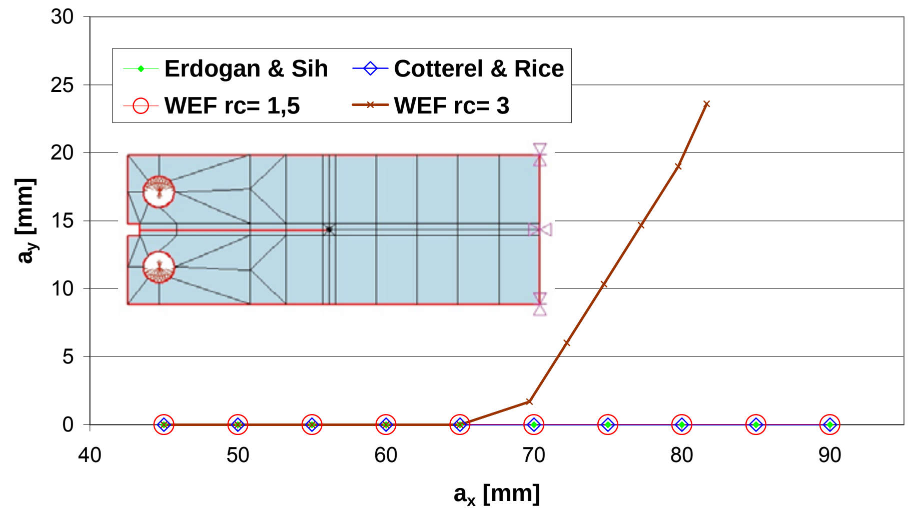

Figure 67: Crack prediction using symmetric boundary conditions.

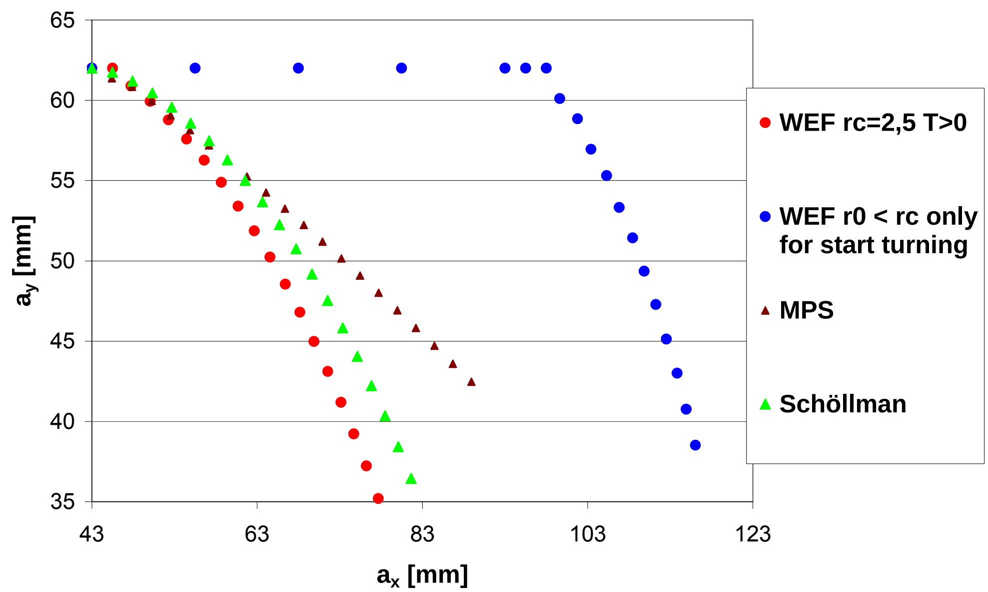

Figure 68: Crack prediction taking into account real boundary conditions and notch effect

7 Fatigue and Fracture of Composites

7.1 Critical State Theory

L. G. Gelimson (RUAG)

For predicting fatigue and fracture of composites [1-3], the critical (limiting, i.e., yield, ultimate, etc.) stresses are usually determined via common strength criteria [4]. None of them applies to arbitrarily anisotropic materials under variably loading (process) with turning the directions of the principal stresses. To generalize [5,6] them, each unordered stationarily indexed principal stress is synchronously reduced via dividing by the modulus of its uniaxial limiting value of the same sign in the same direction. The adequate combination of the ranges of triaxial stress processes stationarily and variably safe is defined with choosing the most dangerous, possibly depending on time, permutations of stationary indexes and with correcting by introducing additional material constants, e.g., to fit the substantial influence [7] of the intermediate normal stress and/or the ratio of the limiting normal and shear stresses. Such universal laws of nature hold for any material arbitrarily loaded and were successfully tested along with these generalization methods. The stress transformations reduce time and money expenses due to consolidating experimental data for distinct materials and are necessary by different strengths in tensions and compressions. This is shown here for data [8] on diverse isotropic ductile and brittle materials in biaxial stress state in the relative principal stresses r_1, r_2 , Figure 69, and in the principal stresses σ_1, σ_2 divided by the limiting stress σ_t in uniaxial tension, Figure 70.

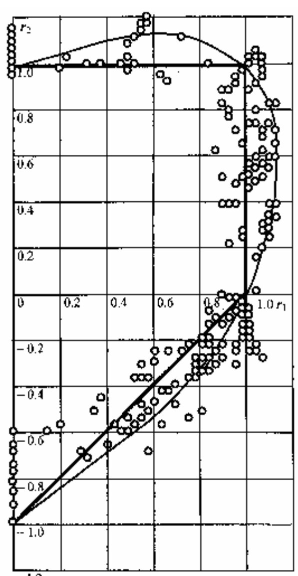

Figure 69: Data of [8] in terms of relative principal stresses compared to maximum shear stress and of distortion energy criteria.

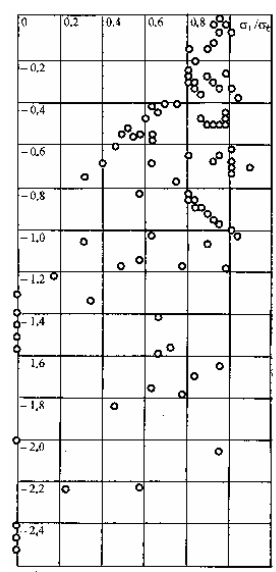

Figure 70: Data of [8] in terms of principal stresses compared to maximum shear stress and of distortion energy criteria.

Here the broken line and the curve show the criteria [4] of the maximum shear stress and of distortion energy, respectively. In the reduced form, the both give values coinciding with theoretical data and fitting many experimental ones [8] for the ratio of the limiting stresses in tension and pure shear. The last criterion determines the applicability range (formerly vague) of the internal friction criterion [4] and naturally generalizes the Hu-Marin criterion [8] for orthotropic materials under static loading, the principal directions of a stress state coinciding with the basic orthotropy directions at the same solid's point.

[1] Brunn, E. F.: Analysis and Design of Flight Vehicle Structures. Jacobs Publishing, Inc., Indianapolis (IN), 1973

[2] Military Handbook. Metallic Materials and Elements for Aerospace Vehicle Structures. MIL-HDBK-5H, 1998

[3] Handbuch Struktur-Berechnung. Prof. Dr.-Ing. L. Schwarmann. Industrie-Ausschuss-Struktur-Berechnungsunterlagen, Bremen, 1998

[4] Pisarenko, G. S. etc.: Manual de Resistencia de Materiales. Editorial MIR, Moscú, 1989

[5] Gelimson, L. G.: General Strength Theory. Abhandlungen der Wissenschaftlichen Gesellschaft zu Berlin, Publisher Prof. Dr. habil. V. Mairanowski, **3** (2003), Berlin

[6] Gelimson, L. G.: Elastic Mathematics. General Strength Theory. The ”Collegium” International Academy of Sciences Publishers, Munich (Germany), 2004

[7] P. W. Bridgman, Collected Experimental Papers, Vols. 1 to 7, Harvard University Press Publ., Cambridge (Massachusetts), 1964

[8] Pisarenko, G. S., and Lebedev, A. A.: Deformation and Strength of Materials in Complex Stress State, Izd. Naukova Dumka, Kiev, 1976 (Russ.)

8 Fatigue and Fracture of Engine Materials and Structures

8.1 Realistic Fatigue Testing of Gas Turbine Blade Materials

M. Bartsch, B. Baufeld, S. Dalkiliç, K. Mull and C. Sick (DLR)

Gas turbine blades for aircraft engines are made from high performance super alloys and coated with metallic and often additional ceramic protective layers. The service lifetime of the component is determined by simultaneously acting and interacting damage processes. Verification of the reliability of the component requires realistic testing of the respective material systems, in order to make sure that lifetime determining mechanisms under testing conditions are the same as in real engines.

Test facilities for Thermal Gradient Mechanical Fatigue (TGMF)

For simulating the service conditions of rotating gas turbine blades a new and unique testing facility has been designed and built [1]. The thermal and mechanical fatigue load occurring during an entire flight cycle, including start, cruising, landing and shut off, can be applied on test specimens. Besides simultaneous cyclic thermal and mechanical loading, a high thermal gradient over the wall of tubular specimens can be applied by external radiation heating and internal air cooling, similar to internally cooled gas turbine blades. In the case of specimens coated with a ceramic thermal barrier the maximum temperatures at the ceramic surface are about 1050° to 1100°C. Because of the controlled thermal gradient over the specimen wall the test cycles are called 'thermal gradient mechanical fatigue' or TGMF-cycles. High heating and cooling rates are achieved by a radiation furnace with concentrating mirrors combined with external air cooling using a shutter technique. The new TGMF facility is shown in Figure 71.

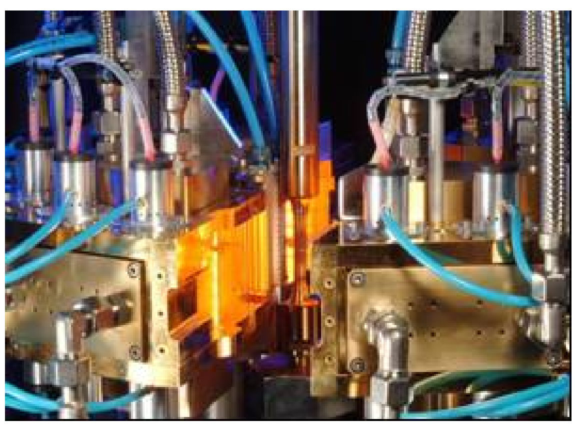

Figure 71: Open radiation furnace (16kW) with clamped specimen

Failure and damage features

The combined thermal and mechanical loading results in local microstructural and chemical changes and damages. The high thermal gradient over the wall of the specimen or the turbine blade, respectively, induces high multiaxial stresses, which are determined by the resultant strain and the mismatch of the physical properties of the substrate and layer materials.

One important damage feature of metallic oxidation protection coatings is rumpling of the surface. Rumpling is drastically enhanced in thermomechanical laboratory testing if a thermal gradient is imposed, which generates multiaxial compressive stresses in the metallic coating, Figure 72 [2].

Thermal barrier coating (TBC) systems on turbine blades often fail by spallation near the interface between ceramic topcoat and underlying oxidation protection layer. In laboratory the complex TGMF cycle results in specific damages, e.g. enhanced TBC spallation due to fatigue cracking parallel to the metal/ceramic interface [3]. Because of their specific feature we called this fatigue cracks 'smiley cracks' Figure 72. Analyses of damage features combined with mechanical analyses by means of finite element methods are used to elucidate the damage mechanisms.

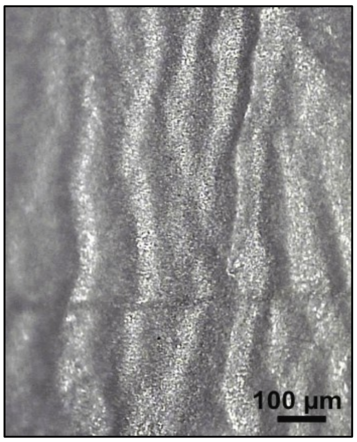

a)

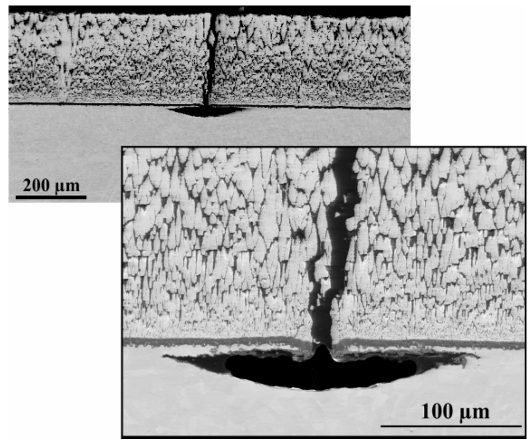

b)

Figure 72: Specific damages features in TGMF-testing, a) rumpling of the surface of a metallic protective coating, b) fatigue cracks in TBC-system, 'smiley crack'.

Lifetime assessment and damage parameter

Failure of the TBC by spallation of the coating requires in realistic testing a high number of about 5000 to 10000 cycles, comparable to the number of flights in service which the TBC system has to survive. In order to achieve reasonable testing times for lifetime assessment, the damage status as function of the loading history needs to be characterized in terms of life consumption long before failure. For the case of final failure by spallation of the ceramic top coat, it is proposed to use the apparent interfacial fracture toughness as damage parameter. Several methods for measuring the apparent fracture toughness of brittle coatings are under investigation with respect to their application to TBC systems [4].

[1] http://www.dlr.de/wf/forschung/htss/wdschichten/pruefung
[2] Bartsch, M and Baufeld, B.: Effects of Controlled Thermal Gradients in Thermal Mechanical Fatigue, *Proceedings of the 5th International Conference on Low Cycle Fatigue*, DVM-Verlag 2004, 183-188.
[3] Bartsch M., Baufeld B., Dalkilic S., Mircea I.: Testing and characterization of ceramic thermal barrier coatings, *Materials Science Forum* Vol. 492-493 (2005) 3-8.
[4] Bartsch M., Mircea I., Suffner J., Baufeld B.: Interfacial fracture toughness measurement of thick ceramic coatings by indentation, *Key Engineering Materials* Vol. 290 (2005) 183-190.

8.2 Low Cycle and Thermo-mechanical Fatigue Behaviour of Niobium Enhanced Intermetalic γ-TiAl alloy of the Third Generation

V. Bauer and H.-J. Christ (USI)

Titanium aluminides provide a suitable alternative to conventional alloys for high temperature applications in advanced energy conversion systems because they combine desirable properties such as low density with high specific strength and stiffness up to 800°C. However, low ductility at room temperature, poor fracture toughness and insufficient oxidation resistance at temperatures above 700°C have limited the use of γ-TiAl based alloys. In past attempts have been made to reduced these disadvantages by additions of specific alloying elements and microstructural modifications. The third generation of γ-based titanium aluminide alloys is characterised by a high oxidation resistance, improved toughness and fairly high ductility. Those properties are achieved by adding 5-10% of Nb.

Since γ-TiAl alloys are intended for use in high-temperature components such as blades in jet engine which are exposed to complex mechanical and thermal load interactions during start-up and shutdown of the technical system, it is necessary to evaluate not only the high-temperature low-cycle fatigue properties but also the resistance to thermomechanical loading.

In this project primarily low-cycle fatigue (LCF) tests where conducted on γ-TiAl alloy with fine duplex microstructure in order to quantify the role of temperature, total strain range, and environment on the deformation behaviour and on the fatigue life. The temperature was varied between 450°C and 800°C and the strain amplitude was varied between 0.3 and 0.6%. Also the effects of strain rate were investigated by conducting the test at two different strain rates of $\dot{\varepsilon} = 4 \cdot 10^{-3} s^{-1}$ and $\dot{\varepsilon} = 1 \cdot 10^{-4} s^{-1}$. Furthermore in order to eliminate the environmental effects on fatigue life fatigue tests at highest strain amplitude were conducted in high vacuum.

In addition thermomechanical fatigue (TMF) tests were performed at a strain amplitude of 0.6% in temperature regions of 450-700°, 500°C-750°C and 550-800°C both in-phase (IP) and out-of-phase (OP) testing mode. OP-tests were performed in vacuum environment too.
The results of the investigation on niobium-alloyed γ-TiAl can be summarised as follows:

The alloy exhibits (compared to previous γ-TiAl alloys) a higher Brittle to Ductile Transition Temperature BDTT at a value of about 750°C. This enables a higher service temperature due to a better creep resistance.

During LCF tests, high plastic deformation of the alloy at high strain amplitudes combined with reasonable fatigue life was observed, Figure 73. The reduction of staking fault energy by adding niobium to the alloy leads to increased formation of mechanical twins and consequently a higher deformability at elevated temperatures as microstructural observations revealed. At lower temperatures the deformation in the two-phase γ-TiAl alloys takes place predominantly in the γ-grains by the slip of ½ <110]-dislocations and dislocation bundles as well as net structures can be detected.

During the TMF deformation both high density of mechanical twins and net and bundle dislocation structure were observed. Also the stress response in the first cycles was comparable with stress values at the same temperature under isothermal conditions. Hence a pseudo isothermal life increases with temperature at lower strain amplitudes, and with increasing strain amplitude the deformation behaviour at beginning of the TMF tests can be assumed.

The fractographical analysis showed that in the isothermal case at lower temperatures and strain amplitudes cracks initiat inside the specimen at the γ-grain clusters or at irregular large lamellar grains. At higher temperatures, crack initiation is oxidation or environmental induced and takes place at the surface. The fatigue fatigue life shows a maximum at 650°C, Figure 73. The TMF results revealed that thermomechanical loading conditions can be considered crucial for the design of γ-TiAl components, Figure 73. In particular, OP loading conditions reduce fatigue life tremendously if compared with the isothermal loading conditions at any temperature within the temperature range of TMF. The short life can be attributed to the accelerated oxidation-induced crack initiation during OP testing. At high temperature an oxide layer is formed which becomes brittle at lower temperatures. In the low temperature part of the cycle (tension) the oxide cracks easily and hence promotes crack initiation. In contrast the IP-life is higher than that under isothermal conditions. The reason might be found in the high value of negative mean stress and in the softening behaviour at high temperature which was observed during the deformation process.

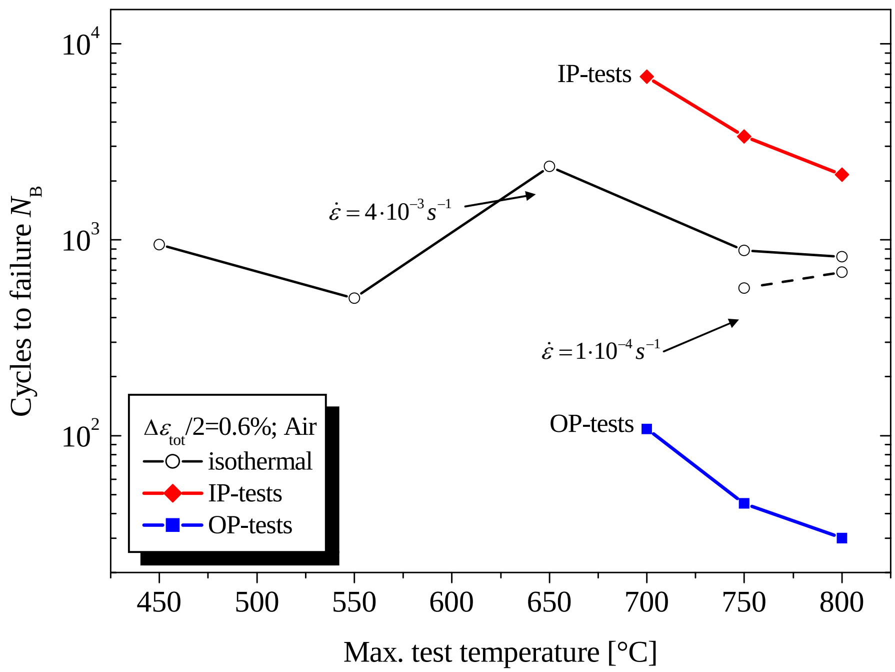

Figure 73: Fatigue life results in dependence on maximal test temperature for isothermal and thermomechanical tests

8.3 Effect of Dwell Times on Fatigue Crack Propagation in the Nickel-Base Superalloy IN 718 – A Study of Dynamic Embrittlement

Ph. E.-G. Wagenhuber and U. Krupp (USI)

The field of high-temperature application of polycrystalline superalloys such as IN 718 is versatile with aircraft turbines or land based turbine constructions as a typical example. An advantage of the superalloy IN 718 is its excellent oxidation resistance due to the high concentration of Chromium and the presence of the BCT γ''-phase (Ni_3Nb) which gives the material a high strength by the addition of 5.1% of Niobium. Further properties, which make the material attractive for engineering application, are good weldability and a maximum service temperature of around 800°C. The favourable cost/performance ratio of IN 718 compared to cobalt-base superalloys means that it is the preferential choice for traders.

Demands to increase the efficiency of turbine applications has resulted in the requirement for higher service temperatures which in turn leads in the case of the alloy 718 to a change in the fracture mode from transgranular to brittle intergranular either if the frequency is decreased or if a dwell time at the maximum stress or strain value of the low-cycle fatigue (LCF) loop is present. The aim of this study is to investigate the environmental effect on the LCF behaviour of IN 718 by applying an increasing dwell time and to show that the governing failure mechanism is “dynamic embrittlement” [1], i.e., diffusion of oxygen into an elastically high-stressed grain boundary ahead of the crack tip lowering the cohesion and eventually leading to crack propagation.

On specimens that were taken in circumferential direction from a forged ring of the alloy IN 718 LCF tests were carried out at a temperature of T=650°C, a total strain amplitude of $\frac{\Delta\varepsilon}{2} = 0.7\%$ and a strain rate of $\dot{\varepsilon} = 3.57 \cdot 10^{-4}$. Prior the LCF tests, the material was solution heat treated for one hour at 1050°C and water quenched, afterwards aged at 718°C for 12 hours, furnace cooled to 620°C and held for 12 hours and finally air cooled to room temperature to get the alloy hardened by the γ’ (Ni_3Al,Cr) and γ’’ (Ni_3Nb).

The impact of applying a dwell time can be seen in Figure 74. SEM studies of the fracture surface revealed a predominantly transgranular fracture mode without dwell time exhibiting fatigue striations Figure 74a compared to the dwell-time tests where the fracture mode changed to time-dependent intergranular cracking, Figure 74b. Figure 74c shows that cyclic stress relaxation occurs and an increasing dwell time leads to a dramatic decrease of the number of cycles to failure.

Further investigations are planned within the scope of the project to describe in detail the mechanism of dynamic embrittlement in the alloy IN 718. To complete the LCF tests and to get more information on the environmental effect vacuum tests will be performed. To identify the detrimental role of oxygen on the crack propagation behaviour under LCF conditions accelerating current potential drop (ACPD) measurement tests in laboratory air and in vacuum are envisioned to find out how this failure mechanism works under dynamic conditions.

[1] Krupp, U.: Dynamic Embrittlement – Time Dependent Quasi-Brittle Intergranular Fracture at High Temperatures, International Material Reviews, 2, 2005, pp. 83-97

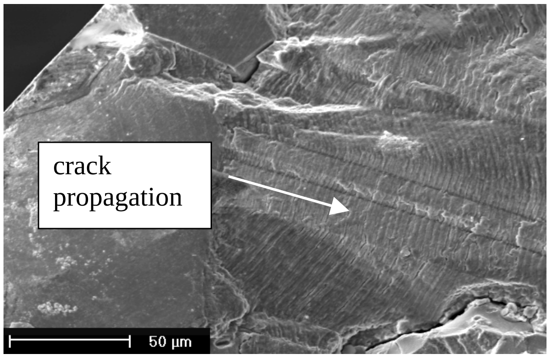

(a)

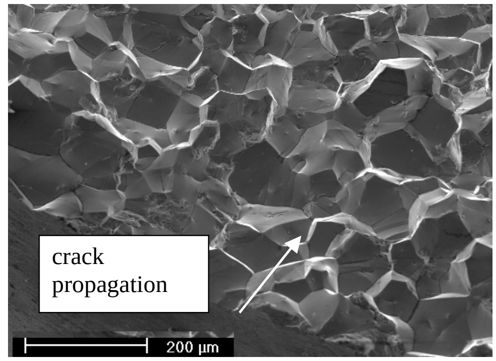

(b)

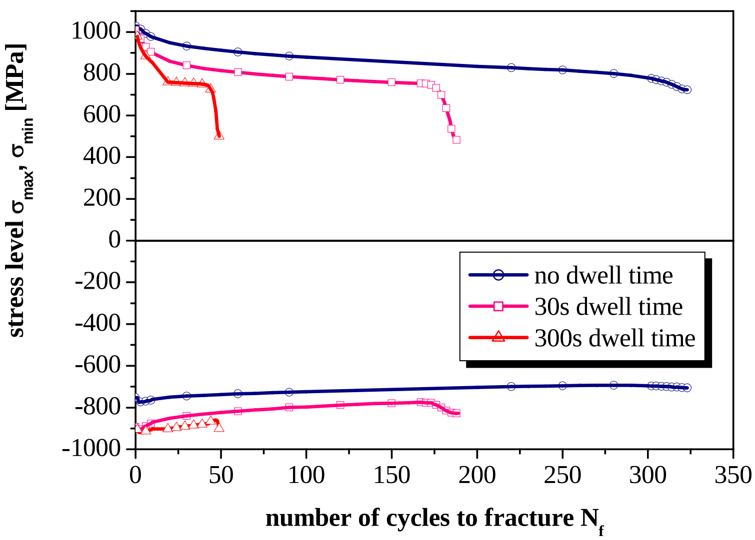

(c)

Figure 74: Fracture surface after fatigue testing without (a) and with a hold-time of 300 seconds (b) and (c) corresponding cyclic deformation curves

8.4 Thermohydrogen Processing (THP) of Metastable Beta Titanium Alloys

G.M. Lohse and H.-J. Christ (USI)

Beta titanium alloys are used for components and assemblies in the aeronautical, aerospace and recently consumer industry due to of their attractive strength-to-density ratio, excellent corrosion resistance, deep hardening heat treatment potential and inherent ductility as a result of the body centered cubic (bcc) structure of the high temperature beta phase of titanium.

In principle hydrogen is known to deteriorate the mechanical properties and lead to brittle fracture behaviour of most structural alloys. Hydrogen uptake mainly takes place during production, surface treatment and in service under respective environmental conditions. As opposed to the embrittling effect of hydrogen, a positive effect on the mechanical properties of titanium alloys may result under certain conditions. This is due to the fact that hydrogen stabilizes the beta phase of titanium and can therefore be used to optimize the microstructure by means of thermo hydrogen processing (THP).

The object of this ongoing study is to investigate the effect of hydrogen on the microstructure and to characterize the variation of the mechanical properties in metastable β titanium alloys by means of thermo hydrogen processing. Especially in the investigated metastable β-titanium alloys hydrogen has strong influence on the microstructure and this provides the possibility to optimise final mechanical properties.

The present study deals with two commercial titanium alloys used in TH processing. β-titanium alloys Timetal®LCB (low cost beta, Ti-6.8Mo-4.5Fe-1.5Al) and Timetal®10V-2Fe-3Al were hydrogenised by means of hydrogen charging from helium/hydrogen gas mixtures during heat treatment with variable hydrogen concentration. Figure 75 shows experimentally determined plots of the hydrogen concentration in Timetal®10V-2Fe-3Al representing the solubility data versus the square root of hydrogen partial pressure in the gas phase. It can be seen that for hydrogen solubility increases with decreasing temperature. Furthermore, the isothermal plot at 770°C indicates that the solubility in the alloy up to a partial pressures of 10 mbar follows strictly the Sieverts' law.

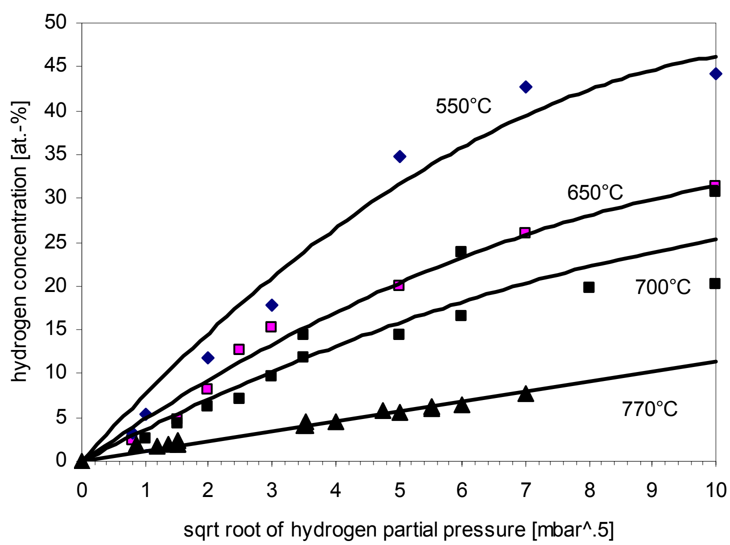

Figure 75: Linear relationship between hydrogen concentration and the square root of partial pressure for hydrogen charging of TIMETAL®10V-2FE-3AL at various temperatures.

Figure 76 a and b show the microstructure of Timetal®10V-2Fe-3Al after heat treatment at 750°C and subsequent water quenching. The hydrogen content of the material shown in Figure 76a is 1.6 at-% and in Figure 76b 5.1 at-%. The heat treatment led in both cases to two-phase microstructures consisting of bcc β-matrix with hcp α-phase. The sample of Figure 76a shows a higher volume fraction of secondary hexagonal α-phase than the sample of Figure 76b, because of the lower hydrogen content.

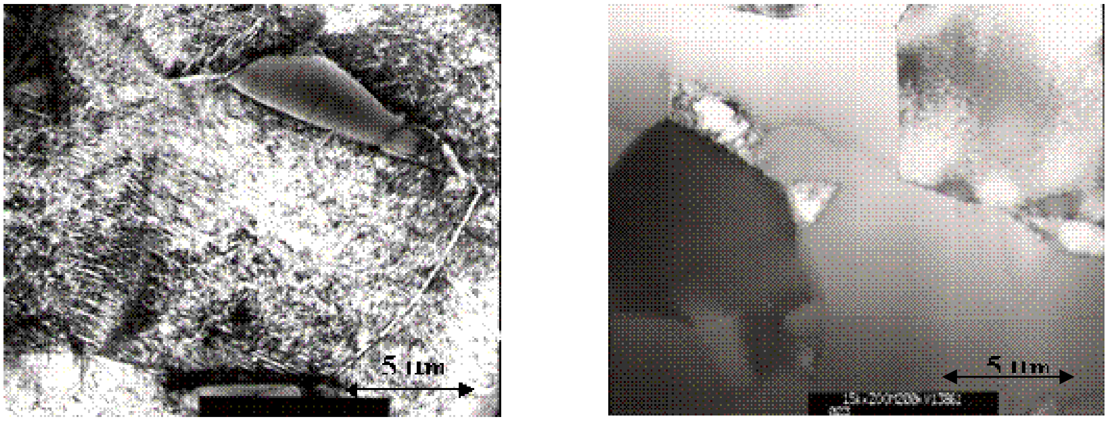

(a) (b)

Figure 76: Transmission electron microscopy images showing the microstructure of TIMETAL®10V-2FE-3AL after heat treatment at 750°C. Hydrogen content in a is 1.6 at-% and in b is 5.1 at-%.

In the study the effect of hydrogen on the kinetics and thermodynamics in the β-titanium alloys to develop a THP treatment procedure, consisting of hydrogen charging, solution annealing above the beta transus in combination with hydrogen release and ageing. This process provides the opportunity to establish a microstructure with less grain growth during solution annealing and higher volume fraction of the strengthening α-precipitates after ageing as compared to the standard heat treatment. The final goal is to optimize mechanical properties in such a way that an improved strength and fatigue limit results.

8.5 High-Temperature Fatigue of Titanium Alloy IMI 834 in an Environmental Scanning Electron Microscope

G. Biallas (DLR), M. Essert and H.J. Maier (Univ. of Paderborn)

The near-α titanium alloy IMI 834 was designed for use in the compressor section of jet engines at upper service temperatures of 600 °C. To mimic conditions experienced by such components, *in-situ* fatigue tests were performed in an environmental scanning electron microscope at 600 °C in both pure water vapour of 12 Torr (corresponds to 60 % relative humidity at ambient room temperature conditions) and ambient air of similar humidity. Completely reversed cycling with a constant plastic strain amplitude of 0.5% was conducted at a frequency of 0.015 Hz. The cyclically very stable equiaxed microstructure of IMI 834 used for this investigation allows an estimate of lower bound for the cyclic properties. Loading direction is vertical on the page for all pictures shown.

Fatigue life was found to decrease distinctly in the case of cycling in pure water vapour ($N_f = 32$) as compared to loading in ambient air ($N_f = 154$). In both environments, cracks not associated with slip bands and oriented perpendicular to the loading direction, Figure 77 and Figure 78, formed in the oxygen-enriched brittle subsurface layer (α case) resulting from inward diffusion of oxygen. The high number of slip bands observed on the specimen surface indicates pronounced cyclic slip activity independent on the environment imposed, Figure 77 and Figure 78. Thus, the rather thick α case does not prevent the evolution of slip bands. However, crack initiation at slip bands only occurred for the test conducted in ambient air. During further cycling, these cracks oriented at about 45° to the loading direction grew and opened in a different manner as compared to the previously mentioned cracks, which had formed in the α case (Figure 78).

Figure 79 compares fracture surfaces formed in 12 Torr pure water vapour and ambient air. Only few but very pronounced cleavage-type facets oriented parallel to the loading direction were observed in case of the 12 Torr pure water vapour environment (Figure 79a). The brittle fracture behaviour is underlined by extensive secondary cracking on the crack surfaces. By contrast, for ambient air the striation-like apperarance with a spacing very close to the per-cycle growth rate of $\approx$ 2 µm (Figure 79b) implies some plastic blunting and a higher cyclic plasticity at the crack tip. Thus, despite the similar number and density of slip bands on specimen surface, the cyclic deformation at the crack tip is different for both environments.

It is well known that hydride formation is enhanced in the triaxially stressed crack tip region and that the tendency towards a hydride-induced fracture mode is increased, if the strain rate is lowered or the temperature is increased [1]. Since hydrides can be stabilized by plastic accommodation, the environmental degradation of titanium alloy IMI834 is attributed to the formation of hydrides even at 600 °C. However, the brittle character of hydrides can not be generalised since thin hydrides deform readily along with the surrounding matrix without brittle fracture [2]. The behaviour observed can be rationalized, if hydride formation is assumed to be affected by the amount of oxygen present in the environment [3]. The proposed coupled mechanism of oxygen-affected hydride formation implies that hydrides become thinner, *i.e*. the embrittling effect is reduced [2] the more oxygen is present at the crack tip. The amount of oxygen available is much higher for ambient air as compared to a pure water vapour atmosphere and, consequently, the number of cycles to failure is also higher. Fine cleavage-type facets accompanied by small secondary cracks correspond to thin deformable hydrides, and thus, a lower crack growth rate. By contrast, only few but pronounced cleavage-type facets observed for the 12 Torr pure water vapour case indicate the formation of thicker hydrides resulting in a higher crack growth rate. Obviously, the free oxygen present in ambient air diminishes the hydrogen induced embrittlement although the amount of water vapour present in the environment remains unchanged.

[1] Shih DS, Robertson IM, Birnbaum HK. Hydrogen embrittlement of α titanium: *In situ* TEM studies. Acta Metall. 1988; 36(1):111-124.

[2] Chen CQ, Li SX, Zheng H, Wang LB, Lu K. An investigation on structure, deformation and fracture of hydrides in titanium with a large range of hydrogen contents. Acta Mater. 2004; 52(12):3697-3706.

[3] Biallas G, Essert M, and Maier HJ. Influence of environment on fatigue mechanisms in high-temperature titanium alloy IMI834. Int. J. Fat., in print.

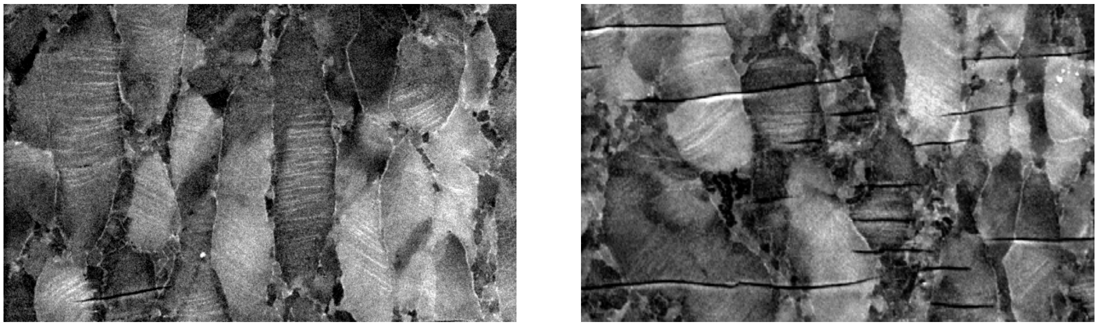

Figure 77: Slip bands and cracks in the specimen cycled in 12 Torr pure water vapor, $N = N_f = 32$. 20 μm

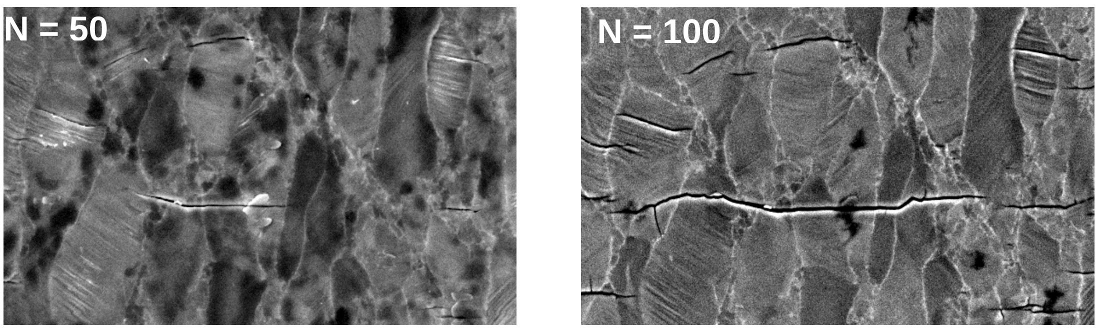

Figure 78: Slip bands and cracks in the specimen cycled in ambient air ($N_f = 154$). 20 μm

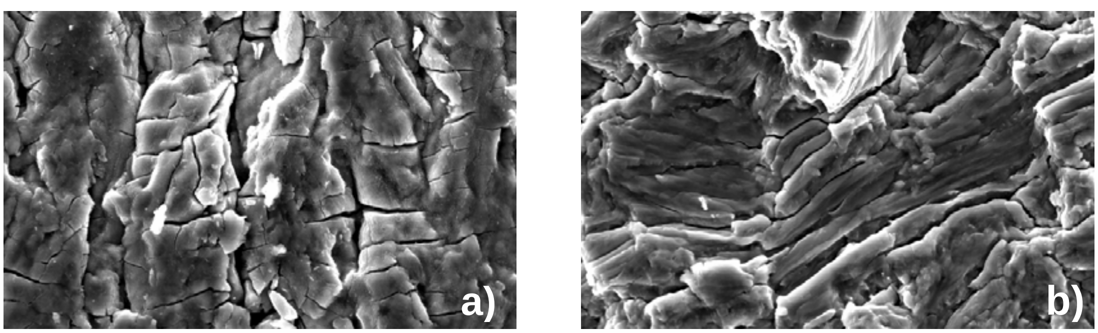

Figure 79: Fatigue fracture surface in (a) 12 Torr pure water vapor and (b) ambient air, respectively. 10 μm

9 Non-Destructive Testing and Structural Health Monitoring

9.1 High-Resolution Ultrasonic Testing of Aluminium Friction Stir Welds

T. Vugrin, G. Staniek and W. Hillger (DLR), C. Dalle Donne (EADS-CRC)

Friction Stir Welding is a novel solid state joining process invented by The Welding Institute in 1991. A rotating tool is being plunged into the material to be welded and moved along the joint line. The rotation and forward motion of the tool cause frictional heat, plastification of the material and severe material movement, thus leading to the joining process [1].

Though Friction Stir Welding is a very stable process, occasionally defects may occur. The defects can be divided into three categories: voids, lack of penetration (located in the root region of the weld) and root flaws. Voids and lack of penetration can be avoided by optimizing the welding parameters and tools. In the case of the root flaw only partial bonding of the material takes place. It is typically the smallest of the mentioned defects and its origination process is least understood. Therefore, during the development of a suitable non-destructive testing technique for friction stir welds, special attention was paid to the detection of the root flaw [2].

Testing Setup

Due to the small size of the root flaw (typically a few hundred microns), a very high resolution of the non-destructive testing is required. The ultrasonic inspection system HFUS 2400 with an ultrasonic transducer coupled to a high-precision scanner is used. The focused transducer has a frequency of 25 MHz and a focal length of 1 inch in water. The relatively high frequency and short focal length enhance the ultrasonic signal leading to superior lateral resolution. The measurements are conducted with water coupling in pulse-echo technique.

Voids are detected by longitudinal ultrasonic waves and a perpendicular incidence of the ultrasonic beam, since they show interfaces oriented perpendicularly to the ultrasonic beam, Figure 80 left. As the root flaw and lack of penetration do not have these interfacial areas, they can not be detected using the same testing setup as that for voids.

The defects in the root region of the welds are detected by an inclined ultrasonic beam. Using an angle of incidence of 20° towards the inspected plate, an ultrasonic shear wave of 45° is created inside the aluminium plate. Thus the ultrasonic wave hits the defect near the bottom of the weld and the flaw can be detected,
Figure 80 right.

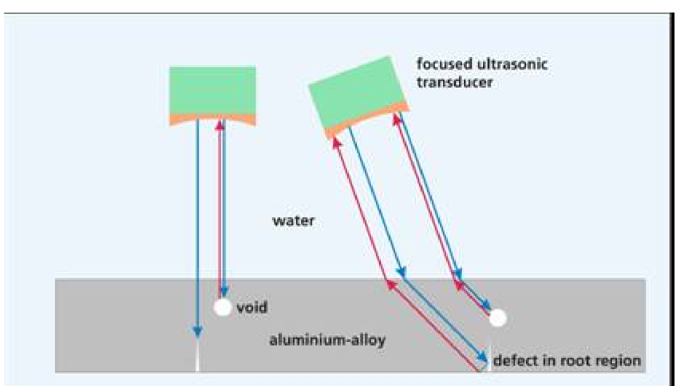

Figure 80: Ultrasonic beam path for the detection of voids (left) and the detection of the root flaw or lack of penetration (right) in friction stir welds.

Results

Figure 81 shows the top view of an ultrasonic “time of flight”-image (D-scan) of a friction stir weld that contains a root flaw from its beginning to its end. The grooves on the top of the plate, left behind by the welding tool shoulder, are indicated in blue colour. The root flaw is indicated as a continuous red line. As the plate was bent slightly at the beginning of the weld, the root flaw there is initially coloured in yellow.

Metallographic sections confirm the ultrasonic testing results and show the small size and the geometry of the root flaw.

Metallographic sections taken at various positions within the welds proof that a suitable and reliable non-destructive testing technique for friction stir welded joints could be established.

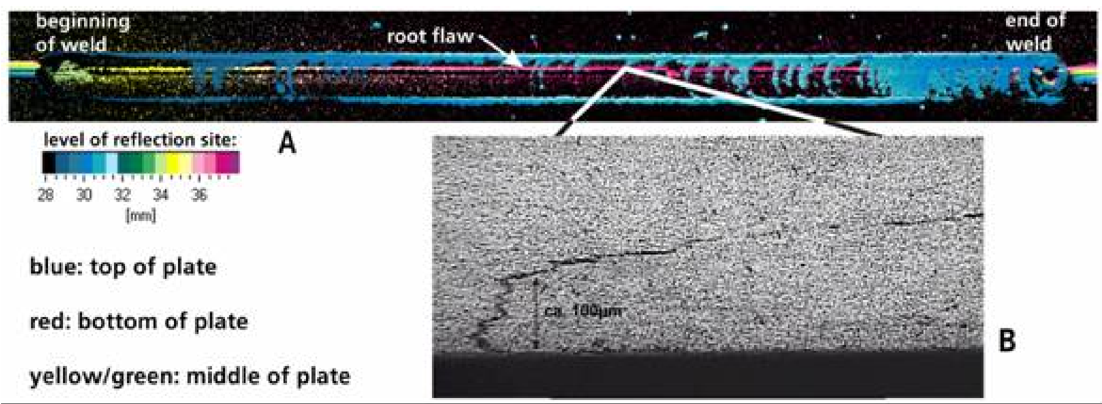

Figure 81: Ultrasonic scan and metallographic section of a friction stir weld containing a continuous root flaw. A: Ultrasonic D-scan (time of flight image), top view. B: Metallographic cross section of the root flaw.

[1] Thomas W. M, Johnson K. I., Wiesner C. S., “Friction Stir Welding-Recent Developments in Tool and Process Technologies”, Advanced Engineering Materials 2003, 5, No. 7

[2] Vugrin T., Staniek G., Hillger W., Dalle Donne C., „Non Destructive Detection of Flaws in FSW and their Metallographic Characterization”, Proceedings 5th International Friction Stir Welding Symposium (CD-ROM), September 2004, Metz, France, ISBN 1-903761-04-2

9.2 Possibilities and Problems with Vibro-Acoustic Diagnostics on Aircraft Engines

R. Rennert and C. Pritzkow (IMA)

In the last years vibro-acoustic diagnostic has been taken into account for health and usage monitoring more and more also in civil aviation. To guarantee safe aircraft operation, condition monitoring on aircraft engines and drive systems by vibration measurement and analysis is a widely accepted subsidiary method.

In a research project IMA GmbH Dresden and partners developed the embedding of a vibro-acoustic diagnosis system into an existing aircraft engine control unit.

The investigation deals with the problem of aircraft engine vibrations from the diagnostician's point of view, especially with some aspects of dealing with memory shortage. Calculation time and memory in aircrafts is strictly limited and high priced. We could show, how it will be possible to perform the extensive diagnosis calculation in a strictly limited aircraft engine control unit.

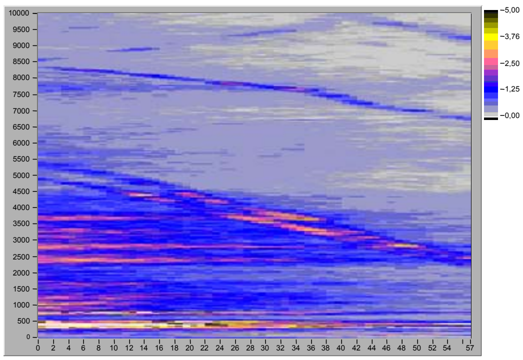

Figure 82: Power spectrum during shut down of an aircraft engine

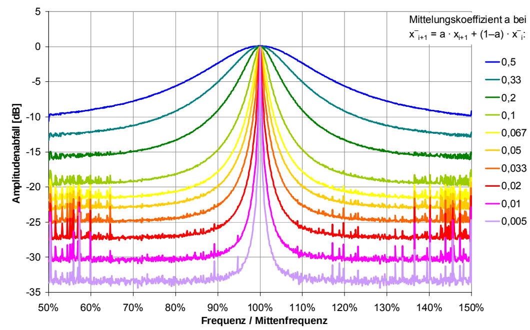

Figure 83: Filter characteristic of new algorithm for unbalance detection with different length of sliding average

All described concepts and methods were putted into practise. Test results show vibration monitoring periods on aircraft engines during test rigs runs. The diagnosis data are collected in intensity plots, this means diagrams with the time history of frequency spectra, from special operation conditions of aircraft engines. The characteristic vibration patterns of the surveyed aircraft engine occur clearly.

At the request of air carriers a new algorithm for online unbalance identification was developed. Using a non-linear curve fit method it allows permanent unbalance identification also under highly variable speeds. The unbalance detection algorithm works like a narrow band filter for one special frequency, in our case the turbine shaft frequencies. We proved the filter characteristics of the new algorithm as well as the effect of influence values like noise level, speed change etc. on the resulting unbalance values. The unbalance detection algorithm was also tested on real aircraft engines.

Result of all investigations is an aircraft engine control unit with the additional functionality of a vibro-acoustic diagnosis system. That could be reached without any hardware extension by complete use of existing vibration sensors, measurement equipment, calculation resources and data transfer paths. So we can provide an economic solution to increase safety on aircraft engines. Due to low costs and flexible implementation that diagnosis extension is especially designed for small and mid-size aircrafts.